Doctoral Dissertations   Graduate School

12-2002

A finite element model updating technique for correcting global geometric errors using multiple models

Charles R. Vining
University of Tennessee

To the Graduate Council:

I am submitting herewith a dissertation written by Charles R. Vining entitled "A finite element model updating technique for correcting global geometric errors using multiple models." I have examined the final electronic copy of this dissertation for form and content and recommend that it be accepted in partial fulfillment of the requirements for the degree of Doctor of Philosophy, with a major in Engineering Science.

<div align="right">

Remi Engels, Major Professor

</div>

We have read this dissertation and recommend its acceptance:

<div align="right">

Accepted for the Council:

Carolyn R. Hodges

Vice Provost and Dean of the Graduate School

</div>

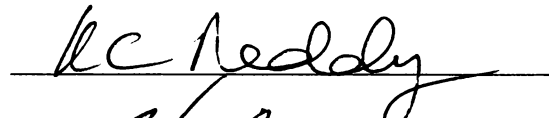(Original signatures are on file with official student records.)

To the Graduate Council:

I am submitting herewith a dissertation written by Charles Vining entitled "A Finite Element Model Updating Technique for Correcting Global Geometric Errors Using Multiple Models." I have examined the final paper copy of this dissertation for form and content and recommend that it be accepted in partial fulfillment of the requirements for the degree of Doctor of Philosophy, with a major in Engineering Science.

_____

Remi Engels, Major Professor

We have read this dissertation and
recommend its acceptance

_____

_____

_____

_____

Acceptance for the Council:

_____

Vice Provost and Dean of
Graduate Studies

A Finite Element Model Updating Technique

For

Correcting Global Geometric Errors Using Multiple Models

A Dissertation

Presented for the

Doctor of Philosophy

Degree

The University of Tennessee

Charles R. Vining

December 2002

Acknowledgements

I would like to thank all of the people who helped me in completing this research effort. First, I would like to thank Dr. Engels for his guidance and for sharing his expertise in structural dynamics and modal analysis. I would also like to thank my committee members for their insight and for serving on my committee. Thanks also go to Mr. Goodman and the staff in the Propulsion Lab at the University of Tennessee Space Institute for their assistance during the experimental phase of this research. Additionally, I would like to thank Mr. Tibbals and Ms. Stevens of Sverdrup Technologies for data systems support.

I would also like to thank my family for their support, encouragement, and patience. Completing this work would not be possible without their support.

Abstract

Finite element model updating has been an area of active research for the past thirty years. The goal is to provide a model that is more representative of the structure. This updated model can then be used for additional analysis to evaluate the design or provide the designer with insight on how to improve the design, if necessary. Despite the extensive amount of research, no one method has emerged that can be applied to all circumstances. The diversity in methods applied can be traced to the inverse nature of the problem. Typically, the amount of information available from modal testing of a structure is limited. The finite element model of the structures can be quite large with hundreds or thousands of degrees of freedom. This leaves the analyst with little choice but to select a region of the finite element model by choosing elements or groups of elements for corrections. The selected elements are parameterized by extracting design parameters directly or by sensitivity methods. The parameter corrections are obtained using the method of least squares. This process usually results in an ill conditioned problem that can be sensitive to small variation or noise in the test data.

An alternate view of the updating problem is that the errors are distributed rather than localized to a specific region of the model. This is the case when variations in geometry can influence the response characteristics of a structure. This research effort proposes a new approach for updating the geometry of a finite element model using a set of models to form a basis for a perturbation space. The method is demonstrated by numerical simulations and by experiment using a series of perturbed flat plates. The numerical simulations indicate that the updating technique produces an updated model

that improves the agreement between the simulated test plate and the model. The application of the method to the experimental data demonstrated that the updated model provided a slight improvement of the nominal model. A new metric for comparing the error between the model and the test data based on the matrix 2-norm is presented.

Table of Contents

List of Figures

List of Tables

1. Introduction

Efforts to reduce the development time for new and increasingly complex engineering systems have resulted in the convergence of the design and experimental processes. The reduction in development time is being achieved by relying on advances in computing power and in analysis tools including finite element analysis while reducing the amount of testing to verify the ability of the design models to predict system performance. As a result of the emphasis on shorter design cycles, new tools to integrate the two processes are being developed and refined. One area where design tools and experimental tools are being integrated is structural dynamics. Dynamic testing is expensive and time consuming. At the very least, special test equipment including shakers, test fixtures, instrumentation, and expensive analyzers are all needed to conduct the test and analyze the results to determine what, if any, design modifications are required to shift or dampen any undesirable vibratory resonance. In some cases, particularly in complex machinery such as turbine engines there is limited access to the parts being evaluated and only response data is available. The limited information available forces additional reliance on the analysis tools to predict the response characteristics away from the measurement locations. Understanding or reducing the discrepancy between the experimental data and the design model is important to ensure the validity of the design model and its ability to accurately predict system performance.

Current methods for predicting the dynamic response of turbo machinery airfoils are based primarily on models that use the nominal blade geometry. These models provide the natural frequencies and mode shapes for the modes of interest that could occur in or near the rotor speed range or a multiple of the speed. Blade-to-blade variations can result in deviations from the nominal blade model in the measured deflections and stress amplitudes for a blade row. These variations can be significant, resulting in a reduction in the high cycle fatigue life [1] of the blades or related structure. There have been several studies directed at predicting the response characteristics of rotor disks and blades. Different approaches to the problem include investigations of the effects of mistuned rotors on blades vibration and studies of the response characteristics of individual blades. The differences in the response characteristics can be caused by several factors including variations in the blade attachment stiffness (boundary conditions), material properties, and blade geometry. The differences in response are most often attributed to blade-to-blade variations in material properties and in geometry [2], [3], [4], [5], [6]. These studies do not address how or to what extent the variations in the material properties and geometry affect the response characteristics.

The objective of aeromechanical testing is to ensure that all excited modes within the operating range of the machine do not have a response that exceeds a predetermined design criterion. A commonly used design criterion is a predetermined margin of safety below the Goodman line [7] for any excited resonant mode. Identifying the modes that exceed the design criteria provides the designer with a starting point for redesign. However, a difficultly in the analysis of the test results can occur when one or more blades on the test article fails to meet the design criteria. The challenge then is to

2

determine which characteristics or properties of the blades that fail the design criteria are the primary causes for the differences between the design model and the structure being tested. This is the juncture where the design and experimental processes converge.

One means of resolving the discrepancies between the model and the experimental results is to adjust or correct the design model to reduce the error. A careful assessment of the quality of the experimental results must be accomplished to ensure that the adjustment of the model is justified. In the area of modal analysis, there are several tools available to assess the quality of the test modes using the modes determined from the baseline model. Once confidence in the test data has been established, it is valid to consider determining the appropriate adjustments to the model to reduce the error between the model modes and the measured modes. The intent of finite element model updating is to determine physically meaningful model corrections to reduce the modeling discrepancies so that the designer can use the model to obtain more accurate vibratory displacements and stresses. The updated model can then be used to assess whether the design should be modified in cases where the structure under test has failed to meet any design criteria specified by the designer.

During the past thirty years of research several methods for updating finite element models have emerged. No one method is best in all circumstances. Model updating algorithms are designed to solve an inverse problem where the necessary adjustments to the model parameters are calculated reducing the error between the model predictions and the experimental results. The nature of the inverse problem requires that the analyst constrain the problem so that the updating analysis can be structured as a forward matrix perturbation problem providing a unique solution. The imposed

constraints or assumptions utilized are problem specific with regard to identifying the regions of the model that are considered to be the largest contributors to the discrepancy between the model predictions and the test results. Global assumptions that also apply to all updating problems include a requirement that the finite element model be suitably structured to avoid numerical errors and that proper test techniques are employed to ensure that noise and experimental setup do not introduce errors into the measured characteristics such as mode shapes and natural frequencies.

The objective of the present study is to develop a finite element updating approach using isoparametric elements that produces an updated model minimizing the error between the model and the experimental results by accounting for variation in geometry. Geometric variations have been identified as having a larger influence on the modal response characteristic of turbo machinery airfoils than variation in material properties [8]. There are no methods currently available using isoparametric elements that either directly or indirectly address variations in geometry. This dissertation presents a non-iterative updating method that uses a nominal model with a set of geometrically perturbed models. The modes for the entire set of models form a set of basis vectors for a modal perturbation space that can approximate the test article modes. An over determined system of equations is generated and prepared in order to solve for the coefficients of the modal basis vectors. These coefficients are then used to determine the contribution of each model's geometry to provide an updated geometry for the test article model. Modal analysis is performed on the updated model using the predicted geometry. A 2-norm for the error matrix formed by taking the difference between the test article modes and the updated model modes at the measurement points is calculated and

4

compared with the 2-norm of the error matrix between the initial model and the test

article to verify the improved performance of the updated model. The model updating

method is demonstrated by numerical simulation and a test conducted with four perturbed

test plates and one unperturbed plate.

2. Literature Survey

Scope of Survey

A literature survey related to the proposed topic was accomplished for two broad areas. The areas covered by the literature survey included research on the vibratory response characteristics of turbo machinery blades including flat and twisted plate representations and research on finite element model updating algorithms. The survey of literature on the vibratory characteristics of turbo machinery focused on modeling and experimental methods to characterize the response of blades. The intent of this review was to make an assessment of the areas where model updating could provide some benefit. The review of the model updating literature was conducted to evaluate different methods for applications where large regions or potentially the entire model may require adjustment.

Mistuned Rotor Dynamic Analysis

There has been a substantial amount of research directed at understanding the response characteristics of axial flow turbo machinery rotors. Srinivasan [9] presented a comprehensive study of blade vibration in 1997 covering a wide range of parameters both aerodynamic and structural that influence the response characteristics of blades. One of the parameters identified was blade geometry during a review of mistuning.

Mistuning refers to the loss of symmetry of a rotor, which can result in large variations in blade response for a rotor stage. The studies reviewed on mistuning can be divided into two categories. The first category developed lumped parameter models of

the blades and the disk allowing for the investigation of blade-to-blade and blade-to-disk stiffness parameters and in some cases damping parameter variations [3]. These studies provide the ability to assess the rotor response characteristics for varying degrees of mistuning by adjusting the mass and stiffness parameters. The second category applies finite element models of a rotor stage to investigate the response characteristic of mistuned rotors [4], [6]. Efforts have been directed at providing reduced order models that allow for the detailed study of the effects of mistuning. These studies have indicated that variations in blade characteristics can result in significant increases in response amplitude and stresses.

The variation of blade characteristics is central to mistuning studies. In one study, inducing a random variation in Young's modulus for each blade was used to represent the degree of mistuning [10]. Here a reduced-order model was solved one thousand times using a Monte Carlo simulation to estimate the statistical properties of the response. This approach does not provide a convenient method for determining how to manipulate the blade design to produce a set of blades with intentionally mistuned characteristics to limit response caused by mistuning.

Several approaches have been attempted to characterize the response characteristics of turbo machinery blades. Varying lumped parameters or material properties, depending on the modeling approach, has resulted in simulations representative of the variations in blade response seen during testing. These methods provide insight into mistuning but they do not provide the designer with a means for placing bounds on geometric tolerances to limit the response levels and control mistuning.

Aeromechanical Test and Analysis Methods

During development testing for turbo machinery, blades are often instrumented with strain gages to measure the resonant strains for comparison with the modal strains and stresses of a nominal finite element model of the blades. In addition to using strain gages, a non-intrusive stress measurement system can be used to measure the blade deflections during component rig testing or engine testing [11]. There are several advantages to using a non-intrusive stress measurement system. Some of these advantages include: 1.) All blades in the blade row can be assessed; 2.) The disk and blades are not influenced by the application of strain gages with the associated wiring and slip ring; and 3.) The system is more durable than strain gages, which can fail during testing. The testing can range from laboratory test of individual blades through full up sea level and altitude engine tests to evaluate the durability of the design against one of many established criterions. Bench testing and finite element models are used to identify vibration modes and selecting strain gage locations. They also provide a means for determining stress and strain ratios from the gage locations to the maximum stress and strain for the blade.

Development of analysis tools for aeromechanical testing continues to be an active area of research. The work reviewed included testing and analysis for various test techniques ranging from shaker table tests of individual blades and component tests through methods used for engine testing. There are several sources of uncertainty in the measurement and modeling process. Finite element models are a necessary component in the process from experiment design through the monitoring and analysis of test data.

The use of finite element models as part of experiment design includes the prediction of the blade's modal strain and stress distributions to determining the optimum locations and orientations for strain gages. Yang and Griffin [5] present a method for selecting the optimum gage locations for closely spaced modes of vibrations. They point

8

out that the actual mode shapes for closely spaced modes are highly sensitive to small variations in geometry. Small variations in geometry make the true mode shape unknown. This method seeks to determine the participation factors of the modes from a nominal model to represent the unknown mode. The error sources compensated for are gage placement errors and gage measurement errors. Here the "nominal" model is error free and a least-squares method is used to determine the participation factors for the participating modes. The gage errors are propagated to the mode participation factor using the strains predicted by the model at the gage locations. The optimization routine minimizes the error in the mode participation factor vector for the gage locations.

Sensmeier and Nichol [12], [13] use a genetic algorithm that defines the optimum location of the gages based on a set of constraints or metrics. One metric is mode identification. The gages can be used to represent reduced mode shape vectors that do not retain their orthogonality. The method maximizes the angle between a mode and all other modes of interest to improve or increase the visibility of the modes. Additional metrics are used to ensure mode visibility (gage output), minimize the influence of gage placement errors, and to ensure that gage spacing exceeds a minimum distance to minimize the influence of the gage on the response of the blade. This method has the advantage that the model need be solved only once for the mode shapes. It also provides an effective method for maximizing the angle between two closely spaced modes for the model geometry.

The numerical representation of strain gages is critical to the effective use of finite element models in the analysis of aeromechanical data. Nichol [14] presented a method for modeling a strain gage that accounts for the averaging effects of the gage. Averaging effects are especially important in areas of high strain gradients. Variations in gage placement in high strain gradients can result in large variations in the strain gage output [15]. Comparing strain gage data with the nodal strains or the element strains of a

finite element model is not practical. Comparison with nodal strains ignores the averaging effects of the gage and comparison with an element strain would require that the gage be aligned with the model mesh. Nichol's method provides the capability to investigate gage placement effects as well as allow for the relocation of gages without having to re-mesh the model. Being able to model the averaging effects of strain gages improves the efficiency of analyzing test data by eliminating the need to rerun the finite element model.

The use of finite element models in the analysis of aeromechanical test results has been used to assess aerodynamic effects on the response characteristics of blades. Kenyon et al [1] presented a study on the effects of aerodynamic damping on variations in the response characteristics for an integrally bladed disk. Their assessment is that the disk was tuned and that mechanical coupling between the blades and the rotor are not responsible for the variation in response. The assumption is made that the small variations in geometry such as blade untwist and airfoil shape influences the aerodynamic damping but not the measured stresses. Gage measurement errors and placement errors are accounted for in their analysis. However, the assumption that the blade-to-blade variations in geometry do not influence the strain gradients at the gage locations ignores the influence of variations in local geometry on the measured response.

Flat and Twisted Plate Testing and Analysis

A review of the past work on testing and analysis of flat and twisted plates was conducted in support of the experimental phase of the proposed research topic. Flat and twisted plates have been used to approximate the characteristics of real turbo machinery blades [16]. The National Aeronautics and Space Administration sponsored a joint research effort on twisted plates [17]. This effort compared several different analytical

10

methods, most being finite element methods, to the results of twenty precision-machined twisted plates for two different aspect ratios and thickness ratios tested at two laboratories. Generally, the analytical methods predicted higher mode frequencies at four twist angles that ranged from zero degrees to sixty degrees in fifteen degrees increments. The resonant frequencies were experimentally repeatable to within 0.5%. The test mode shapes were identified by holographic interferometry. Mode shapes were matched with the analytical mode shapes on a qualitative basis. This was a comprehensive study aimed at validating analytical methods including convergence studies for the various finite element models and at providing an extensive database for the vibration characteristics of twisted plates. The NASA study demonstrated that different finite element methods could be used to predict the dynamic structural performance of flat and twisted plates.

Finite Element Model Updating

Model updating has been an area of active research for the past 30 years. Several methods based on least squares and minimum variance estimators have been developed [18]. It is often assumed that the discrepancy between the test results and the results predicted by the model can be attributed to specific areas of the model. This is a key assumption necessary for the formulation of the problem as a forward perturbation problem. Forward perturbation models retain the nodal connectivity of the original model. Papers on representative updating methods that do not preserve the model structure were not considered. Updating methods that do not preserve the connectivity of the finite element model cannot be used for additional analysis such as fatigue life assessments or forced response. Most research is geared toward improving the model for additional analysis.

There are two major branches of model updating techniques that maintain the nodal connectivity of the baseline finite element model. They are methods based on eigensensitivity analysis and methods based on the error localization equation for perturbed mass and stiffness matrices of the eigenvalue problem. The updated models from these methods maintain the structure of the finite element model allowing for additional analysis. Friswell and Mottershead [18] published a text on finite element model updating that presented an overview of the several different methods. The text placed a great amount of emphasis on sensitivity-based methods. Sensitivity methods are based on taking the derivative of the eigenvalues and/or eigenvectors with respect to the material parameters or when feasible the geometric parameters of the stiffness and mass matrices. These methods are usually iterative, requiring extensive computation at each step to provide the updated model for the next iteration. Most of the sensitivity-based methods reviewed did not use eigenvector derivatives. This is more than likely associated with the computation cost associated with producing these derivatives for several modes iteratively [19].

Finite element updating methods have been applied to all types of elements. Simple elements including bar, beam and plate elements can have either material or geometric parameters that are targeted for updating. Solid model elements are restricted to material properties. Generally, the analyst must determine which elements and parameters should be adjusted regardless of the updating approach used. In one example, Ahmadian [20], et al, recommended the updating of a rigid offset parameter for joints in a truss. The rationale was that the modeling of the truss members away from the joint was more accurate than the modeling of the joints. The offset parameter was preferred over using joint stiffness parameters because it is more sensitive to the errors in the eigenvalues. However, attempts to use the joint parameter updating approach on a welded space outside of the laboratory environment were unsuccessful [21]. The authors

12

noted that either the approach used to update the joints was inadequate or that the assumption that the joints were the primary cause of the difference between the model and the test was in error.

Farhat and Hemez [22], [23] presented an updating method referred to as the Sensitivity-Based Element-by-Element method (SB-EBE) and an extension of the SB-EBE to compensate for the ill conditioning related to the difference magnitude in the residual force error for the mass and stiffness matrices. The residual force $R(\vec{p})$ is an n × 1 vector found by solving the eigenvalue equation using the test eigenvalues and eigenvectors with the original model mass and stiffness matrices. The residual force is

$$R(\vec{p}) = \left(K(\vec{p}) - \omega_t^2 M(\vec{p}) \right) \begin{bmatrix} \vec{\varphi}_t \\ \vec{\varphi}_{ex} \end{bmatrix} \qquad (1)$$

where p is a m × 1 vector for m<<n of generic element parameters targeted for updating, ω_t^2 is the test eigenvalue, K(p) is the n × n stiffness matrix, M(p) is the n × n mass matrix, φ_t is a m × 1vector of the measured components of the eigenvector, and φ_{ex} is a (n-m) × 1 vector of the unknown components of the mode vector found by using a mode vector expansion method [18] to create a test eigenvector of order n × 1. Equation (1) gives the residual force when using the original model parameters with ω_t^2, φ_t, and φ_{ex}. The residual force vector is a result of the error between the test mode and the original model mode. After an updating method is applied, R(p) is made close to zero by substituting the updated parameters p and the remaining (n-m) × 1 original model parameters, that were not targeted for updating. The SB-EBE method uses a two-step process that first identifies the elements with dofs where the residual forces are highest. The elements that have the highest sensitivity to the residuals are then targeted for updating. Usually, the residuals associated with the stiffness matrix are several orders of

magnitude larger than the residuals associated with the mass matrix. This tends to result in corrections for stiffness parameters even when the error is associated with a local change in a density parameter. Farhat and Hemez [23] presented a normalization process that gave equal weighting to the mass and stiffness parameters to reduce the disparity in the sensitivity of stiffness and mass parameters resulting in the correct identification of the local errors in density.

The process of selecting design variables for updating is not intuitive. It requires an assessment by the analyst constructing the updating problem [24]. There are several possible design variables that can be selected to solve a particular problem. A criterion has to be selected to pick the best set. Different criteria that range from allowing several design variables to vary within manufacturing tolerance to iterative methods based on sensitivity for a subset of design parameters have been tried. The elastic modulus, Poisson's ratio, and density are usually selected. These are the only parameters that are easily extracted from the finite element equations for isoparametric elements. Blelloch and Freymiller [24] suggest that automated methods that limit the involvement of the engineer are less effective in delivering a reliable solution. The criterion to select the best set of parameters in one instance was the set that produced the best results on average [25]. In reference [25], model updating experiments were conducted on a three-story space frame using five different sets of parameters. The parameters were: scalar multipliers of substructure stiffness and mass matrices for three different element groups; the mass of the connecting nodes; a joint offset parameter; and the tube thickness. Different combinations of these parameters were used all producing reasonable results. The set that produce the best results on average was also considered the set that best preserved the physical meaning of the model after updating.

Ill conditioning is a problem common to all updating formulations. The updating problem usually results in an over determined set of equations that are solved by using

14

the method of least squares. Ill conditioning manifests itself in numerical simulations by producing large changes in the updated parameters vector p for changes in the quantity represented by the b vector and a large condition number for the A matrix in the least square equation

$$Ap = b \qquad (2)$$

where A is an k × m coefficient matrix obtained by transforming the mass and stiffness matrices from the global coordinate space to the parameter space of the targeted parameters with k>m and the p vector is the m × 1 vector of parameters to be corrected. The dimension k of equation (2) obtained by multiplying the size of the finite element model, n by the number of test modes available for use in equation (2). The k × 1 b vector can represent the residual force defined in equations (1) above of the available test modes or for sensitivity based methods the difference between the measured eigenvalue and the model eigenvalue. Farhat and Hemez [23] suggest that the ill conditioning is caused by the small singular values of A (typically, $<10^{-6}$) and their associated left singular vectors. They point out that these components of the singular value decomposition are responsible for large parameter changes (100% and higher) that are not physically real. There have been several methods proposed for dealing with ill conditioning of the updating problem. Friswell, Mottershead, and Ahmadian [26] present several methods to address the ill conditioning of the least squares problem. They also attribute the errors to the small singular values.

One aspect of the problem that has not been addressed are cases where some b vectors produce acceptable solutions for the parameters, and others where a small change in one component of the eigenvector can produce large changes in the residual force vector of equation (1), that result in unrealistic parameter corrections [27]. The

calculated updated parameters, p_i in equation (2) can be correctly estimated within the simulated noise bounds place on the eigenvectors despite the small singular values of the A matrix. The cases where changes in the parameters p_i are large for small changes in an eigenvector component (<.01%) results in the rotation of the b vector away for the range of A. The relative condition number for perturbations in p_i that arise for certain perturbations in the b vector provides a basis for explaining why certain b vectors from a set with the same noise level can cause large perturbations in p_i and others produce reasonable perturbations within the simulated noise levels. The relative condition number is given by [28]

$$\kappa_r = \frac{\kappa(A)}{\eta \cos(\alpha)} \tag{3}$$

where $\kappa(A)$ is the condition number for the A matrix, α represents the angle between the b vector and the range of A and

$$\eta = \frac{\|A\| \, \|p\|}{\|y\|} \tag{4}$$

where $\| \ \|$ represents the 2-norm for the matrix A and the Euclidian norm for the vectors p and y. The vector y is the projection of b onto the range of A. The number η is a measure of how much the magnitude of y falls short of its maximum given the 2-norm magnitude of A and p. The relative condition number, κ_r is exact for specific perturbations rather than a bounding value as is the cases for the relative condition number between perturbations in the A matrix and the update parameter vector, p.

16

3. Conclusion from Literature Survey

The papers reviewed on the response characteristics of turbo machinery airfoils indicate that variations in the geometry of the blades influence the response characteristics of the airfoils. Current modeling techniques for representing variations in response vary material properties, which do not provide a practical method for correcting a design deficiency, should one occur. Locally controlling the elastic modulus for a rotor disk is not practical. Geometric parameters are available to the designer for controlling the stiffness of individual blades. Determining the specific cause for variations in stress amplitude during testing of a rotor stage is a complicated task. There are several variables that can influence the response. Simplifying assumptions can be made to develop a tractable problem. One assumption that can be made is that all blades experience the same forcing. Applying this assumption permits the investigation of the influence of blade geometry variations on the response characteristics.

Model updating provides one means of investigating the effects of variations in geometry on the response characteristics of turbo machinery airfoils. All of the model updating techniques that have been reviewed are applicable to local variations in material properties or geometry properties for elements that have local coordinate systems in one or two dimensions. The inverse character of the updating problem has prevented any single method for updating to be applicable in all circumstances. A key assumption of all the finite element model updating methods reviewed is that the error between the model

and the test can be attributed to a few elements or a few groups of elements. This assumption is necessary because the structure of the updating problem is constrained by the limited amount of information available from experimental modal testing. The limited amount of information constrains the number of parameters that can be updated for most methods. There have been no research efforts conducted on methods that correct for global variations in geometry. Extending methods based on error localization to account for global variations in geometry is not practical. This suggests that a different approach should be taken to obtain an updated model that reduces the discrepancy between the modal test data and the model.

4. Development of Geometric Updating Method

Existing finite element model updating methods for isoparametric elements target material properties of a small subset of the elements or groups of elements. The material parameters are easily extracted from the element equations. In contrast, extracting the element coordinates for modifications is not practical. The difficultly is related to the element formulation. The isoparametric formulation permits the use of nonrectangular elements that can have curved surfaces depending on the number of nodes and shape functions [29]. The nodal coordinates in the global coordinate system define the element geometry. An auxiliary coordinate system is introduced that has its origin defined as the average of the nodal coordinates in the global system. The auxiliary coordinate system is a function of the global coordinate system. The global coordinates of the nodes are used to define the coefficient of the strain displacement matrix and for defining the determinant of the Jacobian matrix. Both of these quantities are needed for the integration of the stiffness matrix. The determinant of the Jacobian is needed for the integration of the mass matrix. The difficultly in extracting nodal coordinates from the element formulation suggest that an alternative approach needs to be considered when changes in geometry are being considered.

Assumptions

All model-updating problems are inverse problems with the possibility of many feasible solutions. In order to obtain a unique solution constraints are applied to the

system of equations. These constraints are necessary in that there is a limited amount of information available from the test that can be used for updating. The amount of information available from the test is limited by the number of measurement locations and the number of modes that can be identified from the test. The frequency range of the test limits the number of modes that can be defined. Given the constraints on the information available from testing, the updating problem must be structured so that the number of parameters does not exceed the number of measured quantities. Most updating methods constrain the problem by selecting a number of elements or a number of element groups that is less than or equal to the number of measured parameters (e.g. natural frequencies). This process usually results in an over determined problem that can be solved by applying the least-squares method.

In the least squares solution the parameters are free to take on any value that satisfies the minimum norm solution. This can result in parameter corrections that are not physically realizable or unrealistic for the given the problem. Methods that rely on adjusting material properties must define a priori the location or elements that are suspected to be in error. Typically, the number of groups of elements or the number of elements that are targeted for updating is much smaller than the total number of elements in the model. This subset of elements and the selected parameters for these elements translates into changes in a subset of matrix coefficients in the mass and stiffness matrices. Under ideal conditions the elements that are in error are correctly identified, measurement noise is low, and the resulting parameter corrections are physically realizable.

Compensating for errors in geometry is not amenable to updating methods that are formulated based on the ability to localize the error. Engels presented [27] a non-iterative method based on error localization for updating models provided the following three assumptions are met.

20

1. All obvious testing and modeling errors have been eliminated.

2. The structure's geometry is known.

3. All parameters needing change have been identified.

Assumption 2) eliminates geometric variations as an influence on the modal response. Assumption 3) implies that the source of the error can be localized to specific regions of the model. With the error localized the material parameters can be extracted from the mass and stiffness matrices for updating. The influence of variation in geometry on the response characteristic for turbo machinery airfoils implies that a method is needed that relaxes or removes the requirement for assumption 2). The inability to localize the error for arbitrary variations in geometry implies a modification of assumption 3). Assumption 1) is still valid.

The assumptions needed for developing an updating method that corrects for errors based on adjusting the geometry are:

I.   The material properties do not vary from point to point in a structure made of one material.

II. Clamped boundary conditions apply. Small variation in the boundary stiffness do not appreciable influence the mode shapes of the structure

III. Bounds or tolerances can be placed on the variation in geometry.

IV. Geometric variability can be characterized

Assumption I is consistent with the isotropic material assumption generally applied for modeling structures made of a single material. Assumption II is demonstrated

by an example. One of the models used to demonstrate the validity of Assumption II is shown in Figure 1. The boundary stiffness in this model is reduced linearly from middle of the plate to the edge by reducing Young's modulus in three steps. The outer most elements have a Young's modulus that has been reduced by approximately 2.2%. The second model, which is not shown, has the same plate dimensions and the same number of elements with a taper from the center of the plate to one edge in the widthwise direction. The percent change in thickness in the widthwise direction is the same as the percentage change in Young's modulus. Using the same relative change in the Young's modulus and in the thickness of the plate allows for a direct comparison of these modifications with the unperturbed model. The error in percent relative to the nominal model modes for the tapered plate and the change in Young's modulus are shown in Figure 2 for the first bending mode (Errgeo1b and Errstif1b) and the second stripe mode (Errgeo2s and Errstif2s). The bars represent the error in percent for each node point of the top surface of the plate excluding the nodes connected to the clamping block elements. This comparison shows that the young's modulus of the boundary blocks results in a much smaller error in the mode shapes for both modes. It also indicates that variations in geometry of the blade have an increasing impact as the frequency of the mode increases. Assumption III is based on the fact that all parts will have manufacturing tolerances to meet form, fit, and function requirements of the item. The tolerance bounds provide the definition of the variation for an acceptable part. Assumption IV implies that the variations in part geometry are not totally random in nature. These variations are related to the manufacturing process [8]. Manufacturing variations can be related to part positioning errors, tool sharpness changes, and

22
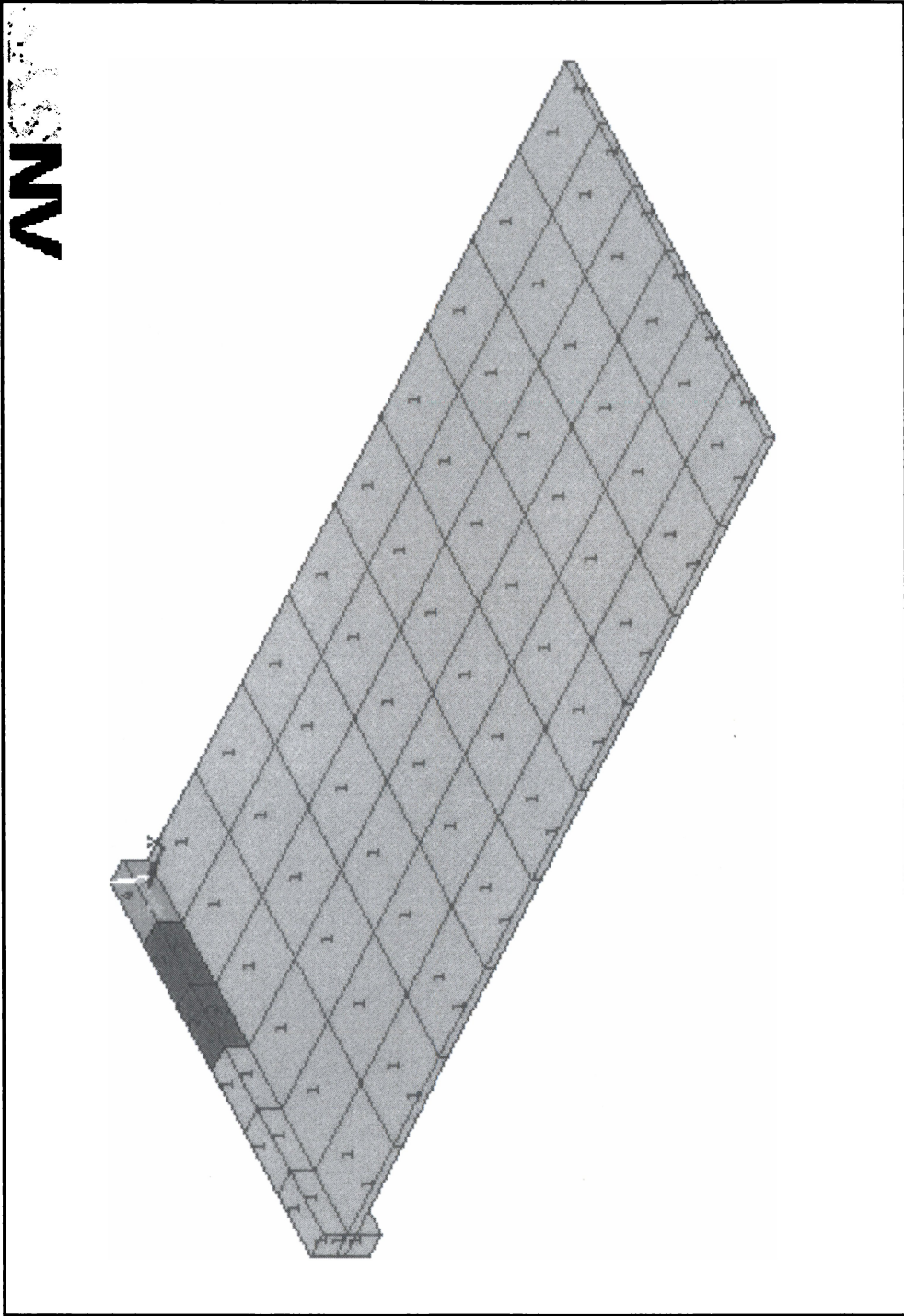
Figure 1. Model for variation of Young's modulus for the clamping elements

Errgeolb

Errstifflb
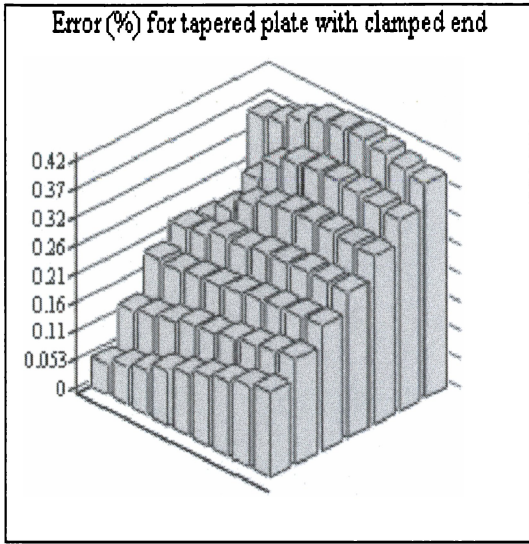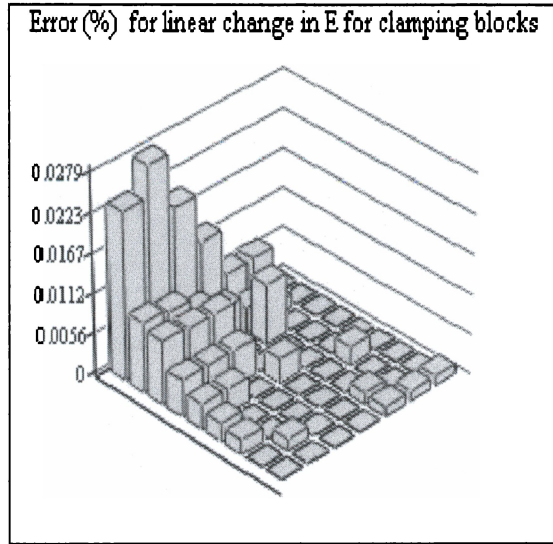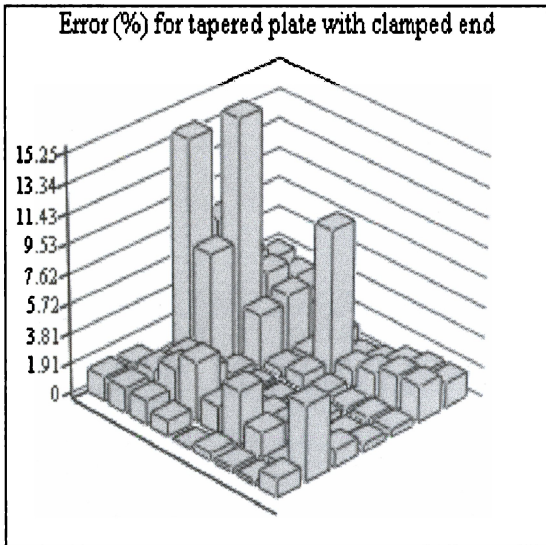
Errgeo2s
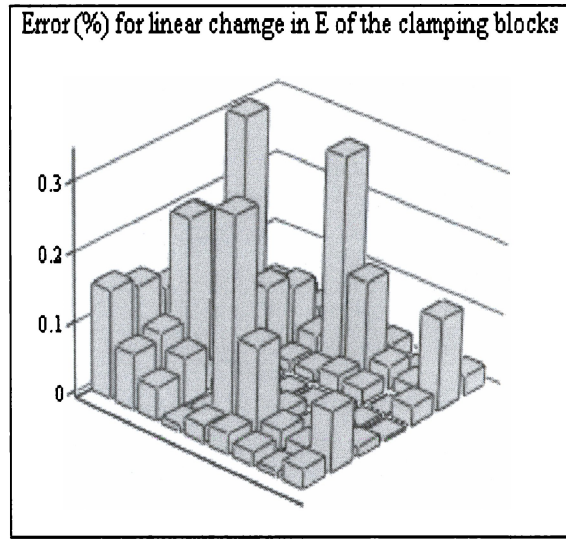
Errstiff2s

Figure 2. Comparison of error for variations in geometry versus variations in boundary stiffness

24

other factors. These assumptions provide the framework for developing an updating method that produces an updated geometry that improves the agreement between the test data and the model.

Rationale for Geometric Updating Method

The updating method must be able to compensate for arbitrary variations in the geometry. As noted in the discussion on Assumption IV, the geometry of parts will typically vary as a result of the manufacturing process within certain tolerances established a priori. The variations are independent of the nominal model, making sensitivity-based analysis of the model impractical for determining the characteristics of the geometry correction. The modal models generated by the finite element method produce positive definite system matrices with real eigenvalues and eigenvectors for the undamped case. The eigenvectors are uniquely determined up to a scalar multiple. The eigenvalues are not necessarily unique. The system matrices can be multiplied by a similarity transform resulting in the same set of eigenvalues with a new set of eigenvectors representing a completely different structure [30]. Based on these characteristics of the eigenvalue problem, an updating method should be based on the eigenvectors rather than the eigenvalues of the structure being evaluated. The eigenvectors are uniquely related up to a scalar multiple to the model matrices in physical space representing the structure being tested. Invoking Assumptions I and II and Assumption 1) used in the Engels method above, the discrepancy between the nominal model and test data can be attributed to variation of the test articles' geometry relative to the nominal model. Assumptions III and IV provide the additional constraints for the formulation of an updating method to adjust the geometry of the nominal model to reduce the error between the modes of the model and the modes of test article.

Formulation of Method

The proposed method uses a set of perturbed models with the nominal model as an n-dimensional perturbation space for estimating the geometric corrections. This approach was outlined by Dr. Kurt Nichol in meetings during May of 2001 [31]. This approach uses the set of models as a set of basis vectors. With the appropriate coefficients, the basis vectors can approximate the modes of the test article to any degree of accuracy with an increasing number of models or perhaps a set of perturbed models that is based on a priori knowledge of the expected geometric variations. The basic equation of the method is

$$\varphi_t^{\langle j \rangle} = \sum_{i=1}^{n} w_i \varphi_{\text{mod}\,i}^{\langle j \rangle} \tag{5}$$

where the superscript j is for the j$^{\text{th}}$ mode for the test and the models, $\varphi_t^{\langle j \rangle}$ is an m × 1 vector of the j$^{\text{th}}$ measured modal displacements, $\varphi_{\text{mod}\,i}^{\langle j \rangle}$ is an m × 1 vector of the j$^{\text{th}}$ mode vector of model at the measurement locations, and w_i are the scalar weight coefficients for the participation of the n models for the jth mode. A unique solution for the weights w_i is obtained for cases when n≤m. In cases where m>n, a unique solution can still be obtained by stacking the j test and model modes to form a least squares solution of the form

$$\begin{bmatrix} \Phi_{\text{mod}}^1 \\ \vdots \\ \Phi_{\text{mod}}^p \end{bmatrix} w = \begin{Bmatrix} \varphi_t^1 \\ \vdots \\ \varphi_t^p \end{Bmatrix} \tag{6}$$

26

where p is the total number of test modes, w is an n × 1 vector of the weighting coefficients, Φ^P_{mod} is an m × n matrix of the pth mode components at the m measurement locations for the n models, and φ^P_t is the pth measured mode. Stacking the p modes allows for cases where there are fewer measurement locations than models m<n while still providing a unique solution provided that p*m $\geq$ n. This formulation permits the use of all of the test modes that can be matched to the model. At this point, the coefficients represent the participation of all of the matched modes for each of the models in representing the test modes. As noted above, the eigenvectors are uniquely determined up to a constant for a specific system of mass and stiffness matrices. This property can be used to apply the coefficients w_i found using Equation (6) to determine the contribution of each model's geometry providing the updated model geometry that best approximates the test modes. The geometry updating equation is given by

$$x_u = \sum_{i=1}^{n} w_i x_{mi} \tag{7}$$

where x_u is the vector of the updated dofs for the model surfaces that were selected for updating, and x_{mi} are vectors of the dofs for the same surfaces of the basis models that have been selected for correcting the geometry of the nominal model. The updated dofs of the surfaces targeted for updating are combined with the unmodified dofs of the nominal model to produce the updated model geometry. The updated model can then be used for additional analysis as required.

An important benefit of this method, which should not be over looked, is that it

does not require the expansion of the mode shapes to obtain mode vectors that are of the

same order as the model. One method of expanding the test mode data to the full order

model modes is accomplish using the following equations [18]

$$\begin{bmatrix} K_{m,m} & K_{m,n-m} \\ K_{n-m,m} & K_{n-m,n-m} \end{bmatrix}\begin{bmatrix} \varphi_{t\,j} \\ \varphi_{\mathrm{mod}\,j} \end{bmatrix} - \omega_{t\,j}^{2}\begin{bmatrix} M_{m,m} & M_{m,n-m} \\ M_{n-m,m} & M_{n-m,n-m} \end{bmatrix}\begin{bmatrix} \varphi_{t\,j} \\ \varphi_{\mathrm{mod}\,j} \end{bmatrix} = \begin{bmatrix} \vec{0} \\ \vec{0} \end{bmatrix} \qquad (8)$$

where $\omega_{t\,j}^{2}$ is the measured eigenvalue for the jth mode, $\varphi_{t\,j}$ is an m × 1 vector of the

measured eigenvector components for jth mode, $\varphi_{\mathrm{mod}\,j}$ is an (n-m) × 1 vector of the

unmeasured eigenvector vector component, M and K are the n × n mass and stiffness

matrices that are partitioned into the measured coordinates m and the unmeasured

coordinate n-m. The full mode vector is obtained by joining the test mode vector

components with the unknown mode components that are found by rearranging the lower

portion of this equation to yield

$$\varphi_{\mathrm{mod}\,j} = -(-\omega_{t\,j}^{2} \cdot M_{n-m,n-m} + K_{n-m,n-m})^{-1} \cdot (-\omega_{t\,j}^{2} \cdot M_{n-m,m} + K_{n-m,m}) \cdot \varphi_{t\,j} \qquad (9)$$

Updating methods based on error localization requires the full mode vector

computed by this method or any other method. The process of expanding the modes

using the original model is done as a convenience. One concern with this approach is

how the measurement noise affects the calculated components. Another concern is that

the measurement points may not be coincident with the regions of the model that are

suspected to be in error. In this case, the mode vector dofs found using equation (9) in

the region where the model is suspected to be in error are in some way influenced by the

28

model that is being updated. An updating approach that does not rely on the expansion of the modes has the potential to avoid ill conditioning, which is a common problem.

Demonstration of the Method

In order to implement the method, several steps must be accomplished which will be outline as the method is demonstrated. All of the algorithms necessary to implement the method were programmed in Mathcad Professional 2000® worksheets. The method is first demonstrated by numerical simulation.

The simulated test articles are representative of three of the test articles used during the experimental validation of the method. The test articles are flat plates with nominal dimensions of 8.5 X 4.0 X 0.094 in inches. The simulated test plates have geometric variations of up to 0.003 inch depth below the top surface of the nominal model the point or the points of maximum deviation. The nodes for the perturbed top surface for the three simulated cases are shown in Figure 3. The first thirteen modes of the solution of the eigenvalue problem for the simulated test plates were used to simulate the test data. The test modes were determined using a modified finite element code from a Mathsoft® electronic book [32] that was extended to solve models with three dofs per node using an eight noded brick element with extra shape functions [29] (see Appendix A). The code was verified by solving the nominal plate and the simulated test plate P2 in ANSYS-ED® and the code shown in Appendix A. The same mesh density and material properties were used in both codes. Both codes produced the same mode frequencies and mode vectors. This validation was done to ensure that the element aspect ratios were acceptable. No error messages or warning were observed during the solve process in ANSYS-ED®. The finite element code worksheet also separates out the model dofs of

Simulated test plate P1

$$XYZ\left(TPMODES^{\langle 2\rangle},98,14\right)$$

Simulated test plate P2
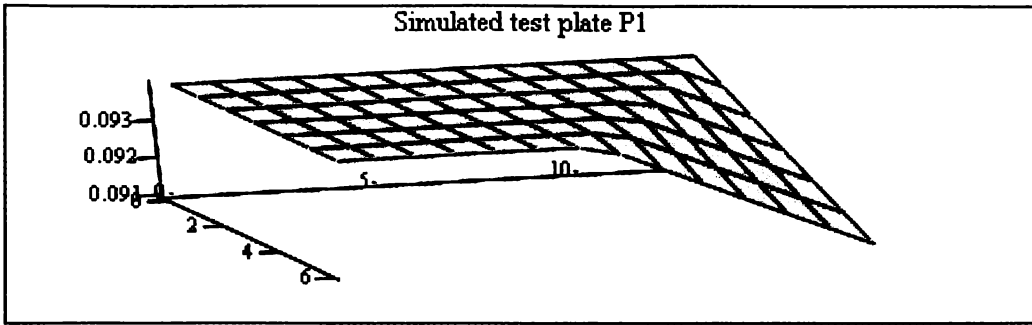
$$XYZ\left(TPMODES^{\langle 2\rangle},98,14\right)$$
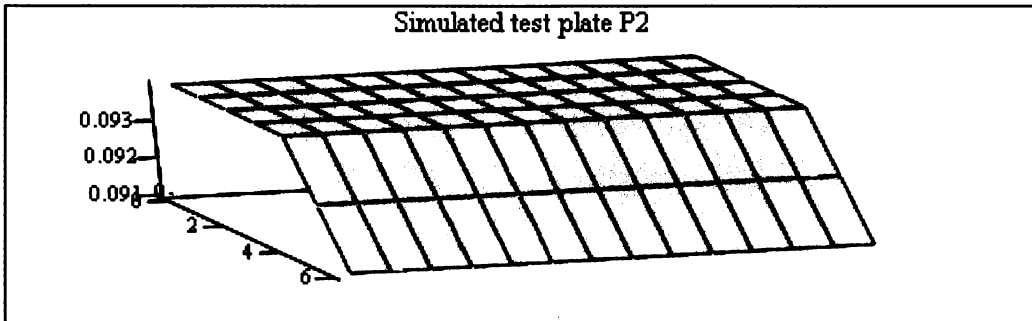
Simulated test plate P3
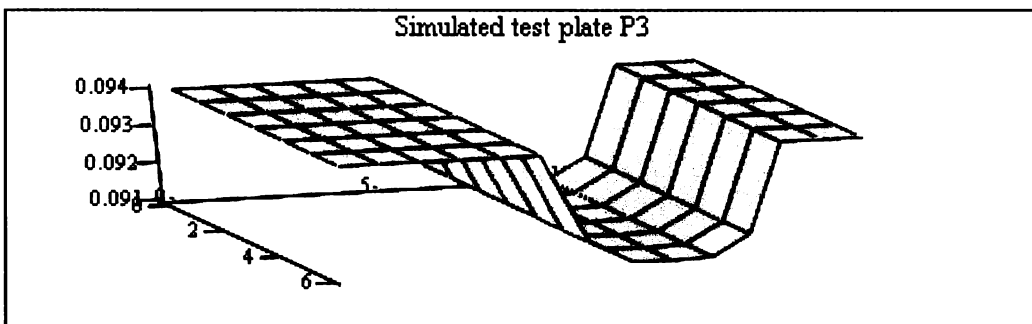
$$XYZ\left(TPMODES^{\langle 2\rangle},98,14\right)$$

Figure 3. Surface node plots of the perturbed surface for the three test cases

30

the perturbed surface for the specified modes. Two modes of the simulated test plate P2 top surface nodes are plotted in Figure 4.

The next step in the process was to develop a set of perturbed models. By definition the nominal model or design model already exists. The nominal model has the plate geometry defined above. The set of perturbed models must be able to approximate symmetric, antisymmetric, and asymmetric plate geometric variations. To do this, the set of models that form the perturbation space must include linear, non-linear, and trigonometric variations in geometry. A total of twenty-five models were used in this demonstration (See Figures 5 and B-1). Plots for the widthwise asymmetric functions are shown in Figure 5 and are not repeated in Figure B-1. All twenty-five models were solved using the worksheet shown in Appendix A. The nodes of top surface for the first thirteen mode vectors were saved to data files for use in the updating worksheet (See Appendix C). The coordinates normal to the surface are extracted from the mode vector and the normal coordinate at the fifteen simulated measurement points where found using spline interpolation.

The next step is to match the test and model modes for use in Equation (2). The modes are matched using the modal assurance criterion (MAC) [18]. The MAC is not an orthogonality check between the test modes and model modes since the mass matrix is not used. The MAC is given by

$$MAC_{j,k} = \frac{\left| \varphi_{t_j}^T \varphi_{m_k} \right|^2}{\left(\varphi_{m_k}^T \varphi_{m_k} \right) \left(\varphi_{t_j}^T \varphi_{t_j} \right)} \tag{10}$$

where φ_{t_j} is an m × 1 vector of the measured components of the jth test mode, $\varphi_{m_k}^T$ is an m × 1 vector of the kth mode of the model at the measurement locations, and $MAC_{j,k}$ is the
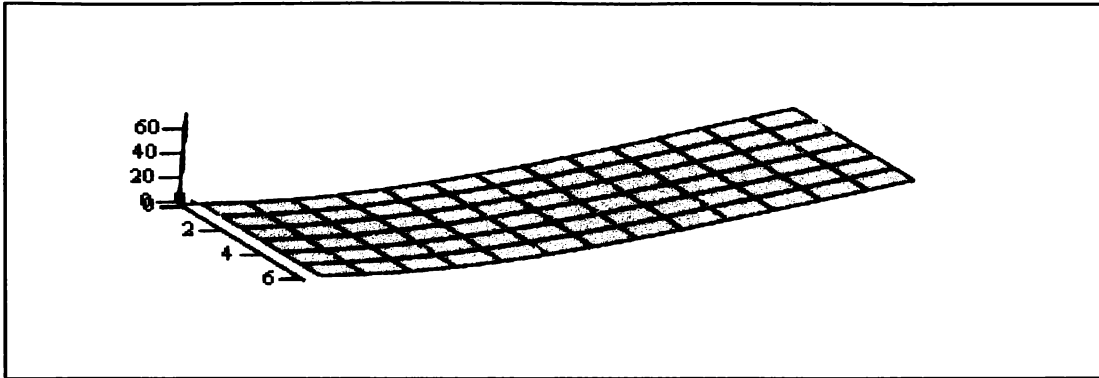
B1
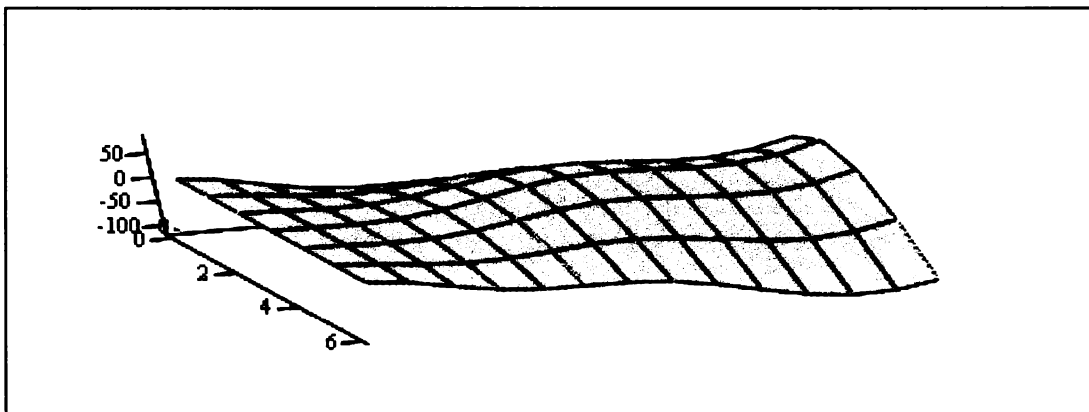
S2

Figure 4. First bending and second stripe modes shown for the top surface nodes of the simulated plate P2

32
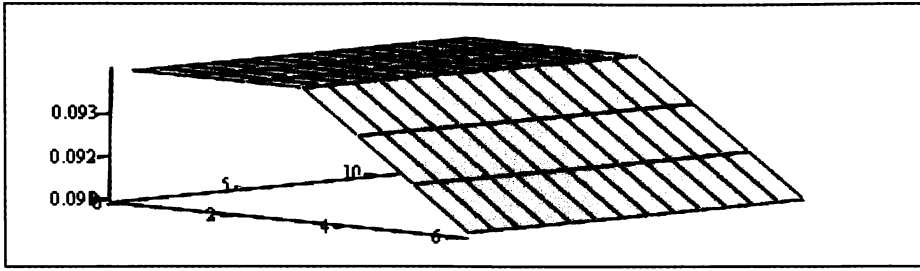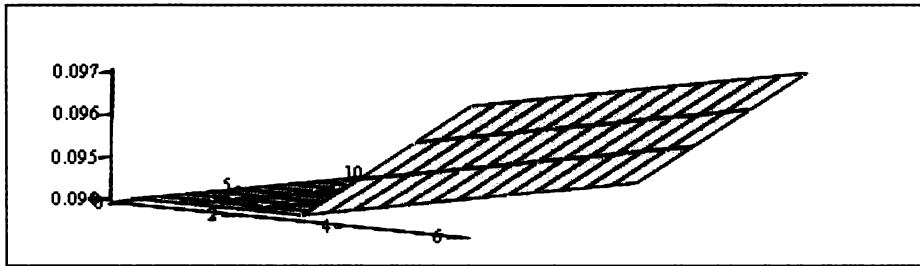
plotgeo(Nodpa1w)

plotgeo(Nodpa2w)
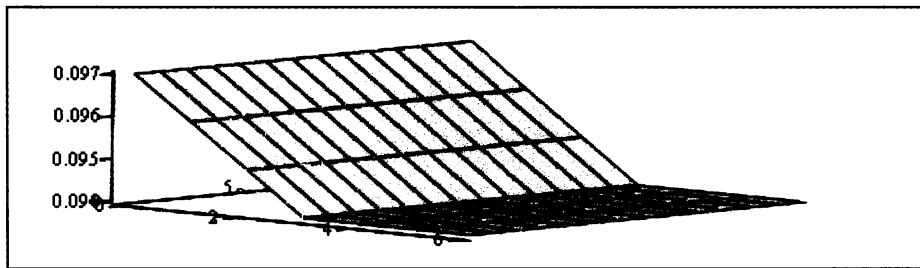
plotgeo(Nodpa3w)
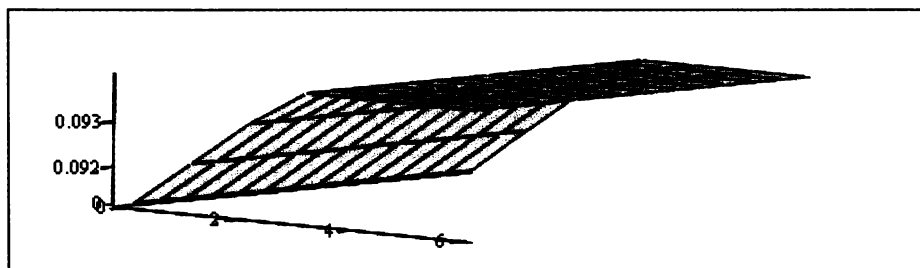
plotgeo(Nodpa4w)

Figure 5. Asymmetric geometric perturbation functions for the top surface nodes in the width direction

(j,k) coefficient of the MAC matrix. When the modes are strongly correlated, the $MAC_{j,k}$ coefficient will be close to unity and the other components in the corresponding j^{th} row and k^{th} column will be near zero. Typically, MAC values above 0.85 for a pair of modes are considered as well correlated modes. There is no need to scale the test modes to the model modes. The ease of application of this method makes it a popular tool in matching test and analytical modes for further analysis. The MAC is a 13×13 matrix for the numerical simulations. All twenty-five models were matched with the simulated test plates. The modes for the simulated test plates and the model set were placed in order from the first mode through the thirteenth mode.

With the test and model modes paired, the model modes are ready to be scaled to the test modes for use in Equation (1). The scaling is accomplished using the modal scale factor [18] given by

$$ msf = \frac{\varphi_{t_i}^T \varphi_{m_i}}{\varphi_{m_i}^T \varphi_{m_i}} \tag{11} $$

where φ_{t_i} is the ith test mode vector and φ_{m_i} is the ith model mode vector. The modal scale factor does not require that the test and model modes to have the same phase. However, the test and model modes must be in phase to determine the weighting coefficients, w_i. An additional check is required to ensure that the modes are in phase. This is accomplish by using the following logic

$$ \text{If} \mid \varphi_{t_i} - \varphi_{m_i} \mid > \mid \varphi_{t_i} \mid \text{Then } \varphi_{cp_i} = -\varphi_{m_i} \tag{12} $$

$$ \varphi_{cp_i} = \varphi_{m_i} \text{ Otherwise} $$

34

where φ_{t_i} is ith component of the test mode vector whose phase is being matched, φ_{m_i} is the ith component of the model mode whose phase is being adjusted based on the condition, and φ_{cp_i} is the ith component of the phase corrected model mode vectors to be used in Equation (6).

The next step is to solve for the weighting coefficients, wi, for the modal basis vectors of Equation (6). Then these coefficients are used to estimate the updated model geometry using the model geometry basis vectors in Equation (7). The vectors of Equation (7) are the normal dof of the surface nodes targeted for modification. The Mathcad program for the procedure outlined above is shown in Appendix C. The updated geometry and the simulated test plate geometry for the demonstration using simulated test plate P2 are shown in Figure 6. The solid surface is the simulated test plate P2 and the transparent surface is the updated geometry. A direct comparison between the simulated test plate geometry and the updated geometry can be accomplished. Three cases are presented showing the effects of increasing noise on the accuracy of the estimated geometry. As the noise increases, the approximation of the geometry degrades. An assessment of the error caused by adding noise to the test eigenvectors is accomplished by comparing the error between the updated surface and the simulated test plate at each node for plate P2. In all cases, the total percent error in the geometry was within the bounds of the noise added to the eigenvectors. The results for P2 are shown in Table 1. This summary shows the maximum and minimum within the bounds of the simulated noise. Several trials were conducted at each noise level to observe the characteristics of the solution under the influence of noise. The noise can result in a plate

Simulated noise free eigenvectors
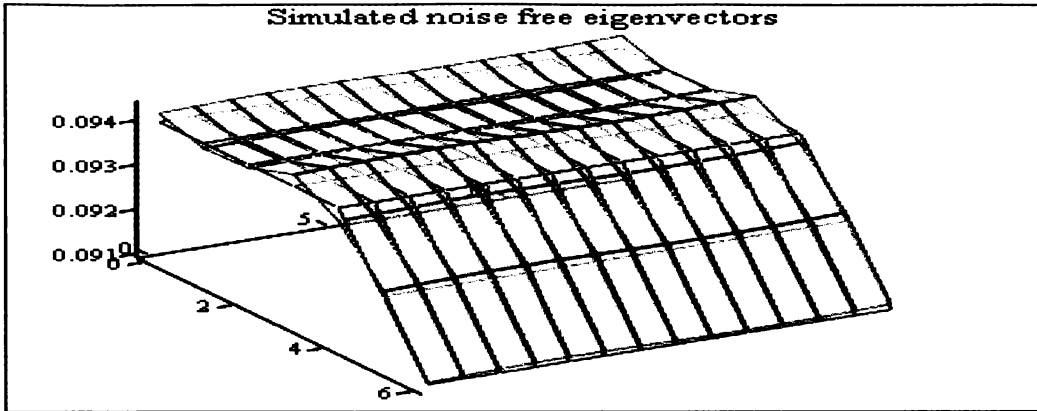
$$XYZ\left(\mathrm{nfr}^{\langle 2 \rangle},98,14\right),XYZ\left(\mathrm{stp}^{\langle 2 \rangle},98,14\right)$$

plate p2 +/- 2% noise

Simulated plate top surface (typical all plots)

Updated top surface (typical all plots)
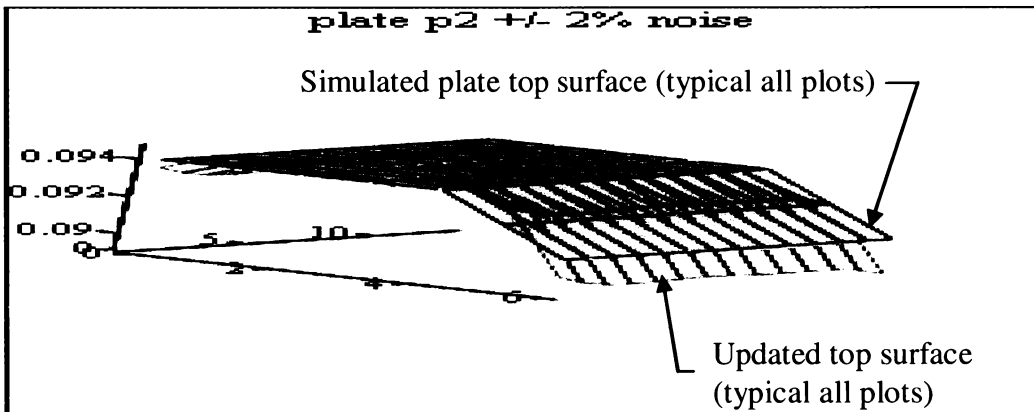
$$Gwl,XYZ\left(\mathrm{TPMODES}^{\langle 2 \rangle},98,14\right)$$
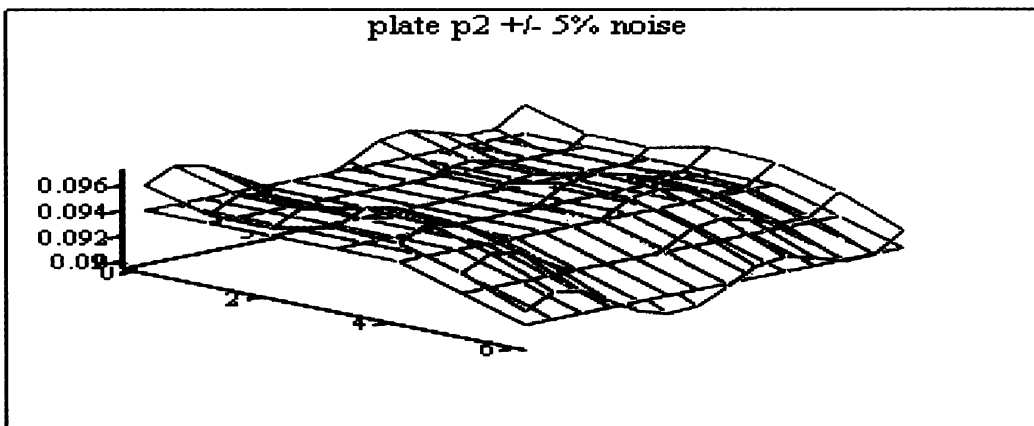
plate p2 +/- 5% noise

$$Gwl,XYZ\left(\mathrm{TPMODES}^{\langle 2 \rangle},98,14\right)$$

Figure 6. Comparison of updated surface nodes for P2 showing the effects of noise

36

Table 1. Summary of geometric error for Plate P2 showing the influence of increasing noise

Case	Eigenvector Uniform noise Percent	Minimum Relative Error Percent	Maximum Relative Error Percent	Total Error Band Percent
1	Noise free	-0.051	0.549	0.60
2	+/- 2	-0.38	1.49	1.87
3	+/- 5	-1.493	3.299	4.792

that is biased either thicker or thinner or ones where the transcendental basis functions cause oscillations about the simulated plate geometry. These effects are amplified with increasing noise levels. This highlights the importance of having instrumentation that has high measurement accuracy and excellent signal-to-noise performance.

Additional comparisons were made for plates P1 and P3. The results are similar to the result for P2. The plots comparing the updated geometry to the simulated test plate geometry are shown in Figure 7 and in Figure 8, respectively. Table 2 shows a comparison of the node-by-node relative error for plates P1 and P3, respectively. The relative error slightly exceeds the noise bounds for these cases. In both cases several trials were conducted. The results were bounded. However, noise levels at or above 5 percent resulted in errors that would not be acceptable. This is true especially when the noise caused the updated nodes to be either all above or all below the simulated test plate surface.

plate p1 noise free

0.094
0.093
0.092
0.09

2
4
6

$Gw1,XYZ(TPMODES^{(2)},98,14)$

plate p1 +/- 2% noise

Updated top surface (typical all plots)

0.095
0.094
0.093
0.092
0.09

2
4
6

Simulated plate surface (typical all plots)

$Gw1,XYZ(TPMODES^{(2)},98,14)$

plate p1 +/- 5% noise

0.098
0.096
0.094
0.092
0

2
4
6
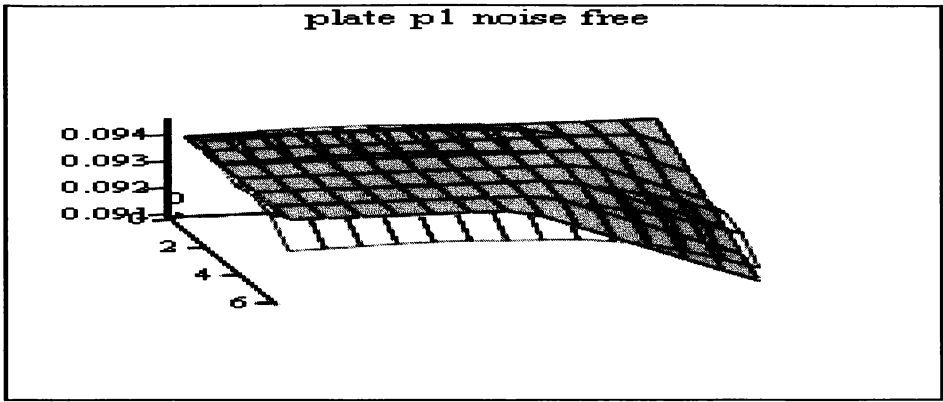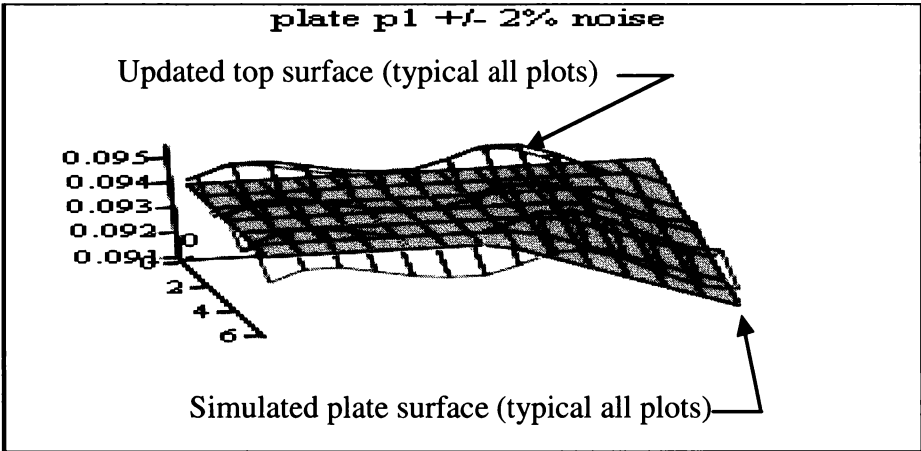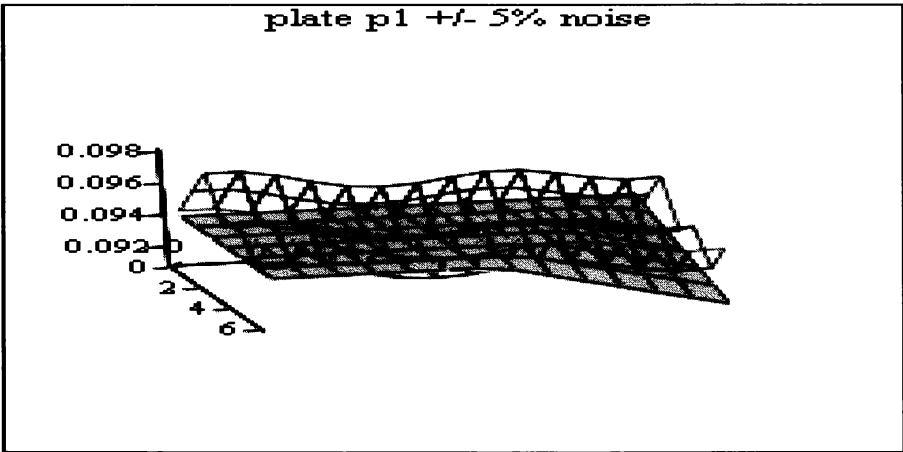
$Gw1,XYZ(TPMODES^{(2)},98,14)$

Figure 7. Comparison of updated geometry for P1 showing the effects of noise

38

plate p3 noise free

$\mathrm{Gwl,XYZ\left(TPMODES^{\langle 2\rangle},98,14\right)}$

plate p3 noise +/- 2%

Updated top surface (typical all plots)

Simulated test plate (typical)

$\mathrm{Gwl,XYZ\left(TPMODES^{\langle 2\rangle},98,14\right)}$

plate p3 +/- 5% noise
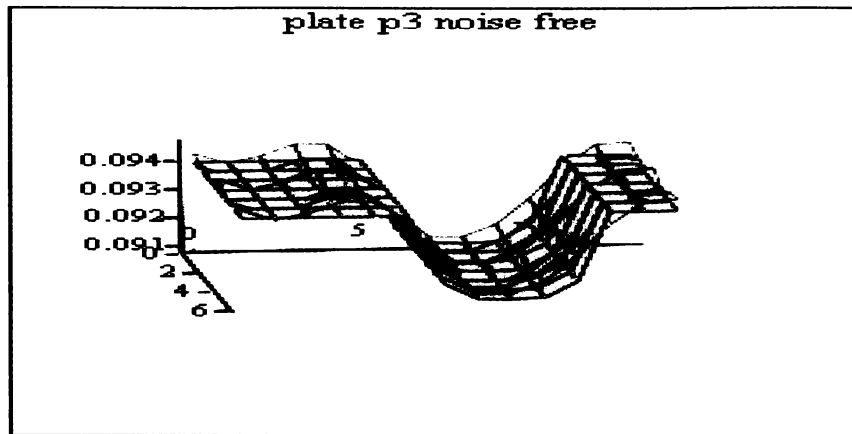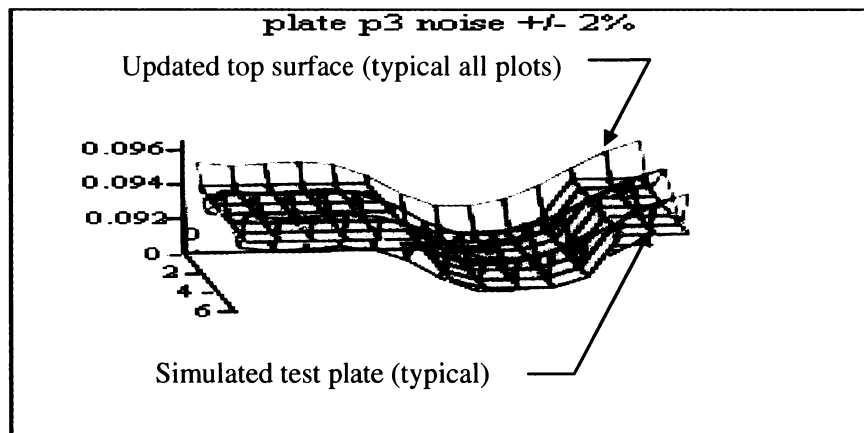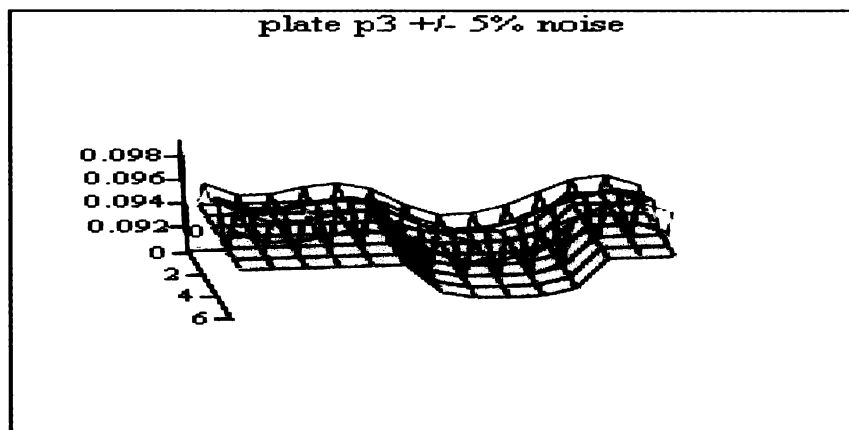
$\mathrm{Gwl,XYZ\left(TPMODES^{\langle 2\rangle},98,14\right)}$

Figure 8. Comparison of Updated geometry for P3 showing the effects of noise

Table 2. Summary of geometric errors for plates P1 and P3 showing the influence of increasing noise

Case	Eigenvector Uniform noise Percent	Minimum Relative Error Percent	Maximum Relative Error Percent	Total Error Band Percent
P1-1	Noise free	-1.39	0.85	2.24
P1-2	+/- 2	-1.28	1.49	2.77
P1-3	+/- 5	-1.43	4.29	5.72
P3-1	Noise free	-0.79	1.11	1.48
P3-2	+/- 2	-2.04	2.56	4.60
P3-3	+/- 5	-1.92	6.43	8.35

In general, the geometry of the structure or structures may not be readily available for measurement. A performance measure is needed that assess whether the updated model improves the prediction of the test results over the original model. The number of test modes available is far fewer than the number of modes predicted by the finite element model. The test modes form an orthogonal subspace for the structure under test.

This subspace can be compared to the model subspace for the paired modes. Eigenvectors of the order of the finite element model are available for comparison with the test modes. This represents an approximation of the true structure. A metric that can be used to evaluate the performance is given by the 2-norm of the difference between the test eigenvector components and the model predictions at the test measurement locations given by

40

$$ER_{abs} = \left\| \Phi_t - \Phi_m \right\| \tag{13}$$

where Φ_t is a 15×13 matrix of the simulated test modes for all three cases above and

Φ_m is a 15×13 matrix of the model mode vectors at the simulated measurement points.

This formulation represents an absolute error between the test modal subspace and the

modal subspace of the updated model. A relative error can be obtained by

$$ER_{rel} = \frac{ER_{abs}}{\left\| \Phi_t \right\|} \tag{14}$$

An assessment of the updated model in comparison with the nominal or design model can

be made by comparing the improvement of the relative error. These are shown in Table 3

for the simulated test cases of plates P1, P2 and P3. The noise free cases have the best

performance using this metric. The metric also indicates the degradation in performance

with increasing noise. The performance of test plate P1 indicates that the set of models is

not adequate for reducing the error in the model geometry. This is also true for case (1),

which is noise free. This metric provides a consistent method for assessing the degree of

improvement of the updated model in representing the test article. The performance

summarized in Table 3 also indicates that the metric will identify situations where no

improvement is possible or that the test data needs additional analysis for errors.

An assessment of the participation of the models for the simulation cases is

needed to evaluate adequacy of the model set used for this study. This check is necessary

to determine if the updated model is represented by or can be represented by a smaller

number of models. The evaluation is accomplished using the noise free simulation cases

for all three test plates. The participation of the weighting coefficients for the model set

Table 3. Summary of 2-norm relative error metric for simulated test plates

Error metric	P1 Relative error Percent	P2 Relative error Percent P2	P3 Relative error Percent
Error - nominal model	1.56	2.77	2.74
Error - noise free updated model	1.51	0.21	0.31
Error - +/-2% uniform noise updated model	1.59	1.29	1.53
Error - +/-5% uniform noise updated model	2.58	8.54	4.68
Error - +/-5% uniform noise updated model	2.58	8.54	4.68

is shown in Figure 9. The weight category names in Figure 9 are taken from the

nomenclature used in Figures 5 and B-1. For example, the first plot in Figure B-1 is the

top surface of the nominal model, xyz_{nom}, which corresponds with weight, wnom in

Figure 9. The plot shows the relative contribution of all twenty-five perturbed models. A

larger number of models show significant participation for plate P1 relative the model

with the maximum weight, wg1xy. This is due in part to the fact that this plate is not

symmetric with respect to the either axis. Also there is no model in the set that

approximates this shape. The performance of this model with respect to the relative error

for the geometry and the 2-norm error metric suggest that additional models are needed to

estimate the perturbed geometry of the top surface of P1. Plate P2 is very close in shape

to the first surface perturbation function shown in Figure 5. This results in a high

weighting of this model with the value of the weight coefficient, wp1aw of approximately

0.91. However, the participation of the other models is important in improving the

prediction of the surface even though the magnitudes of the weights are small. Models

42
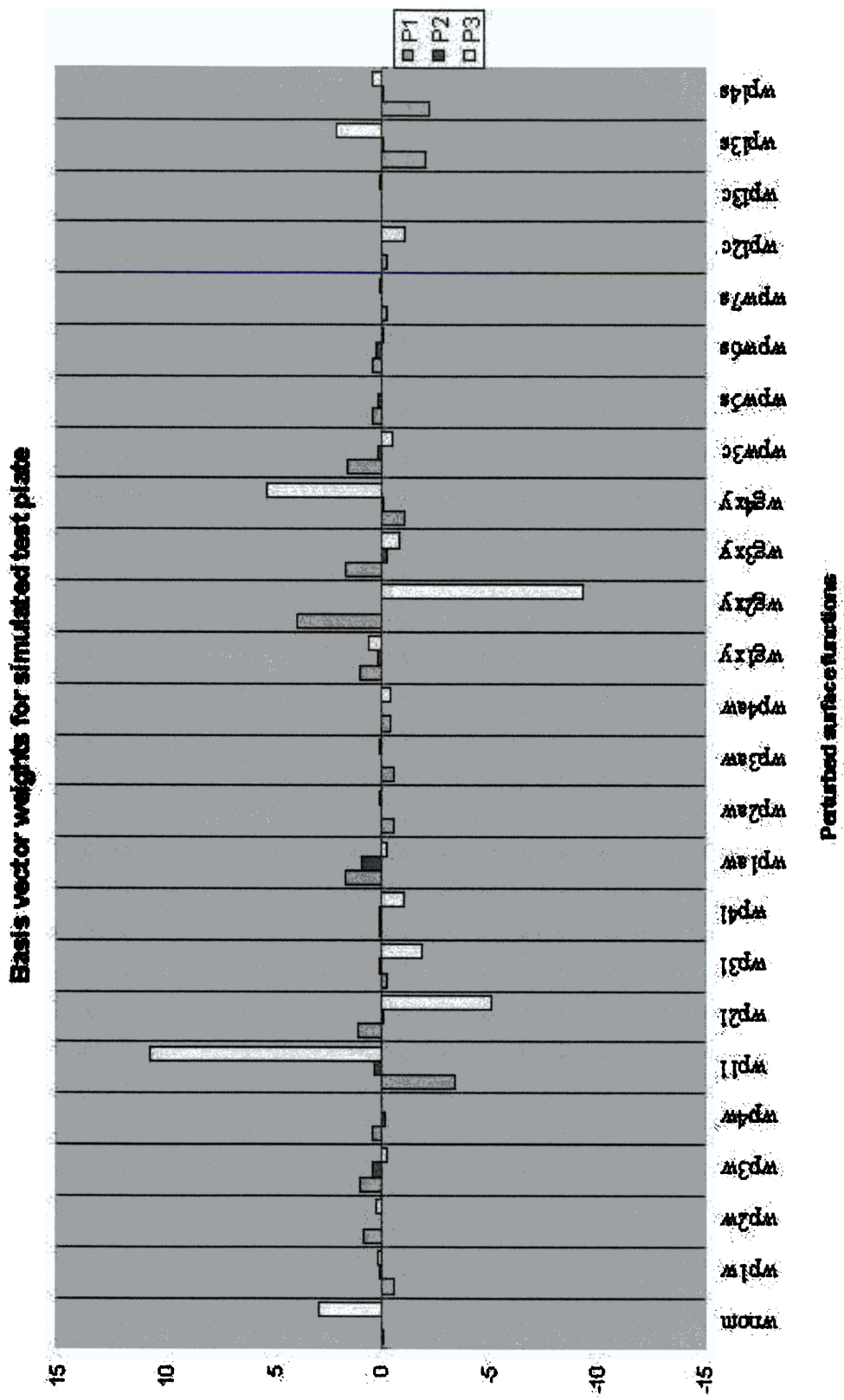
Figure 9. Plot of calculated basis vector weights for the simulated plates

that represent lengthwise geometric perturbations dominate the weighting coefficient participation of the model set for plate P3. This is expected given the shape of the top surface of P3. The participation of the nominal model does not dominate the response for any of the simulated cases.

Next the sensitivity of the updating method to the number of measurement points is considered. The effect of using fewer measurement points is evaluated using the total error band on the geometry. The influence of noise was not considered in the sensitivity analysis. The simulation trials carried out above used fifteen simulated measurements points shown in Figure 10. Different combinations of points in the lengthwise and widthwise direction where used to assess the sensitivity of the method to the number of measurement points. The first case shown in Table 4 is the baseline case that includes all fifteen points. The remaining cases include: 1.) Twelve points closest to the free end; 2) nine points closest to the free end; 3.) Six points closest to the free end; 4.) Four edge and four centerline points closest to the free end; 5.) Three edge and three centerline points closest to the free end; and 6.) Two edge and two centerline points closest to the free end. The total error increased for all three plates as the number of points decreased. Plate P1 is the worst performing plate of the three. It showed the largest increase in the error with the decreasing number of measurement points. The total error increase as the number of points decreased can be attributed to the influence of the geometry on the higher order modes in the data set. The influence of geometry on the higher modes was documented by Yang and Griffin [5] and can also be observed in comparing the plots of the first bending mode and the second stripe mode of the error for the tapered plate shown in Figure 2. The method is less sensitive to a reduction in the number of measurement point

44
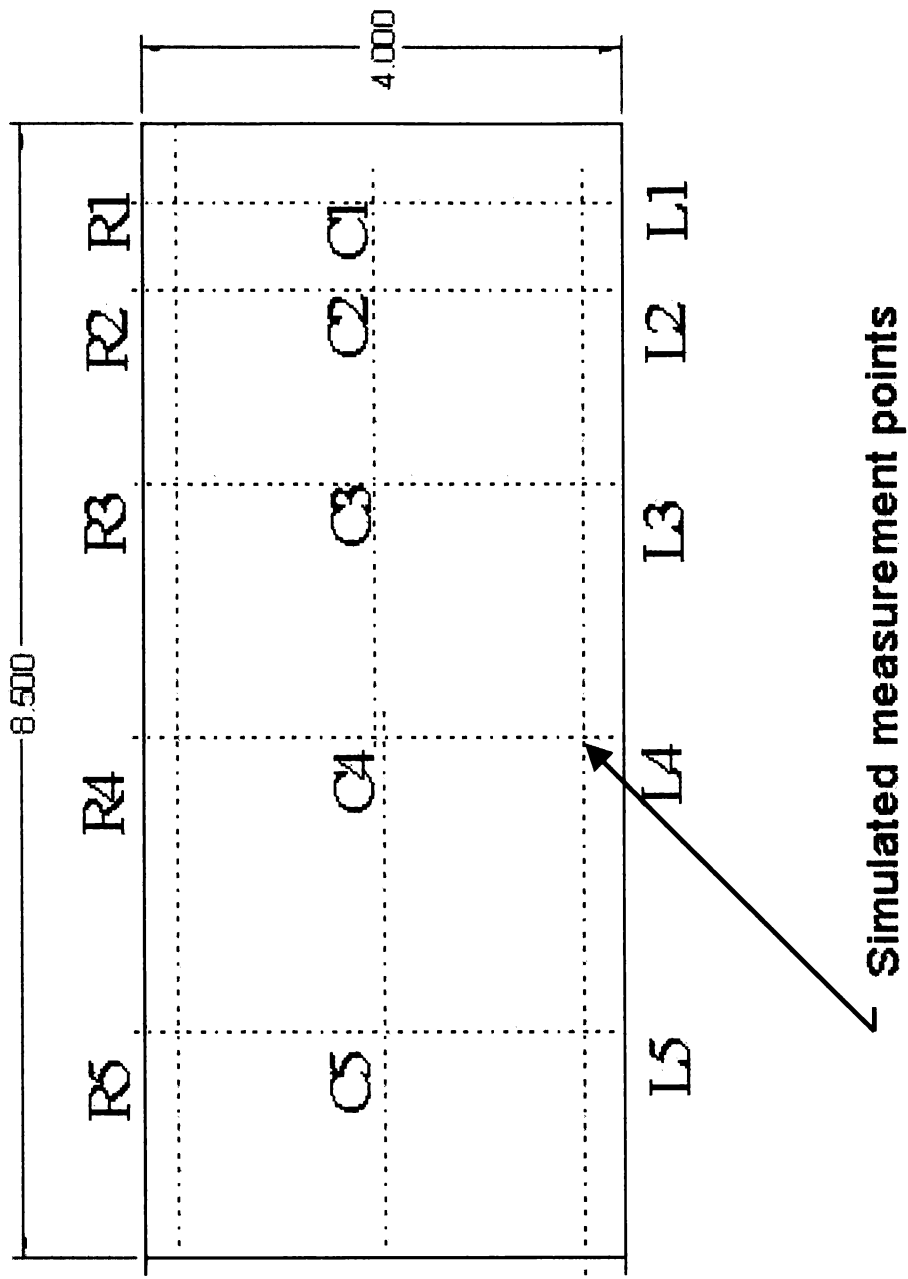
Figure 10 Simulated measurement points for sensitivity analysis

Table 4. Summary of geometric error sensitivity to the number of measurement points

Case	P1			P2			P3		
no. of data pts.	min percent	max percent	Total error percent	min percent	max percent	Total error percent	min percent	max percent	Total error percent
(1) 15 baseline	-0.99	1.319	2.309	-0.119	0.427	0.546	-0.568	0.913	1.481
(2) 12 closest to free end	-1.368	1.33	2.688	-0.164	0.784	0.948	-0.789	0.909	1.698
(3) 9 closest to free end	-1.899	1.34	3.339	-0.291	0.796	1.087	-0.866	1.366	2.032
(4) 6 closest to free end	-1.481	1.683	3.164	-1.209	3.393	4.602	-3.835	2.662	6.497
(5) 8 lengthwise (edge/C.L)	-1.331	2.818	4.149	-0.115	0.778	0.893	-0.747	1.096	1.843
(6) 6 lengthwise (edge/C.L)	-1.48	2.37	3.85	-0.187	0.774	0.961	-0.484	1.767	2.251
(7) 4 lengthwise (edge/C.L)	-3.608	18.36	21.966	-0.457	0.833	1.29	-1.285	3.219	4.494

46

in the lengthwise direction. This can be attributed to the fact that the higher mode shapes can be better approximated using the lengthwise points. Increasing the number of lengthwise points can compensate for errors in curvature associated with the higher modes. The better performance of lengthwise measurement points can be seen by comparing cases (4) and (6) from Table 4. Next the method will be evaluated with test data from four perturbed plates and one nominal plate.

5. Experimental Validation of Geometric Updating Using Multiple Perturbed Models

Test Plates

The test plates used to validate the updating method presented in Chapter 4 were based on a plate designed and reported by Nichol [16], denoted as plate number 4. This plate was selected because it has vibratory model characteristics similar to turbo machinery airfoils and up to ten modes of vibration in the frequency range used for the experimental phase of this research. Figure 11 shows the nominal plate used in the present study, which shall be referred to as R2. The intersections of scribe lines put on the plates were used to identify the measurement locations on all five plates. The scribe lines were placed on the opposite side of the perturbed surfaces for plates P1 through P4. The four perturbed plates P1 through P4 are shown in Figure 12. The plates were machined and then hand blended to produce the final perturbations. Limitations in time and financial resources prevented detailed measurements of the plates after machining. All plates were fabricated from a single sheet of Aluminum 6061-T6, ASTM B209. The material properties used for all calculations can be found in the material properties library of ANSYS-ED®. The material properties are; Young's Modulus, E= 10587920 psi $(7.3 \times 10^4$ Mpa); Poisson's ratio v=0.33; and density, ρ=2.526768x10^{-4} lbm/in3 (2700 kg/m). the nominal plate thickness is 0.94 in (2.388mm).

Test Apparatus

The test apparatus included a Ling Electronics Shaker (model no. B335), a Data Physics Corporation Vibration controller (model no. DP550win), and a Polytec Laser

4.000

8.500

R5 R4 R3 R2 R1

C5 C4 C3 C2 C1

L5 L4 L3 L2 L1

Measurement points (typ.)
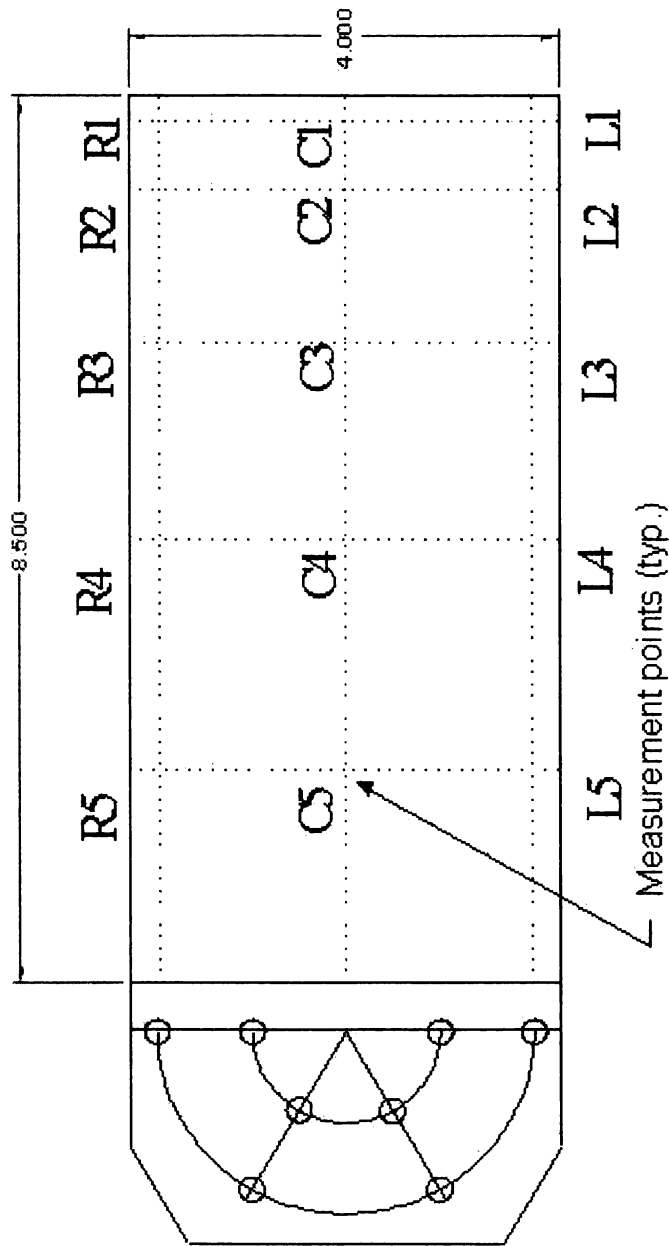
PN: R2
Material: 6061-T6 ASTM B206
Nominal thickness: 0.094 in.

Figure 11. Test plate R2 showing the measurement locations
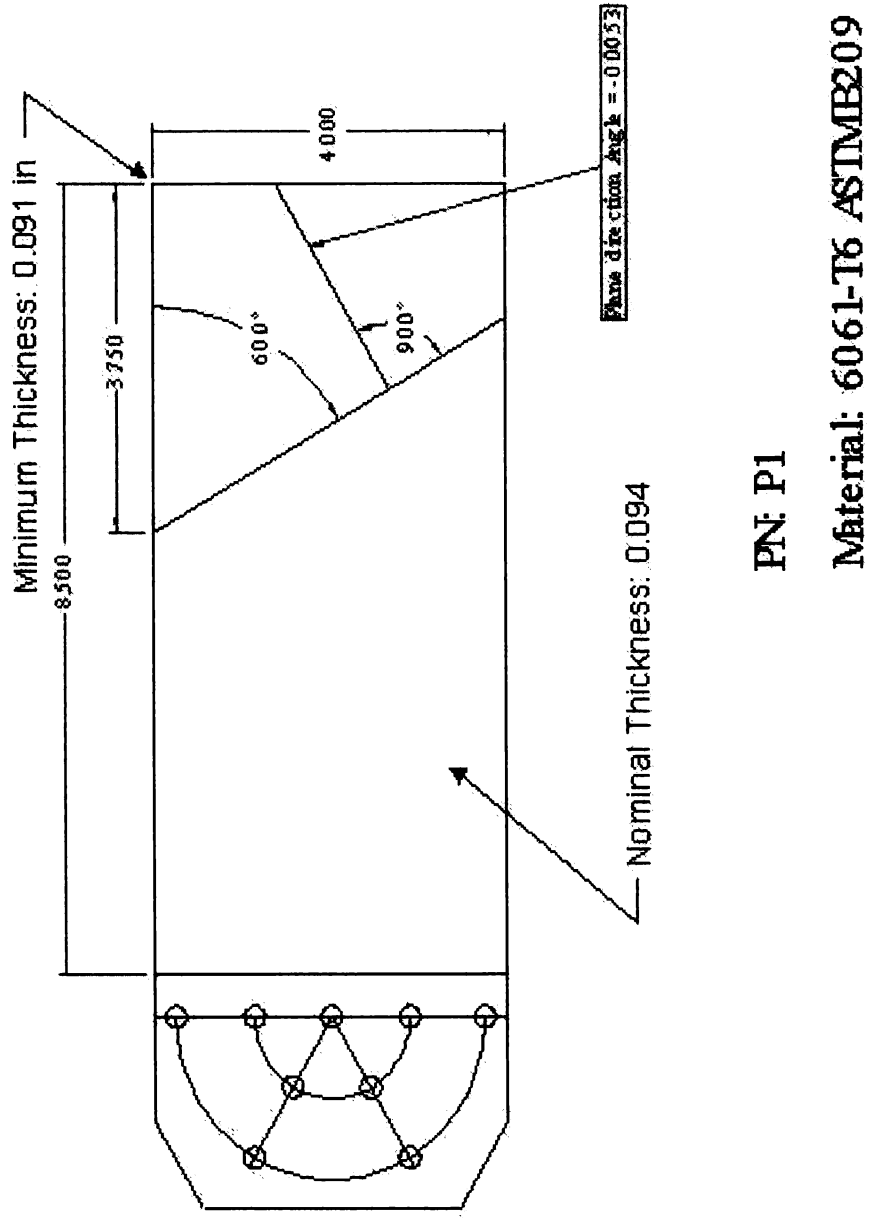
Figure 12. Perturbed test plates
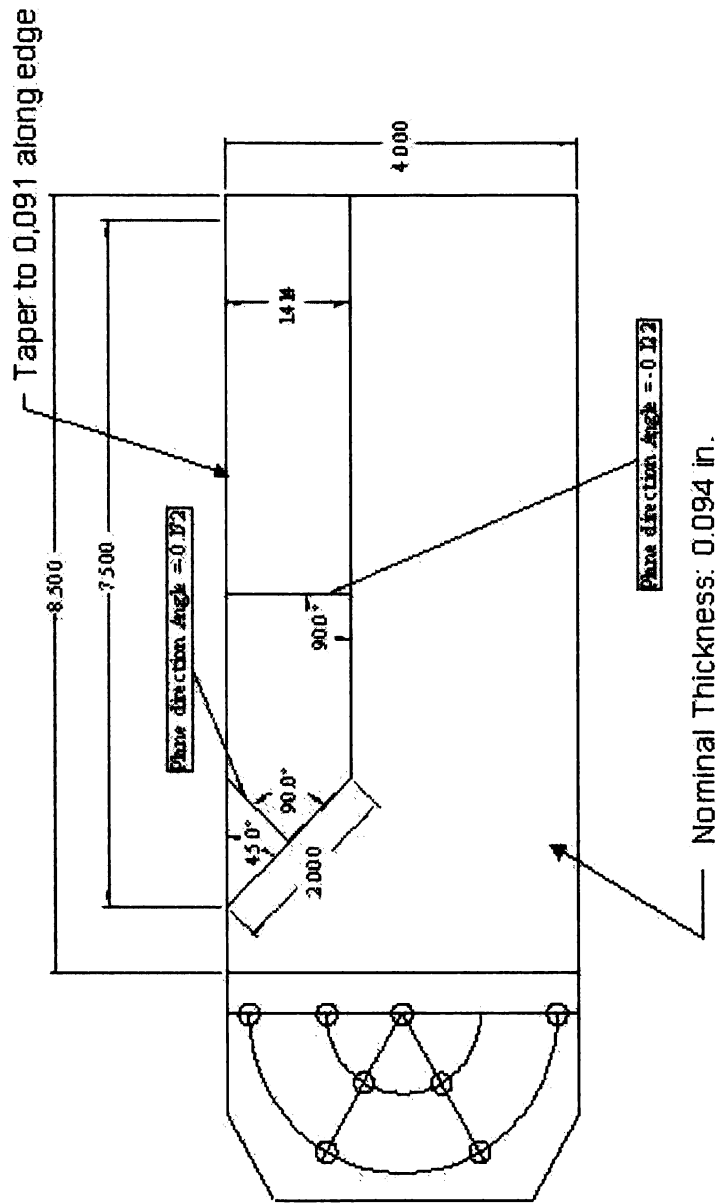
Taper to 0.091 along edge

8.500

7.500

4.000

1.4 in

Taper direction. Angle = 0.172

90.0°

45.0°

90.0°

2.000

900.0°

Plane direction. Angle = -0.112

Nominal Thickness: 0.094 in.

PN P2
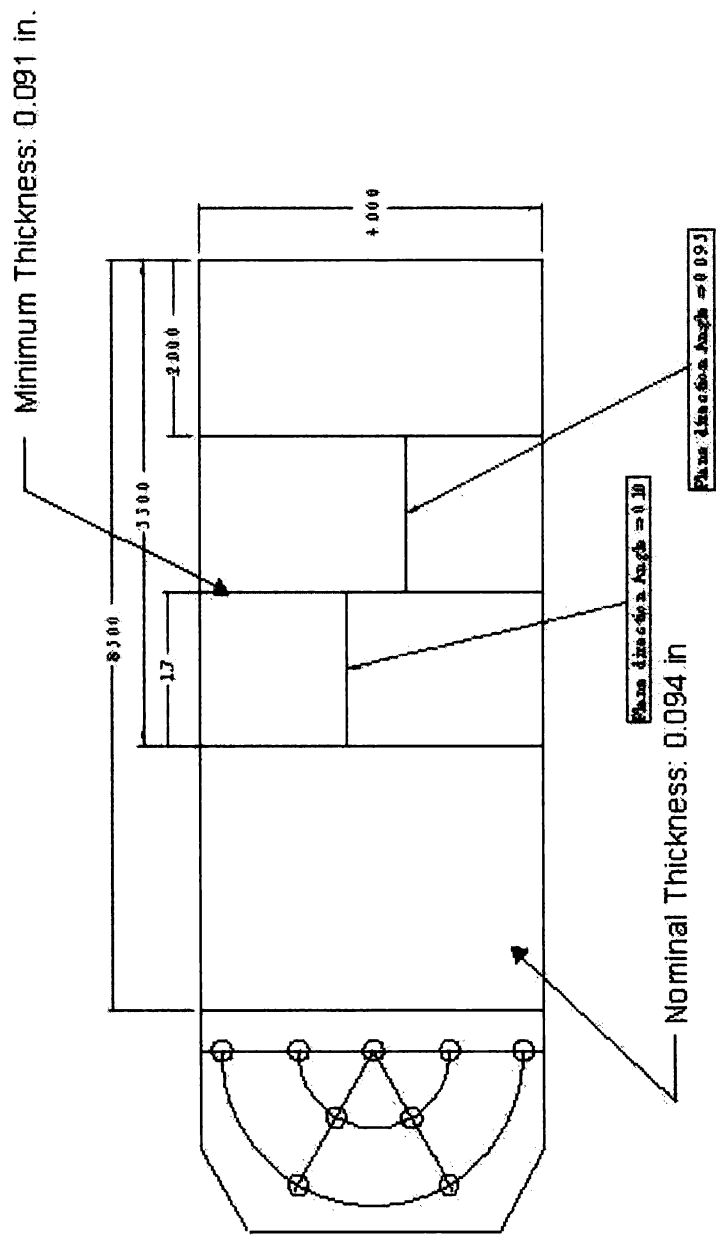
Materials: 6061-T6 ASTMB209

Figure 12. Perturbed test plates (continued)

Figure 12. Perturbed test plates (continued)

Figure 12. Perturbed test plates (continued)

Vibrometer (model no. OFV303). Figure 13 shows a diagram of the test setup. The Ling shaker is capable of producing up to 150 G maximum acceleration, a maximum peak-to-peak velocity of 70 in/sec, a maximum peak-to-peak displacement of 1 inch, and has a frequency range of 10 to 3000 Hz. The shaker has a resonant frequency of 2350 Hz. The vibration controller is a PC based system that was configured with a channel for closed loop control of the shaker and two measurement channels. The closed loop control of the shaker ensures that the same acceleration profile was applied during each test run. The controller data acquisition channels included the table accelerometer for control, an accelerometer on the fixture, and the velocity signal from the laser vibrometer. The Data Physics system stored the data in engineering units for the velocity and the displacement data. The data was stored in text files as peak values at the corresponding frequency. The frequency resolution was approximately 1 Hz from 10 Hz to 2000 Hz. The laser vibrometer has an excellent signal to noise ratio. Measurement resolution is 1 μm/sec or $3.94*10^{-5}$ in/sec for the measurement range 125mm/sec/Volt or 4.92 in/sec/Volt. The signal output voltage was limited to +/- 2.5 Volts to accommodate the data system used for the follow on test. Using the following formula, the displacement resolution, d, is approximately $8*10^{-14}$ m or approximately $3.0*10^{-9}$ in, where

$$d = \frac{v}{2\pi f} ,$$
(14)

v is the velocity, and f is the frequency. The displacement resolution increases with frequency.

Test Methodology

The test program for this research effort was accomplished with the shaker table described above. The initial testing was conducted using reference plate R1, which is

54
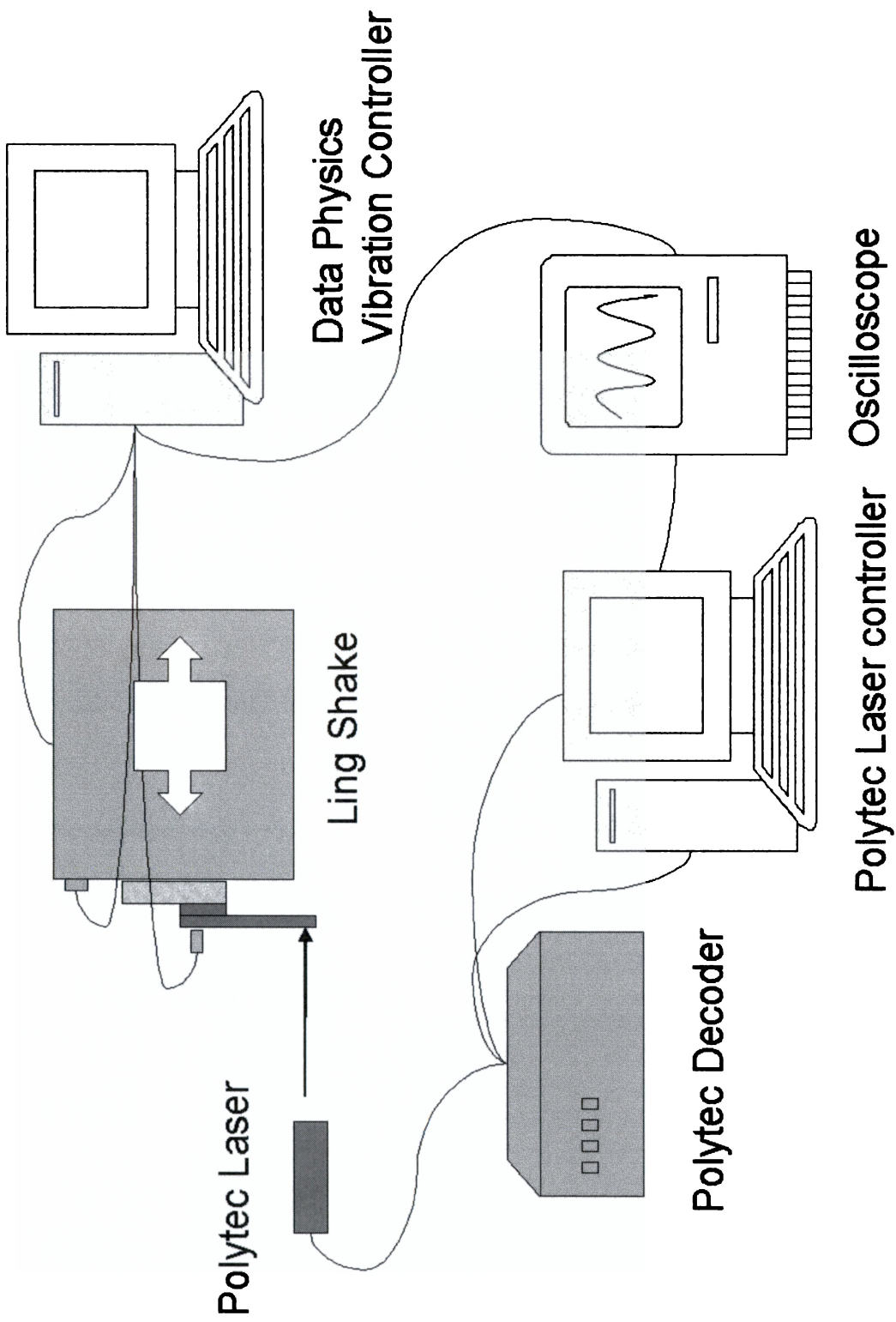
Figure 13. Diagram of test setup

identical to R2, with the exception that R1 had three holes drilled for the mounting of an accelerometer. The accelerometer was mounted in the center position during testing with test plate R1 (See Figure 14). Testing with R1 was done to assess the adapter plate that mounts the test plate to the shaker, to ensure that it did not have any resonance in the frequency range for the test. Ensuring that the adapter plate did not have a resonance in the operating range was essential since the adapter plate and test fixture are not part of the model. The test plate and fixture are bolted to the adapter plate. The plates were modeled with clamped boundary conditions at the fixture. The plate tests were conducted by sweeping the shaker table through a frequency range of 10 Hz to 2000 Hz with an acceleration profile shown in Figure 15 for all five of the test plates. A different acceleration profile was used for test plate R1 shown installed in Figure 14. The profile for R1 required substantially higher accelerations because of the damping caused the attachment of an accelerometer and its cabling (see Figure 14). The damping was high enough that no vibratory modes were observed over 1000 Hz. In contrast, the test plates R2 and P1 through P4 had five modes above 1000 Hz. Measurements were made at the fifteen points where the scribe lines intersected on all of the test plates (see Figure 11). The Laser Vibrometer was aimed at each of these points. The frequency was swept through the measure range fifteen times for each plate to obtain the test mode shape data. The data was saved to test file for post processing and plotting.
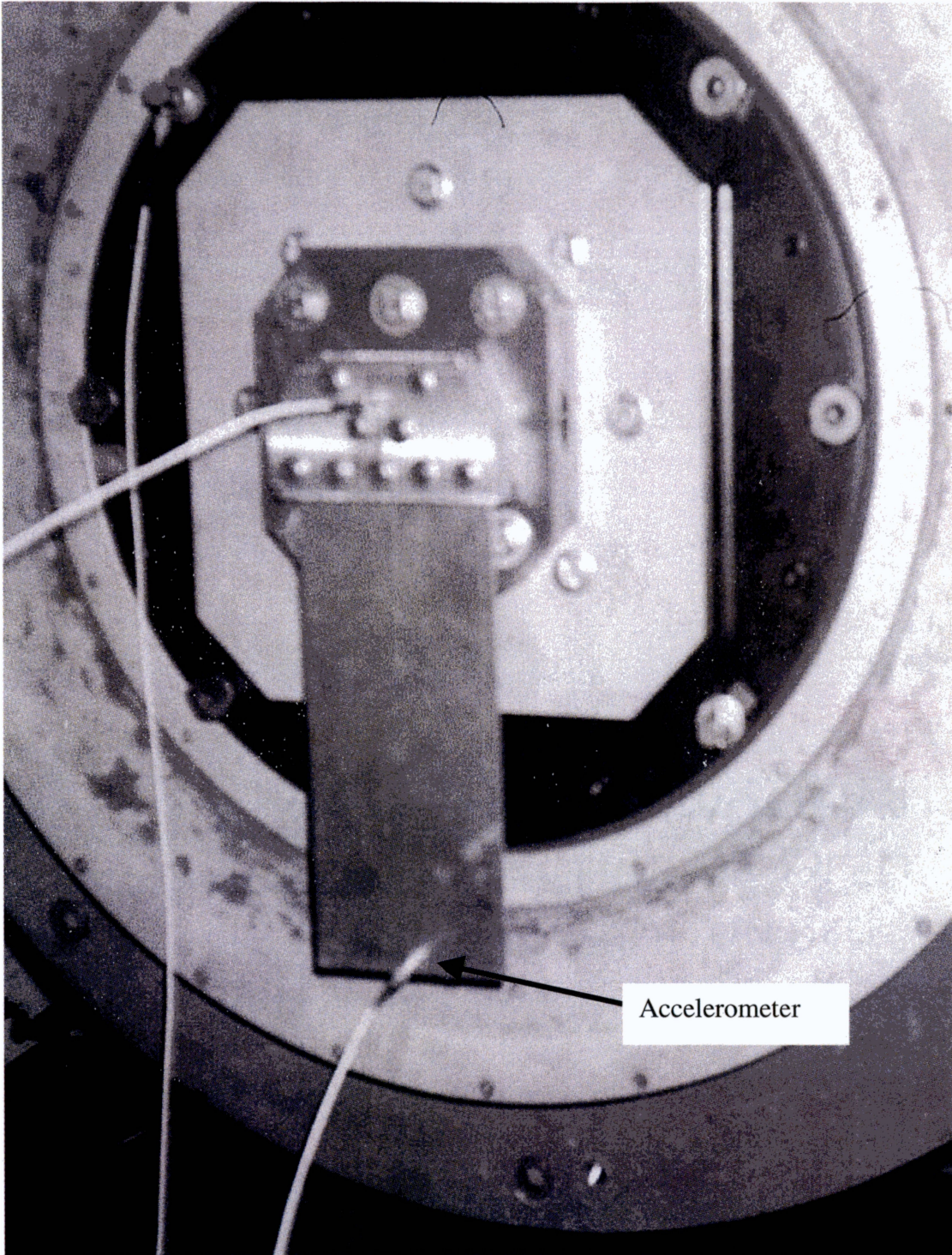
Figure 14. Reference plate R1 mounted in test fixture with accelerometer

Acceleration Profile for R2 and P1 through P4
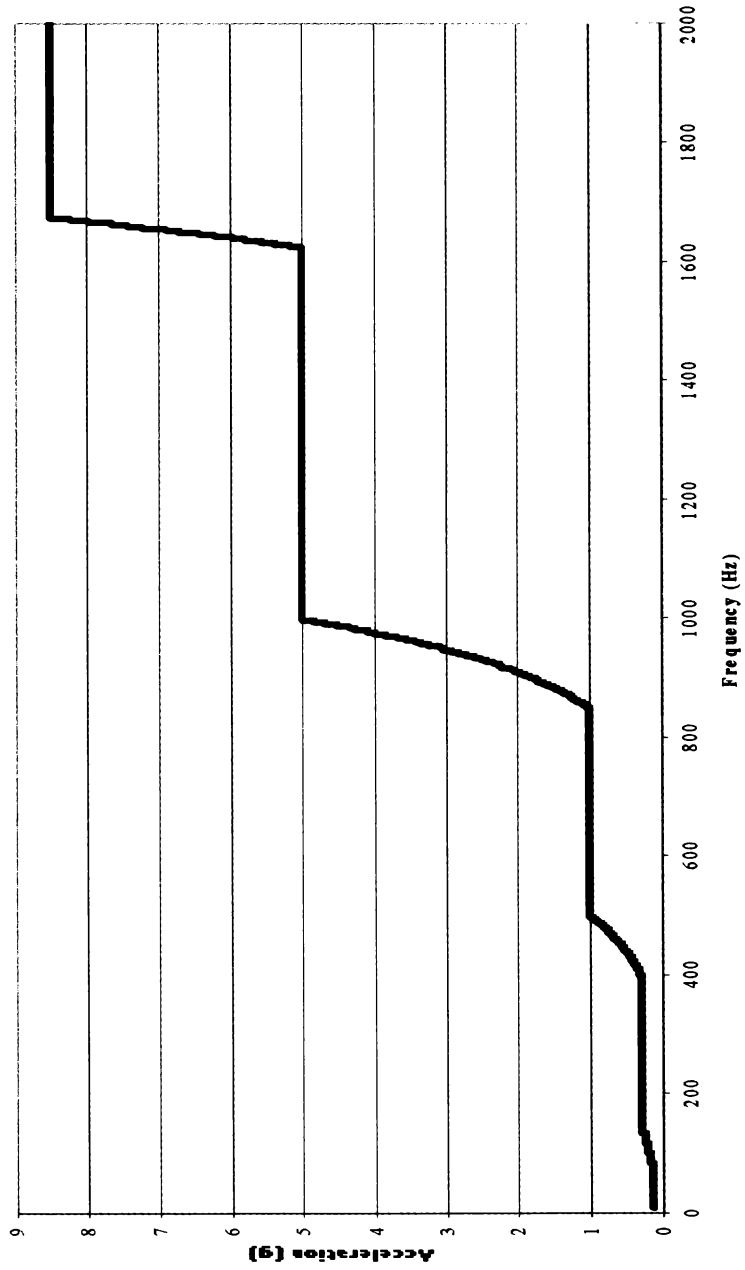
Figure 15. Acceleration profile for test plates R2 and P1 through P4

58

Experimental Results

A total of 75 frequency sweeps were conducted on the five test plates. Each frequency sweep was saved by run number. The text files saved by the Data Physics system include the real and imaginary components of the peak response listed by frequency from 10 Hz to 2000 Hz. There were fifteen runs for each plate. These files were combined into an EXCEL® workbook for each plate. The mode frequencies were identified by plotting the peak magnitude against the frequency. The peaks in this plot identified the mode frequencies. The data sheet for the plot was then analyzed around the peaks to extract the mode frequency and peak displacements at that frequency for all fifteen-measurement locations. The mode frequencies identified for each plate and the corresponding model frequencies for the nominal model are shown in Table 5. The plots for the displacements are shown in Figures D-1 through D-5, where the last to characters of the data trace label refer to the measurement locations shown in Figure 10. These plots include all fifteen measurement points. As can be seen from the plots, the location of the mode frequencies is reasonable well defined. The peak displacements at these frequencies for each plate were used to plot the mode shapes. Since the data saved is peak values only, a new absolute value based modal assurance criterion would be required to match the modes to the model. The absolute value modal assurance criterion is given by

$$AMAC_{ij} = \frac{\left\| \left| \varphi_{mi}^T \right| \varphi_{tj} \right\|^2}{\left(\varphi_{mi}^T \varphi_{mi} \right)\left(\varphi_{tj}^T \varphi_{tj} \right)} \tag{15}$$

where the $\left| \varphi_{mi}^T \right|$ is absolute value of the components of the ith model mode vector of dimension 18×1 (see Table D-1), φ_{tj} is the test mode vector (18×1) of peak response recorded by the data system. These vectors include zeros at the three boundary points for plotting the modes in Figures D-6 through D-10.

Table 5. Frequency summary for nominal model and test plates

PLATE NO.	M1	M2	M3	M4	M5	M6	M7	M8	M9	M10
MODEL	44.455	200.46	278.73	659.67	795.88	1289.2	1377.8	1621.6	1867.4	2181.5
REF2	44.025	-	272.48	-	759.53	1201.9	1340.9	1522.7	1762.8	1987.9
P1	44.998	-	275.4	-	763.42	1200.9	1326.3	1520.7	1754	1964
P2	44.025	195.88	268.59	628.29	746.89	1182.4	1335	1498.4	1749.2	1931
P3	44.025	189.85	261.79	-	740.09	1171.7	1303	1485.7	1718.1	1919.3
P4	44.998	-	271.51	-	748.84	1176.6	1299.1	1497.4	1728.8	1928.1

A qualitative assessment of the AMAC was carried out by plotting the absolute value of the mode shapes for a few modes from a finite element analysis of the reference plate. A comparison of the absolute value plot of the fourth bending mode for the model and the peak value data for test plate R2 is shown in Figure 16. The second strip mode comparison is shown in Figure 17. These plots were done to provide a comparison of the result of the AMAC. The difference in resolution between the model and the test data makes a visual comparison difficult. The only points compared for the test data using the AMAC criterion are the measure points along the centerline and near the lengthwise free edges of the plates. Looking at these points on the figures verifies that the criterion will work based on the similarity of the surfaces at these points. Normally, the off diagonal elements of the MAC are small. The generally accepted criterion for the MAC with the modes paired by increasing frequency specifies that the diagonal element of the MAC matrix should be greater than 0.85 for the matching of the test and model modes [18]. However, when the AMAC is used the off-diagonal components can be large. This limits the use of this criterion to modes that are highly correlated where the diagonal elements of the AMAC must be equal to or exceed 0.95.

The AMAC is implemented in the Mathcad® worksheet for updating the geometry (see Appendix C) by taking the absolute value of the model mode vectors prior to implement the MAC function. The modes vectors obtained from the finite element code in Appendix A are not sorted in ascending order prior to calculating the AMAC. This requires the use of a permutation matrix, which is obtained by setting all of the matrix coefficients in the AMAC that are greater than or equal to 0.95 equal to 1 and all

Absolute value for the 4th bending mode of the model
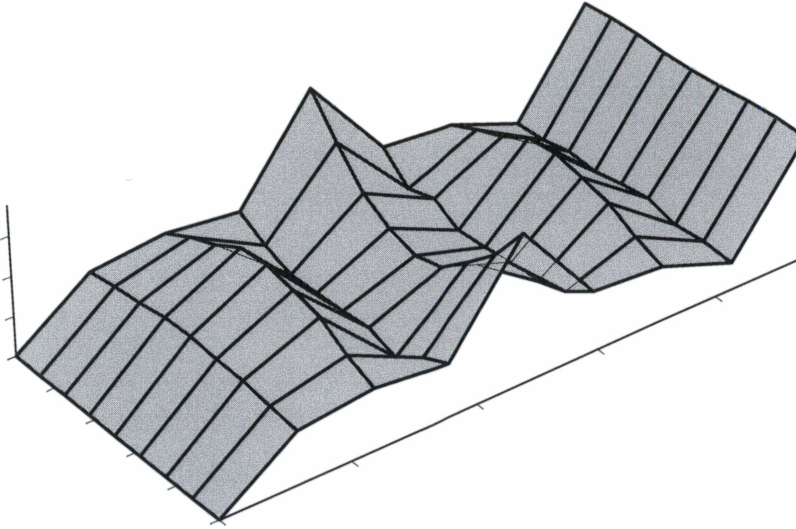
Test data for 4th bending mode
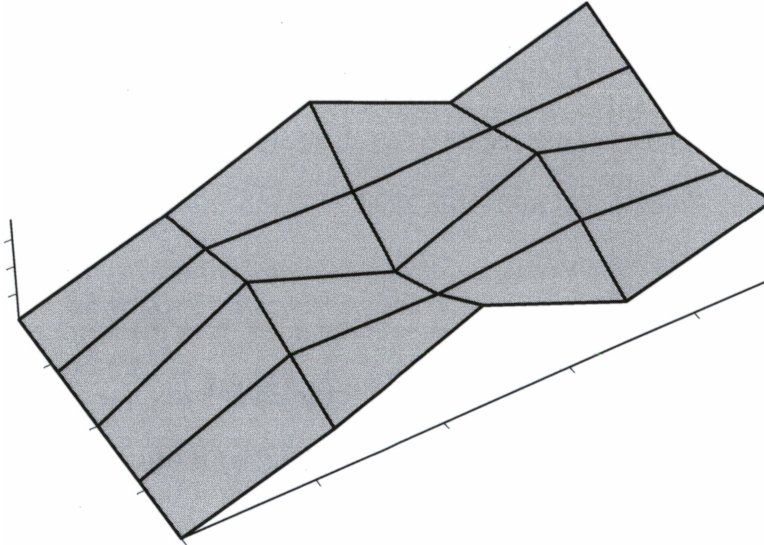
Figure 16. Comparison of 4th bending modes between absolute value of model and test data for R2

Absolute value for 2-strip mode
for the model
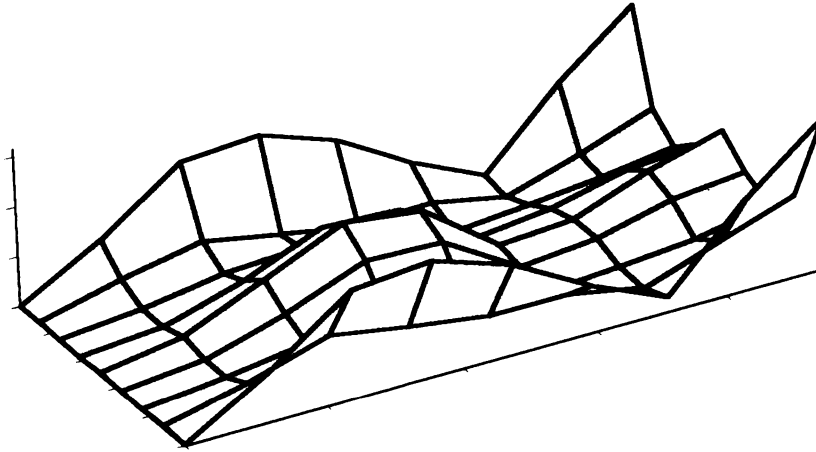
Test data for 2-strip mode
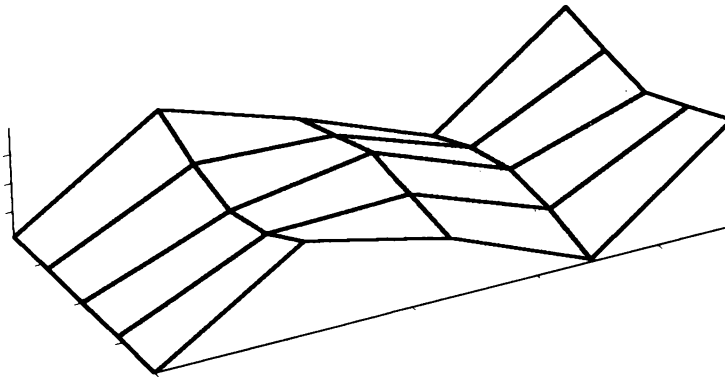
Figure 17. Comparison 2nd strip mode between absolute value of model and test data for R2

other entries equal to 0. The appearance of a column of zeroes in the permutation matrix identifies the occurrence of an incorrectly identified test mode, which should not be used in used in Equation 2.

Validation of Geometric Updating Method

The initial reduction of the data provided the set of test modes to be matched with the model models using the AMAC. The next step is to convert the test modes from peak displacements (absolute value) of the mode at the measurement point to modes with the proper sign. This is accomplished using the following formula

$$\Phi_{tp_{i,j}} = \frac{\Phi_{t_{i,j}} \Phi_{m_{i,j}}}{\left| \Phi_{m_{i,j}} \right|} \tag{16}$$

where $\Phi_{t_{i,j}}$ is the (i,j) component of matrix of test modes for the test plate (see Tables D-2 through D-6), $\Phi_{m_{i,j}}$ is the (i,j) component of the matrix of model modes (see Table D-1), $\left| \Phi_{m_{i,j}} \right|$ is the absolute value of the (i,j) component of the model matrix, and Φ_{tp} is matrix of the phase corrected test mode shapes. The phase corrected test mode shape matrix is then used to adjust the phase of the perturbed models mode shaped matrices. This is necessary to ensure that the test mode shapes and all of the model mode shapes have the same phase prior to determining the basis coefficients for the model modes.

The updating algorithm was applied to all five of the test plates. The results are shown in Figure 18. The two plates where the method performed the best for correcting the geometry of the model are plates R2 and P2. The updated geometry for R2 shows variations of less than .002 inch. The dimensions of the R2 plate were checked using a micrometer. The micrometer measurements where taken at the points R1 through R5 and
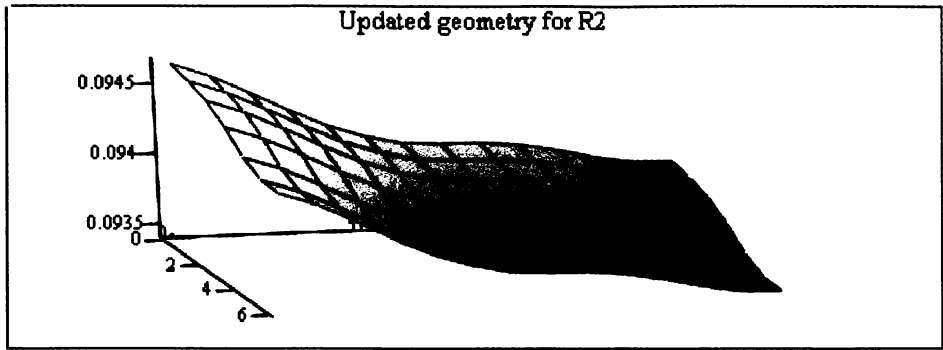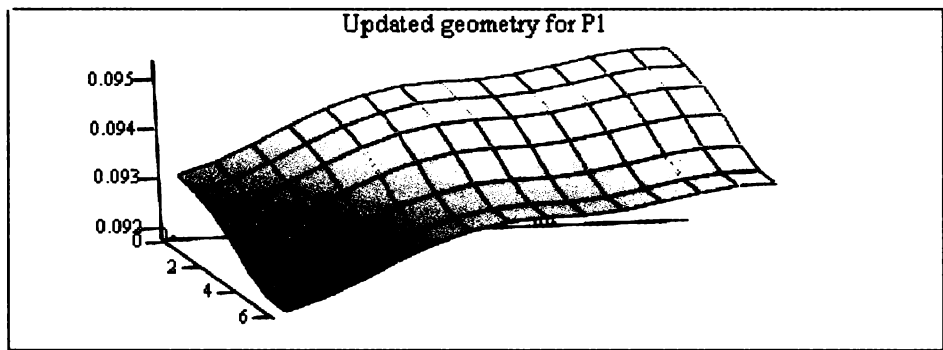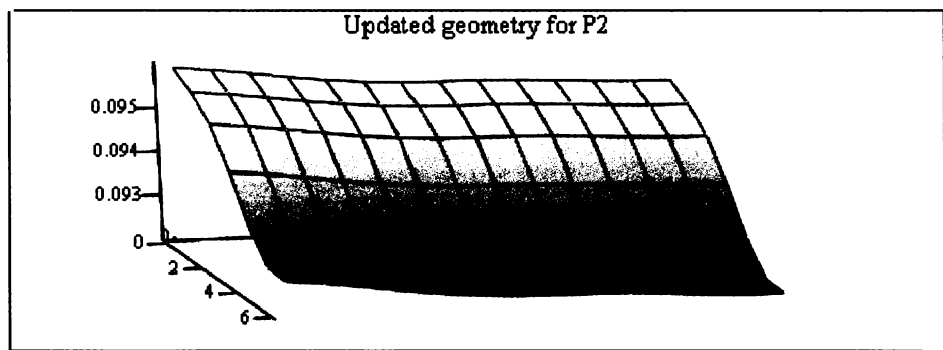
64

Updated geometry for R2

Gwl

Updated geometry for P1

Gwl

Updated geometry for P2

Gwl

Figure 18. Updated nodes for the top surface of the test plates

Updated geometry for P3

Gwl

Updated geometry for P4

Gwl
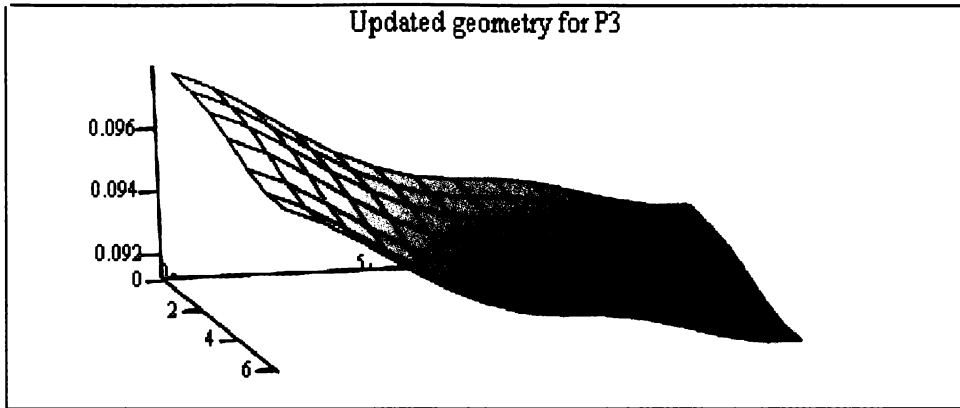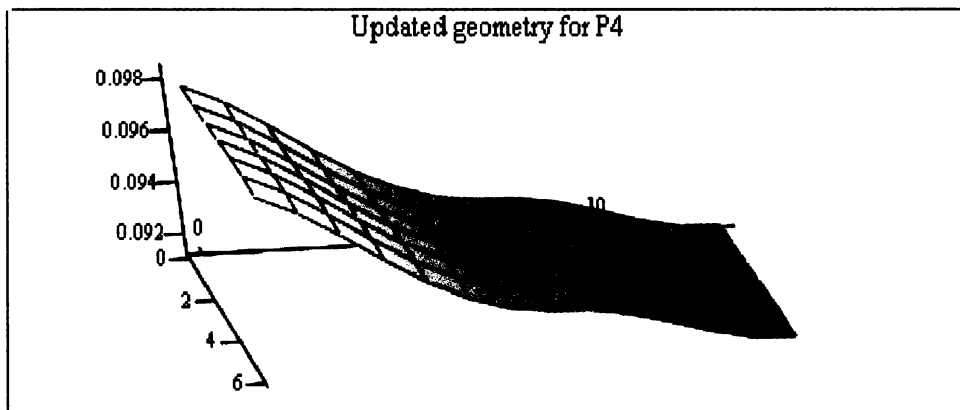
Figure 18. Updated nodes for the top surface of the test plates (continued)

L1 through L5 shown in Figure 10. The micrometer measurements by coordinate location of the test measurement points for plate R2 and the updated geometry at the test measurement points are shown for comparison in Table 6. Both show a change in thickness in the widthwise direction. However, the updated geometry also shows a thickness change in the lengthwise directions. In general, the updated plate geometry is consistent with the measured plate geometry.

The comparison between the measured geometry and the updated geometry for plate P2 shows that the method predicted the general characteristics of the test plate geometry (see Table 7). The amount of variation in the change in thickness is underestimated in this case, since the updated model underestimates the thickness change in the lengthwise direction for the measurement locations L2 through L5 in the widthwise direction. The updated geometries of the remaining plates P1, P3, and P4 deviate from actual geometries depicted in Figure 12 in that the updated geometry for plate P1 showed an inverse characteristic (see Table 8) where as the updated geometry is thinner at the clamped end and increases in thickness where the test plate decreases in thickness. The updated geometries of plates P3 and P4 both taper in thickness from the clamped end out to the free end and also in the widthwise direction. Both of these test plates have a variation in thickness in the lengthwise direction. However, plate P3 first decreases in thickness and then increases in thickness towards the free end of the actual plate. Plate P4 maintains a uniform thickness for half of the plate closest to the clamped end and then reduces in thickness to the free end. The thickness changes for plates P3 and P4 are shown in Table 9 and Table 10, respectively. These measurement checks were made to provide an assessment of the updating method. The method produced bounded results. In all of the cases above, the updated model geometries were reasonable there were no geometry changes that were excessive.

Table 6. Comparison of measured and updated plate thickness for plate R2

		Widthwise			
Measurement		**Experimental Plate R2 (in)**		**Updated model R2 (in)**	
Locations		**L**	**R**	**L**	**R**
Lengthwise	**1**	.0955	.0945	.0943	.0939
	2	.0950	.0948	.0940	.0936
	3	.0950	.0948	.0939	.0936
	4	.0955	.0945	.0938	.0935
	5	.0955	.0945	.0938	.0935

Table 7. Comparison of measured and updated plate thickness for plate P2

		Widthwise			
Measurement		**Experimental Plate P2 (in)**		**Updated model P2 (in)**	
Locations		**L**	**R**	**L**	**R**
Lengthwise	**1**	.0910	.0945	.0928	.0955
	2	.0895	.0940	.0922	.0953
	3	.0890	.0940	.0921	.0953
	4	.0890	.0944	.0920	.0952
	5	.0885	.0945	.0920	.0952

Table 8. Comparison of measured and updated thickness for plate P1

		Widthwise			
Measurement		**Experimental Plate P1 (in)**		**Updated model P1 (in)**	
Locations		**L**	**R**	**L**	**R**
Lengthwise	**1**	.095	.0945	.0929	.0941
	2	.095	.0948	.0935	.0947
	3	.092	.093	.0937	.0950
	4	.091	.093	.0940	.0952
	5	.0885	.090	.0940	.0952

Table 9 Comparison of measured and updated thickness for plate P3

		Widthwise			
Measurement		**Experimental Plate P3 (in)**		**Updated model P3 (in)**	
Locations		**L**	**R**	**L**	**R**
Lengthwise	**1**	.0945	.0955	.0941	.0955
	2	.091	.092	.0926	.0941
	3	.0955	.0945	.0921	.0936
	4	.0960	.0945	.0917	.0930
	5	.096	.095	.0916	.0931

Table 10. Comparison of measured and updated thickness for plate P4

Measurement		Widthwise			
		Experimental Plate P4 (in)		Updated model P4 (in)	
Locations		L	R	L	R
Lengthwise	1	.096	.096	.0949	.0954
	2	.0958	.0958	.0930	.0935
	3	.092	.0930	.0923	.0929
	4	.0905	.0910	.0916	.0921
	5	.0898	.0900	.0917	.0923

A plot of the model set weights for all of the test plates is shown in Figure 19. The participation or weights for the models shows a higher relative participation for more of the models than the simulation trials shown in Figure 9. The weights for the simulation cases (see Figure 9) are obtained using noise free modes from a model that has the same number of dofs as the model set. Where as the actual test modes may be influenced by test technique.

An evaluation of the 2-norm metric is needed to see if it produces results consistent with the updated geometry shown in Figure 18. The 2-norm relative error metric provides a means for gauging the improvement of the updated model relative to the nominal model. This step is important to determine whether this metric can be used in cases where it is not feasible to obtain measurements of the structure under test. It is important to note that the metric indicates the size of the error between the model (updated or nominal) and the test modes at the measurement points. A perfect match would result in a value of zero.

70

Figure 19. Plot of calculated basis vector weights for test plates

The results for all five plates are shown in Table 11. The metric indicates that the updated models for the five plates offer minimal improvement in reducing the error between the measured test mode vectors and the mode vectors predicted by the nominal model. Plates P3 and P4 showed the best performance even though the updated geometry is not fully consistent with the measured geometry. There are three factors that could account for the marginal performance of the method with the test data. They are: 1.) Test methodology, 2.) Instrumentation noise, and 3.) Resolution of the finite element models.

Test methodology is the most likely source of error. A review of the test results conducted by Nichol [16] and Gwinn [33] indicate that the sweep rate was too high in the lower frequencies. The first two modes (M1 and M3, see Table 6) used for this research were not correctly identified. The frequencies reported separately by Nichol and Gwinn were lower than the frequencies obtained in this effort for both of the modes identified above. The primary concern with the test method used here is the frequency sweep rate used during testing. A low sweep rate is needed to approximate steady state measurement conditions. The comparison of the frequencies measured for the first two modes and those reported by Nichol and Gwinn indicates that the rate was too high. Sweeping through a speed range is common practice in structural survey testing for turbo machinery [1]. This is similar to sweeping through a frequency range on a shaker as was done here. The effect is the same.

However, the accuracy of the mode shape may not be reliable obtained during frequency sweep testing. A sweep and dwell test approach should have been used. In all cases, eight of the ten modes in the frequency range of the test were identified. The two modes that were not matched were the 1st torsion and 2nd torsion modes. It should be noted that in theory the antisymmetric modes could not be excited using the type of shaker used. Plate P2 showed small peaks near the model frequencies for these modes. Plate P3 exhibited a response near the 1st torsion mode only. In both cases the AMAC

72

Table 11. Summary of relative error metric for the nominal and the updated models

Relative Error Metric	Test Plates				
	R2	P1	P2	P3	P4
Nominal Model	1.18	1.03	0.61	0.91	1.09
Updated Model	1.17	1.00	0.58	0.70	0.86

criterion indicated that these peaks were not modes. A review of the test mode shapes plotted for all identified responses shows that these are not modes (see Appendix D). The criterion indicated that these peaks were not modes. The asymmetry of the plates was enough to excite the higher antisymmetric modes (e.g. 3rd and 4th torsion modes). A sweep and dwell test may have been able to excite the 1st and 2nd torsional modes. Even though the eight of the ten modes were correctly identified and the response characteristics were qualitatively consistent with expectations of the author, the response levels measured during testing may not have representative of the true mode shapes for the plates. This is the mostly likely cause for the marginal performance of the method using the test data.

Instrumentation errors were not considered to have an effect on the performance of the method. The instrumentation was closely monitored using the diagnostic features available. The Polytec laser vibrometer has excellent diagnostic capabilities and the signal quality was also monitored using an oscilloscope.

The resolution of the model may also contribute to the error. A higher resolution model using more degrees of freedom would provide more accurate predictions of the mode frequencies. However, the mode frequencies are not used in this updating approach. The maximum modal displacement will also change with increased mesh density, but not to the degree that the mode frequency of the higher order modes will

change for the mode frequencies. A comparison for the first bending mode between the measure deflections at the free end of plate R2 with the deflections of the nominal model at the measurement points indicates that the test plates are more flexible in the widthwise direction than the model. A high-resolution model (26,000 dof) using ten node tetrahedron elements did not result in an increase in widthwise flexibility over the model used in this study (588 dof) that would suggest that the model resolution is a significant source of error.

74

6. Conclusions

Discussion of Results

This research effort presented a method for correcting or updating the geometry of the nominal model of a test article using a set of models that represented a perturbation space necessary for finding the model geometry to reduce the error between the test modes and an updated model. The numerical simulation indicated that the method was capable of producing an updated model geometry that approximated the simulated test article geometry. The simulations carried out indicated that the geometry perturbations can be approximated with a combination of linear, nonlinear, and transcendental functions that describe the perturbed geometries. The simulations carried out also indicated that minimizing measurement noise is critical to the success of this method for systems experiencing small perturbations. A sensitivity analysis for the use of the method with a reduced number of test points for the noise free case was also conducted. The analysis showed that the method is sensitive to the number and location of measurement points. The method was less sensitive to a reduction in measurement points in the lengthwise direction for two of the simulated test plates.

A new absolute value modal assurance criterion was introduced and applied effectively to the test data. This criterion can be used to match modes when only the peak displacement data is available. Limits for the use of the absolute value modal assurance criterion were identified. An efficient metric for comparing modes obtained from finite element models with modes acquired during testing was also introduced. This metric gauges the closeness of the model modes to the test modes without requiring expansion of the modes or the mass matrix. The metric is based on the matrix 2-norm

formed by taking the difference between the model predictions at the test locations and the test measurements.

The performance of geometric updating method under experimental validation showed marginal improvement of the updated model over the nominal model for all of the test plates. Comparison of the measured thickness of the test plates with the thickness predicted by the updated model using the 2-norm metric indicated that the improvement was marginal. Deficiencies in the test methodology were identified that contributed to the marginal performance of the method when applying it to experimental data. Additionally, issues with the model resolution were raised that could also improve the performance of the updating technique presented. The numerical simulations did demonstrate that the method was robust and numerically stable providing bounded results.

Recommendations for Additional Research

- Investigate the apparent higher flexibility of the test plates in the widthwise direction when compare with the finite element model predictions.
- Conduct experiments with increased number of measurement locations using a scanning laser vibrometer.
- Investigate the feasibility of using strain gage and displacement measurements.
- Developing geometric updating approaches including parametric methods for more complex structures such as turbo machinery airfoils.
- Investigating the influence of the geometric tolerance for perturbed models.
- Implementing the method using the programming features of a commercial finite element package.

76

- Consider methods that would incorporate frequency to compensate for bias in the result (e.g. in this case either thicker or thinner than expected).
- Investigate the possibility of using an iterative method with a small set of perturbed models.

List of References

[1] Kenyon, James A. and Rabe Douglas C., "Aerodynamic Effects on Blade Vibratory Stress Variations", *Journal of Propulsion and Power*, Vol. 15, No. 5 1999, pp. 675-680.

[2] Chen, S. and Sinha, A., "Calculating the Statistics of the Maximum Amplitude of a Mistuned Bladed Disk Assembly", In the Proceedings of *33rd AIAA/ASME/ASCE/AHS/ASC Structures, Structural Dynamics and Materials Conference,* Dallas TX, 1992, pp. 1296-1302.

[3] Ewins, D. J. and Han, Z. S., "Resonant Vibration Levels of a Mistuned Bladed Disc", Vibrations of Bladed Disk Assemblies, Present at the *9th Biannual Conference on Mechanical Vibration and Noise of the Design and Production Engineering Technical Conferences,* Dearborn, MI, September, 1983, pp. 127-136.

[4] Castanier, M. P., Ottarsson, G., and Pierre C., "A Reduced Order Modeling Technique for Mistuned Bladed Disks", *Journal of Vibration and Acoustics*, Vol. 119, 1997, pp.439-447.

[5] Yang, M. T. and Griffin, J. H. "Theory and Methodology of Optimally Measuring Vibratory Strains in Closely Spaced Modes," *Journal of Engineering for Gas Turbines and Power*, Vol. 120, 1998, pp.801-807.

[6] Kruse, Marlin and Pierre Christophe, "Dynamic Response of an Industrial Turbomachinery Rotor", *Presented at the 32nd AIAA/ASME/SAE/ASEE Joint Propulsion Conference,* Lake Buena Vista, FL July 1-3, 1996.

[7] Dowling, Norman E., Mechanical Behavoir of Materials, *Prentice-Hall, Inc.*, Upper Saddle River, NJ, 1993, pp.371-374.

[8] Nagpal, Vinod K., Rubinstein, Robert, and Chamis, Christos C., "Probabilistic structural anslysis to quantify uncertainties associated with turbopump blades," *In the*

79

proceeding of the 28th Structures, Structural Dynamics and Materials Conference, Monterey, CA, April 6-8, 1987, pp. 268-274.

[9] Srinivasan, A.V., "Flutter and Resonant Vibration Characteristics of Engine Blades", *Journal of Engineering for Gas Turbines and Power,* Vol. 119, 1997, pp. 742-775.

[10] Kruse, Marlin and Pierre, Christophe, "Forced Response of Mistuned Bladed Disks Using Reduced-Order Modeling", *In the proceedings of the 32nd AIAA/ASME/SAE/ASEE Joint Propulsion Conference,* Lake Buena Vista, FL July 1-3, 1996.

[11] Beachkofski, Brian K., and Grandhi, Ramana V., "Probabilistic Modal Analysis for Turbine Engine Blades," *42nd AIAA/ASME/ASCE/AHS/ASC Structures, Structural Dynamics and Materials Conference and Exhibit,* Seattle, WA April 16-19, 2001.

[12] Sensmeier, M. D. and Nichol, K. L., "Optimum Placement of Sensors for Vibration Measurement on Turbine Engine Blades", In the Proceedings of the 39th *AIAA/ASME/ASCE/AHS/ASC Structures, Structural Dynamics and Materials Conference and Exhibit,* Long Beach, CA, Apr. 20-23, 1998, pp1315-1320.

[13] Sensmeier, Mark D. and Nichol, Kurt L., "Improved Vibration Monitoring Through Optimization of Sensor Placements," ASME Turbo Expo 2000 Munich, Germany, May 2000 AEDC PA 2000-034, Feb. 22, 2000.

[14] Nichol, Kurt L., "Numerical Strain Gage Representation", In the Proceedings of the 39th *AIAA/ASME/ASCE/AHS/ASC Structures, Structural Dynamics and Materials Conference and Exhibit,* Long Beach, CA, Apr. 20-23, 1998, pp. 198-203.

[15] Nichol, K. L., "Strain-Gage Placement Considerations for Dynamic Data Analysis", Proceedings of the 32nd *AIAA/ASME/ASCE/AHS/ASC Structures, Structural Dynamics and Materials Conference and Exhibit,* Baltimore, MD, Apr. 8-10, 1991, pp. 2576-2582.

80

[16] Nichol, Kurt L., "The Enhancement of Analytical Structural Models Including Consideration of Elastic Boundary Conditions", Doctoral Dissertation, University of Tennessee, Knoxville, TN, 1995.

[17] Kielb, Robert E., et al, "Joint Research Effort on Vibrations of Twisted Plates," RP-1150, September 1985, NASA.

[18] Friswell, M. I., Mottershead, J. E., Finite Element Model Updating in Structural Dynamics, *Kluwer Academic Publishers*, Dordrecht, Netherlands, 1995.

[19] Sutter, Thomas R., et al, "Comparison of Several Methods for Calculating Vibration Mode Shape Derivatives," *AIAA Journal, Vol. 26, No. 12, December 1988, pp. 150-1511.*

[20] Ahmadian, H., Mottershaed, J., and Friswell, M., "Joint Modeling for Finite Element Model Updating," *Proceedings of the 14th International Modal Analysis Conference,* pp.591-596, 1996.

[21] Horton, B. Gurgenci, H., Veidt, M., Friswell, M. I., "Finite Element Model Updating of A Welded Space Frame," *Proceedings of IMAC-XVIII: A Conference on Structural Dynamics,* San Antonio, TX, February 7-10, 2000, pp. 529-535.

[22] Farhat, Charbel, and Hemez, Francois M., "Updating Finite Element Dynamic Models Using an Element-by-Element Sensitivity Methodology," *AIAA Journal, Vol. 31, No.9,* September, 1993, pp1702-1711.

[23] Farhat, Charbel., and Hemez, Francois M., "Bypassing numerical difficulties associated with updating simultaneously mass and stiffness matrices," *AIAA Journal, Vol. 33, No.3,* March, 1995, pp. 539-546.

[24] Blelloch, Paul A., Freymiller, James E.,"Tunning Finite Element Models Using Design Sensitivity," *AIAA/ASME/ASCE/AHS/ASC Structures, Structural Dynamics and*

Materials Conference and Exhibit, St. Louis, MO, April 12-15, 1999, Vol. 3, pp.2102-2108.

[25] Mottershead, J. E., et al, "Model updating of an aluminium space-frame using different parameters sets," *Proceedings of IMAC-XVIII: A Conference on Structural Dynamics*, San Antonio, TX, February 7-10, 2000, pp. 576-582.

[26] Friswell, M. I., Mottershead, J. E., and Ahmadian, H., "Fininte-element model updating using experimental test data: parameterization and regularization," *Philosophic Transaction,* The Royal Society, London, England, January, 2001, Vol. 359, pp 169-186.

[27] Engels, Remi C., Final Report, Advanced Finite Element Model Modification Algorithms Development, Contract No. F406-94-D-0001 Task 98-02, The University of Tennessee Space Institute. October, 1998.

[28] Trefethen, Lloyd N., Bau III, David, Numerical Linear Algebra, Society for Industrial and Applied Mathematics, Philadelphia, PA, 1997, pp.129-133.

[29] Cook, Robert D., Finite Element Modeling For Stress Analysis, John Wiley & Sons, New York, New York, 1995.

[30] Noble, Ben, and Daniel, James W., Applied Linear Algebra, *Prentice-Hall, Inc.*, Englewood, New Jersey, 1977, pp. 278-279.

[31] Nichol, Kurt L., Private correspondence, May 2001.

[32] Pintur, David A., Finite Element Beginnings, Mathsoft Inc., 1998.

[33] Gwinn Jr., Allen Fort, "A Finite Element Model Updating Technique for Adjustment of Parameters Near Boundaries," Doctoral Dissertation, University of Tennessee, Knoxville, TN, 1998.

Appendices

Appendix A
Finite Element Model Code

Input Region for eight node isoparametric model:

Top :=

	1	2
1	2	10
2	10	11
3	11	12
4	12	13
5	13	14
6	14	9

:=

C:\..\nodes updated geometry sim p1 wxl nl05.xls

pid :=

	1
1	1
2	2
3	3

Mat :=

	1
1	$1.06 \cdot 10^7$
2	0.33
3	0

Restraints :=

	1
1	1
2	2

$Tnodes := Nodes^T$

Process Initialization
Total number of nodes --->
Total number of elements->
Degrees of freedom per node
Number of nodes per element

$$\begin{pmatrix} n_{nodes} \\ n_{el} \\ ndof_{pn} \\ nn_{pe} \end{pmatrix} := \begin{pmatrix} rows(Nodes) \\ rows(Top) \\ 3 \\ cols(Top) \end{pmatrix}$$

85

$$\begin{pmatrix} E \\ v \\ \rho \end{pmatrix} := \begin{pmatrix} Mat_1 \\ Mat_2 \\ Mat_3 \end{pmatrix}$$

Define two range variables which will be used at all times:

$ie := 1 .. n_{el}$

$in := 1 .. n_{nodes}$

$$\begin{pmatrix} n_{nodes} \\ n_{el} \\ ndof_{pn} \\ nn_{pe} \end{pmatrix} = \begin{pmatrix} 196 \\ 78 \\ 3 \\ 8 \end{pmatrix}$$

Loop for elements
Loop for nodes

$j := 1 .. 8$

$$\begin{pmatrix} X_{n_{j,ie}} \\ Y_{n_{j,ie}} \\ Z_{n_{j,ie}} \\ NodeLabels_{j,ie} \end{pmatrix} := Tnodes^{\langle (Top_{ie,j}) \rangle}$$

Properties :=

	1
1	1

$$\begin{pmatrix} E \\ v \\ \rho \end{pmatrix} = \begin{pmatrix} 10587920 \\ 0.33 \\ 0.0002526768 \end{pmatrix}$$

$x_{nm} := \left(Tnodes^T \right)^{\langle 1 \rangle}$

$y_{nm} := \left(Tnodes^T \right)^{\langle 2 \rangle}$

$z_{nm} := \left(Tnodes^T \right)^{\langle 3 \rangle}$

Shape Functions:

86

$$N(s,t,r) := \begin{bmatrix} \dfrac{1}{8}\cdot(1-s)\cdot(1-t)\cdot(1-r) \\[6pt] \dfrac{1}{8}\cdot(1+s)\cdot(1-t)\cdot(1-r) \\[6pt] \dfrac{1}{8}\cdot(1+s)\cdot(1+t)\cdot(1-r) \\[6pt] \dfrac{1}{8}\cdot(1-s)\cdot(1+t)\cdot(1-r) \\[6pt] \dfrac{1}{8}\cdot(1-s)\cdot(1-t)\cdot(1+r) \\[6pt] \dfrac{1}{8}\cdot(1+s)\cdot(1-t)\cdot(1+r) \\[6pt] \dfrac{1}{8}\cdot(1+s)\cdot(1+t)\cdot(1+r) \\[6pt] \dfrac{1}{8}\cdot(1-s)\cdot(1+t)\cdot(1+r) \end{bmatrix}$$

$$dNds(s,t,r) := \begin{bmatrix} \dfrac{-1}{8}\cdot[(1-t)\cdot(1-r)] \\[6pt] \dfrac{1}{8}\cdot[(1-t)\cdot(1-r)] \\[6pt] \dfrac{1}{8}\cdot[(1+t)\cdot(1-r)] \\[6pt] \dfrac{-1}{8}\cdot[(1+t)\cdot(1-r)] \\[6pt] \dfrac{-1}{8}\cdot[(1-t)\cdot(1+r)] \\[6pt] \dfrac{1}{8}\cdot[(1-t)\cdot(1+r)] \\[6pt] \dfrac{1}{8}\cdot[(1+t)\cdot(1+r)] \\[6pt] \dfrac{-1}{8}\cdot[(1+t)\cdot(1+r)] \end{bmatrix}$$

$$dNdr(s,t,r) := \begin{bmatrix} \dfrac{-1}{8}\cdot(1-s)\cdot(1-t) \\[6pt] \dfrac{-1}{8}\cdot(1+s)\cdot(1-t) \\[6pt] \dfrac{-1}{8}\cdot(1+s)\cdot(1+t) \\[6pt] \dfrac{-1}{8}\cdot(1-s)\cdot(1+t) \\[6pt] \dfrac{1}{8}\cdot(1-s)\cdot(1-t) \\[6pt] \dfrac{1}{8}\cdot(1+s)\cdot(1-t) \\[6pt] \dfrac{1}{8}\cdot(1+s)\cdot(1+t) \\[6pt] \dfrac{1}{8}\cdot(1-s)\cdot(1+t) \end{bmatrix}$$

$$dNdt(s,t,r) := \begin{bmatrix} \dfrac{-1}{8}\cdot(1-s)\cdot(1-r) \\[6pt] \dfrac{-1}{8}\cdot(1+s)\cdot(1-r) \\[6pt] \dfrac{1}{8}\cdot(1+s)\cdot(1-r) \\[6pt] \dfrac{1}{8}\cdot(1-s)\cdot(1-r) \\[6pt] \dfrac{-1}{8}\cdot(1-s)\cdot(1+r) \\[6pt] \dfrac{-1}{8}\cdot(1+s)\cdot(1+r) \\[6pt] \dfrac{1}{8}\cdot(1+s)\cdot(1+r) \\[6pt] \dfrac{1}{8}\cdot(1-s)\cdot(1+r) \end{bmatrix}$$

$$dNdt_{esf}(s,t,r) := \begin{pmatrix} 0 \\ -2\cdot t \\ 0 \end{pmatrix}$$

$$dNdr_{esf}(s,t,r) := \begin{pmatrix} 0 \\ 0 \\ -2\cdot r \end{pmatrix}$$

$$dNds_{esf}(s,t,r) := \begin{pmatrix} -2\cdot s \\ 0 \\ 0 \end{pmatrix}$$

$$\text{dNds}_{EF}(s,t,r) := \text{stack}\left(\text{dNds}(s,t,r), \text{dNds}_{esf}(s,t,r)\right)$$

$$\text{xyz}(N,ie) := \begin{pmatrix} N \cdot X_n^{(ie)} \\ N \cdot Y_n^{(ie)} \\ N \cdot Z_n^{(ie)} \end{pmatrix}$$

$$\text{dNdt}_{EF}(s,t,r) := \text{stack}\left(\text{dNdt}(s,t,r), \text{dNdt}_{esf}(s,t,r)\right)$$

$$\text{dNdr}_{EF}(s,t,r) := \text{stack}\left(\text{dNdr}(s,t,r), \text{dNdr}_{esf}(s,t,r)\right)$$

$$J(s,t,r,ie) := \text{augment}(\text{xyz}(\text{dNds}(s,t,r),ie), \text{xyz}(\text{dNdt}(s,t,r),ie), \text{xyz}(\text{dNdr}(s,t,r),ie))^T$$

$$\text{detJ}(s,t,r,ie) := \left| J(s,t,r,ie) \right|$$

$$J_{calc}(J,v1,v2,v3) := \text{augment}\left[\left(J_{1,1} \cdot v1 + J_{1,2} \cdot v2 + J_{1,3} \cdot v3\right), \left(J_{2,1} \cdot v1 + J_{2,2} \cdot v2 + J_{2,3} \cdot v3\right), J_{3,1} \cdot v1 \ldots \atop + J_{3,2} \cdot v2 + J_{3,3} \cdot v3 \right]$$

$$\text{DNdxyz}(s,t,r,ie) := J_{calc}\left(J(s,t,r,ie)^{-1}, \text{dNds}_{EF}(s,t,r), \text{dNdt}_{EF}(s,t,r), \text{dNdr}_{EF}(s,t,r)\right)$$

$$\text{NM}(N) := \begin{pmatrix} N_1 & 0 & 0 & N_2 & 0 & 0 & N_3 & 0 & 0 & N_4 & 0 & 0 & N_5 & 0 & 0 & N_6 & 0 & 0 & N_7 & 0 & 0 & N_8 & 0 & 0 \\ 0 & N_1 & 0 & 0 & N_2 & 0 & 0 & N_3 & 0 & 0 & N_4 & 0 & 0 & N_5 & 0 & 0 & N_6 & 0 & 0 & N_7 & 0 & 0 & N_8 & 0 \\ 0 & 0 & N_1 & 0 & 0 & N_2 & 0 & 0 & N_3 & 0 & 0 & N_4 & 0 & 0 & N_5 & 0 & 0 & N_6 & 0 & 0 & N_7 & 0 & 0 & N_8 \end{pmatrix}$$

$$N_m(s,t,r) := \text{NM}(N(s,t,r))$$

$$\text{MBN1}(N) := \begin{pmatrix} N_{1,1} & 0 & 0 \\ 0 & N_{1,2} & 0 \\ 0 & 0 & N_{1,3} \\ N_{1,2} & N_{1,1} & 0 \\ N_{1,3} & 0 & N_{1,1} \\ 0 & N_{1,3} & N_{1,2} \end{pmatrix}$$

$$\text{MBN2}(N) := \begin{pmatrix} N_{2,1} & 0 & 0 \\ 0 & N_{2,2} & 0 \\ 0 & 0 & N_{2,3} \\ N_{2,2} & N_{2,1} & 0 \\ N_{2,3} & 0 & N_{2,1} \\ 0 & N_{2,3} & N_{2,2} \end{pmatrix}$$

$$\text{MBN36}(N) := \begin{pmatrix} N_{3,1} & 0 & 0 & N_{4,1} & 0 & 0 & N_{5,1} & 0 & 0 & N_{6,1} & 0 & 0 \\ 0 & N_{3,2} & 0 & 0 & N_{4,2} & 0 & 0 & N_{5,2} & 0 & 0 & N_{6,2} & 0 \\ 0 & 0 & N_{3,3} & 0 & 0 & N_{4,3} & 0 & 0 & N_{5,3} & 0 & 0 & N_{6,3} \\ N_{3,2} & N_{3,1} & 0 & N_{4,2} & N_{4,1} & 0 & N_{5,2} & N_{5,1} & 0 & N_{6,2} & N_{6,1} & 0 \\ N_{3,3} & 0 & N_{3,1} & N_{4,3} & 0 & N_{4,1} & N_{5,3} & 0 & N_{5,1} & N_{6,3} & 0 & N_{6,1} \\ 0 & N_{3,3} & N_{3,2} & 0 & N_{4,3} & N_{4,2} & 0 & N_{5,3} & N_{5,2} & 0 & N_{6,3} & N_{6,2} \end{pmatrix}$$

$$\text{MBN78}(N) := \begin{pmatrix} N_{7,1} & 0 & 0 & N_{8,1} & 0 & 0 \\ 0 & N_{7,2} & 0 & 0 & N_{8,2} & 0 \\ 0 & 0 & N_{7,3} & 0 & 0 & N_{8,3} \\ N_{7,2} & N_{7,1} & 0 & N_{8,2} & N_{8,1} & 0 \\ N_{7,3} & 0 & N_{7,1} & N_{8,3} & 0 & N_{8,1} \\ 0 & N_{7,3} & N_{7,2} & 0 & N_{8,3} & N_{8,2} \end{pmatrix}$$

$$\text{MBN}_{\text{esf}}(N) := \begin{pmatrix} N_{9,1} & 0 & 0 & N_{10,1} & 0 & 0 & N_{11,1} & 0 & 0 \\ 0 & N_{9,2} & 0 & 0 & N_{10,2} & 0 & 0 & N_{11,2} & 0 \\ 0 & 0 & N_{9,3} & 0 & 0 & N_{10,3} & 0 & 0 & N_{11,3} \\ N_{9,2} & N_{9,1} & 0 & N_{10,2} & N_{10,1} & 0 & N_{11,2} & N_{11,1} & 0 \\ N_{9,3} & 0 & N_{9,1} & N_{10,3} & 0 & N_{10,1} & N_{11,3} & 0 & N_{11,1} \\ 0 & N_{9,3} & N_{9,2} & 0 & N_{10,3} & N_{10,2} & 0 & N_{11,3} & N_{11,2} \end{pmatrix}$$

$\text{MAKEBN}(N) := \text{augment}\big(\text{MBN1}(N), \text{MBN2}(N), \text{MBN36}(N), \text{MBN78}(N), \text{MBN}_{\text{esf}}(N)\big)$

$\text{BN}(s,t,r,ie) := \text{MAKEBN}(\text{DNdxyz}(s,t,r,ie))$

$$\text{C1}(pk1) := pk1 \cdot \begin{pmatrix} 1 & 0 & 0 & 0 & 0 & 0 \\ 0 & 1 & 0 & 0 & 0 & 0 \\ 0 & 0 & 1 & 0 & 0 & 0 \\ 0 & 0 & 0 & .5 & 0 & 0 \\ 0 & 0 & 0 & 0 & 0.5 & 0 \\ 0 & 0 & 0 & 0 & 0 & .5 \end{pmatrix}$$

$$\text{C2}(pk2) := pk2 \cdot \begin{pmatrix} -1 & 1 & 1 & 0 & 0 & 0 \\ 1 & -1 & 1 & 0 & 0 & 0 \\ 1 & 1 & -1 & 0 & 0 & 0 \\ 0 & 0 & 0 & -1 & 0 & 0 \\ 0 & 0 & 0 & 0 & -1 & 0 \\ 0 & 0 & 0 & 0 & 0 & -1 \end{pmatrix}$$

$\text{C2}_p(ie) := \text{C2}\left[\text{Properties}_{\left(\text{pid}_{ie,2}\right),3}\right]$

$\text{C1}_p(ie) := \text{C1}\left[\text{Properties}_{\left(\text{pid}_{ie,2}\right),2}\right]$

$$C(E,\nu) := \frac{E}{(1+\nu)\cdot(1-2\cdot\nu)}\cdot\begin{pmatrix} 1-\nu & \nu & \nu & 0 & 0 & 0 \\ \nu & 1-\nu & \nu & 0 & 0 & 0 \\ \nu & \nu & 1-\nu & 0 & 0 & 0 \\ 0 & 0 & 0 & \dfrac{1-2\cdot\nu}{2} & 0 & 0 \\ 0 & 0 & 0 & 0 & \dfrac{1-2\cdot\nu}{2} & 0 \\ 0 & 0 & 0 & 0 & 0 & \dfrac{1-2\cdot\nu}{2} \end{pmatrix}$$

$C(ie) := C\left[\text{Properties}_{\left(\text{pid}_{ie,2}\right),2},\nu\right]$

$M(s,t,r,ie) := \rho\cdot xyz(N(s,t,r),ie)^T xyz(N(s,t,r),ie)\cdot detJ(s,t,r,ie)$

$\text{MakeK}(BN,C) := BN^T\cdot C\cdot BN$

$M1(s,t,r,ie) := \rho\cdot N_m(s,t,r)^T\cdot N_m(s,t,r)\cdot detJ(s,t,r,ie)$

$K(s,t,r,ie) := \text{MakeK}(BN(s,t,r,ie),C(ie))\cdot detJ(s,t,r,ie)$

$gp := \begin{pmatrix} -.577350269189626 \\ .577350269189626 \end{pmatrix}$

$w := \begin{pmatrix} 1.0 \\ 1.0 \end{pmatrix}$

$i := 1..2$

$j := 1..2$

$k := 1..2$

$K_e(ie) := \displaystyle\sum_k\sum_j\sum_i w_k\cdot w_j\cdot w_i\cdot K\left(gp_i,gp_j,gp_k,ie\right)$

$M_{el}(ie) := \displaystyle\sum_k\sum_j\sum_i w_k\cdot w_j\cdot w_i\cdot M1\left(gp_i,gp_j,gp_k,ie\right)$

$K_{ee}(ie) := \text{submatrix}\left(K_e(ie),1,24,1,24\right)$

$K_{ef}(ie) := \text{submatrix}\left(K_e(ie),25,33,25,33\right)$

$K_{fe}(ie) := \text{submatrix}\left(K_e(ie),25,33,1,24\right)$

$K_{el}(ie) := K_{ee}(ie) - K_{fe}(ie)^T\cdot K_{ef}(ie)^{-1}\cdot K_{fe}(ie)$

$\text{Vect}(M) := \begin{array}{|l} V \leftarrow M^{(1)} \\ \text{for } i \in 2..cols(M) \quad\quad \text{if } cols(M) > 1 \\ \quad V \leftarrow stack\left(V,M^{(i)}\right) \\ V \end{array}$

$\text{Pack}(V,p,q) := \begin{array}{|l} \text{for } j \in 1..q \\ \quad \text{for } i \in 1..p \\ \quad\quad \begin{array}{|l} M_{i,j} \leftarrow V_{i+p\cdot j} \text{ if } i+p\cdot j < rows(V) \\ M_{i,j} \leftarrow 0 \text{ otherwise} \end{array} \\ M \end{array}$

$\text{ndof}_{pe} := \text{ndof}_{pn}\cdot nn_{pe}$

$nK := n_{nodes} \cdot ndof_{pn}$

$K_{nK,nK} := 0$

$M_{nK,nK} := 0$

$KT^{\langle ie \rangle} := Vect\left(K_{el}(ie)\right)$

$MT^{\langle ie \rangle} := Vect\left(M_{el}(ie)\right)$

$i := 1 .. nn_{pe}$

$j := 1 .. nn_{pe}$

$p := 1 .. ndof_{pn}$

$q := 1 .. ndof_{pn}$

$row(i,j,n) := (j-1) \cdot n + i$

$K_{\left[\left(Top_{ie,i}-1\right) \cdot ndof_{pn}+p\right],\left(Top_{ie,j}-1\right) \cdot ndof_{pn}+q} := K_{\left[\left(Top_{ie,i}-1\right) \cdot ndof_{pn}+p\right],\left(Top_{ie,j}-1\right) \cdot ndof_{pn}+q} \cdots$
$$+ KT_{row\left[(i-1) \cdot ndof_{pn}+p,(j-1) \cdot ndof_{pn}+q,ndof_{pe}\right],ie}$$

$M_{\left[\left(Top_{ie,i}-1\right) \cdot ndof_{pn}+p\right],\left(Top_{ie,j}-1\right) \cdot ndof_{pn}+q} := M_{\left[\left(Top_{ie,i}-1\right) \cdot ndof_{pn}+p\right],\left(Top_{ie,j}-1\right) \cdot ndof_{pn}+q} \cdots$
$$+ MT_{row\left[(i-1) \cdot ndof_{pn}+p,(j-1) \cdot ndof_{pn}+q,ndof_{pe}\right],ie}$$

$band_{el_{ie}} := max\left[\left(Top^T\right)^{\langle ie \rangle}\right] - min\left[\left(Top^T\right)^{\langle ie \rangle}\right] + 1$

$halfban := max\left(band_{el}\right) \cdot ndof_{pn}$

$halfban = 582$

$J := 1 .. ndof_{pn}$

$n_{rr} := \sum_J \sum Restraints^{\langle J.2 \rangle}$

$J =$

1
2
3

$n_{rr} = 42$

$map(i,j) := (i-1) \cdot ndof_{pn} + j$

$BC_{4,nK} := 0$

$i := 1 .. rows(Restraints)$

$j := 1 .. ndof_{pn}$

$j =$

1
2
3

$$BC^{\langle map(Restraints_{i,1},j)\rangle} := \begin{pmatrix} if\left(Restraints_{i,j\cdot2},1,0\right) \\ Restraints_{i,j\cdot2+1} \\ if\left(Restraints_{i,j\cdot2},Restraints_{i,1},0\right) \\ if\left(Restraints_{i,j\cdot2},j,0\right) \end{pmatrix}$$

Our boundary condition bookkeeping table....

	1	2	3	4	5	6	7	8	9	10
1	1	1	1	1	1	1	1	1	1	1
2	0	0	0	0	0	0	0	0	0	0
3	1	1	1	2	2	2	3	3	3	4
4	1	2	3	1	2	3	1	2	3	1

BC = (above table)

Kmod := K

And,

Mmod := M

$i := 1 .. nK$

$j := 1 .. nK$

$$\begin{pmatrix} Kmod_{i,j} \\ Kmod_{j,i} \\ Kmod_{i,i} \end{pmatrix} := \begin{pmatrix} if\left(BC_{1,i},0,Kmod_{i,j}\right) \\ if\left(BC_{1,i},0,Kmod_{j,i}\right) \\ if\left(BC_{1,i},1,Kmod_{i,i}\right) \end{pmatrix}$$

$$\begin{pmatrix} Mmod_{i,j} \\ Mmod_{j,i} \\ Mmod_{i,i} \end{pmatrix} := \begin{pmatrix} if\left(BC_{1,i},0,Mmod_{i,j}\right) \\ if\left(BC_{1,i},0,Mmod_{j,i}\right) \\ if\left(BC_{1,i},1,Mmod_{i,i}\right) \end{pmatrix}$$

$nc := rows(Restraints)\cdot ndof_{pn} + 1$

$nc = 43$

Tlam := genvals(Kmod,Mmod)

TLStm := csort(Tlam,1)

$$Freq := \frac{\sqrt{Tlam}}{2\cdot\pi}$$

TLStest := submatrix(TLStm,nc,14 + nc,1,1)

Fr := csort(Freq,1)

FR := submatrix(Fr,nc,nc + 11,1,1)

C:\..\Kmodco.txt

Kmod

Modfr := submatrix(Tlam,rows(Kmod) − 11,rows(Kmod),1,1)

modevecs := genvecs(Kmod,Mmod)

C:\..\modelfreqgeomup.txt

Modfr

C:\..\Mmodco.txt

Mmod

$m := modevecs^T \cdot Mmod \cdot modevecs$

$i := 1 .. rows(m)$

$mn_i := \dfrac{1}{\sqrt{m_{i,i}}}$

$ModVecMn := modevecs \cdot diag(mn)$

$ModVec := submatrix(ModVecMn, 1, rows(Mmod), cols(Mmod) - 12, cols(Mmod))$

Mode vectors for comparison with expanded modes.

$Modelfreq := submatrix(Tlam, rows(Mmod) - 12, rows(Mmod), 1, 1)$

C:\..\lamdas 4elem.xls

Modelfreq

C:\..\mode vectors 4 elem.txt

ModVec

$FR_m := \dfrac{\overrightarrow{\sqrt{Modelfreq}}}{2 \cdot \pi}$

C:\..\modelfreq 4 Elem lz.xls

FR_m

	1
1	45.46241
2	207.47648
3	285.13044
4	695.49389
5	822.02806
6	1399.09157
7	1432.25412
8	1612.43347
9	1706.19266
10	2023.84015
11	2447.49824
12	2968.23238

FR =

$FR_m =$

	1
1	$3.078 \cdot 10^3$
2	$2.968 \cdot 10^3$
3	$2.447 \cdot 10^3$
4	$2.024 \cdot 10^3$
5	$1.612 \cdot 10^3$
6	$1.706 \cdot 10^3$
7	$1.432 \cdot 10^3$
8	$1.399 \cdot 10^3$
9	822.028
10	695.494
11	207.476
12	285.13
13	45.462

$nr := rows(ModVec)$

$nr = 588$

$nc := cols(ModVec)$

$nc = 13$

$LamFR := augment(Modelfreq, FR_m)$

$LamFR =$

	1	2
1	$3.741 \cdot 10^8$	$3.078 \cdot 10^3$
2	$3.478 \cdot 10^8$	$2.968 \cdot 10^3$
3	$2.365 \cdot 10^8$	$2.447 \cdot 10^3$
4	$1.617 \cdot 10^8$	$2.024 \cdot 10^3$
5	$1.026 \cdot 10^8$	$1.612 \cdot 10^3$
6	$1.149 \cdot 10^8$	$1.706 \cdot 10^3$
7	$8.098 \cdot 10^7$	$1.432 \cdot 10^3$
8	$7.728 \cdot 10^7$	$1.399 \cdot 10^3$
9	$2.668 \cdot 10^7$	822.028
10	$1.91 \cdot 10^7$	695.494
11	$1.699 \cdot 10^6$	207.476
12	$3.21 \cdot 10^6$	285.13
13	$8.16 \cdot 10^4$	45.462

$XYZ(\Phi, nr, nc) :=$ | $cc \leftarrow 1$
| $rc \leftarrow 0$
| for $i \in 1 .. nr$
| | $rc \leftarrow rc + 1$
| | $M_{cc,rc} \leftarrow \Phi_i$
| | if $rc \geq nc$
| | | $cc \leftarrow cc + 1$
| | | $rc \leftarrow 0$
| M

This section of the work sheet is for calculating the permutation matrix for reordering the model dof for expanding the test dof.

$$\text{Modes}(\Phi, \text{geom}) := \left\| \begin{array}{l} \left(\begin{array}{l} \text{nr} \leftarrow \text{rows}(\Phi) \\[4pt] \text{nc} \leftarrow \text{cols}(\Phi) \\[4pt] \text{MV} \leftarrow \Phi^{\langle 1 \rangle} \\[4pt] \text{MM1} \leftarrow \text{XYZ}(\text{MV}, \text{nr}, 3) \\[4pt] \text{for } j \in 2 .. \text{nc} \\[4pt] \quad \left| \begin{array}{l} \text{M1} \leftarrow \Phi^{\langle j \rangle} \\[4pt] \text{MM} \leftarrow \text{XYZ}(\text{M1}, \text{nr}, 3) \\[4pt] \text{MMode} \leftarrow \text{augment}(\text{MM1}, \text{MM}) \\[4pt] \text{MM1} \leftarrow \text{MMode} \end{array} \right. \end{array} \right) \\[4pt] \text{MM1} \\[4pt] \text{MWN} \leftarrow \text{augment}(\text{Nodes}, \text{MMode}) \end{array} \right.$$

$\text{M1} := \text{Modes}(\text{ModVec}, \text{Nodes})$

$\text{SM1} := \text{csort}(\text{M1}, 5)$

$$\text{SM} := \text{submatrix}\left(\text{SM1}, \frac{\text{rows}(\text{SM1})}{2} + 1, \text{rows}(\text{SM1}), 1, \text{cols}(\text{SM1}) \right)$$

C:\..\sim p1 n05 nwxl mode.xls

SM

C:\..\sim p1 n05 wlx freq.xls

LamFR

95

Appendix B
Plots of the Perturbations Functions for the Model Set
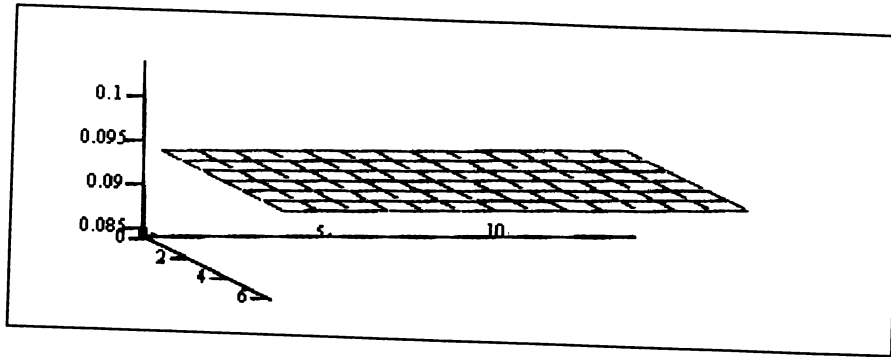
$$XYZ\left(xyz_{nom}^{(2)},98,14\right)$$
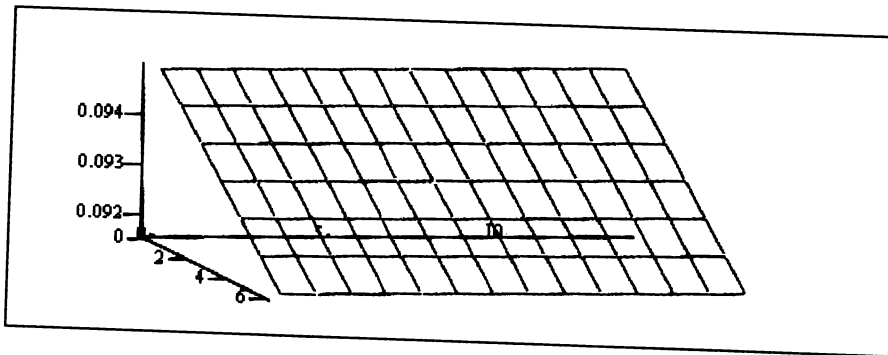
$$XYZ\left(xyz_{p1w}^{(2)},98,14\right)$$
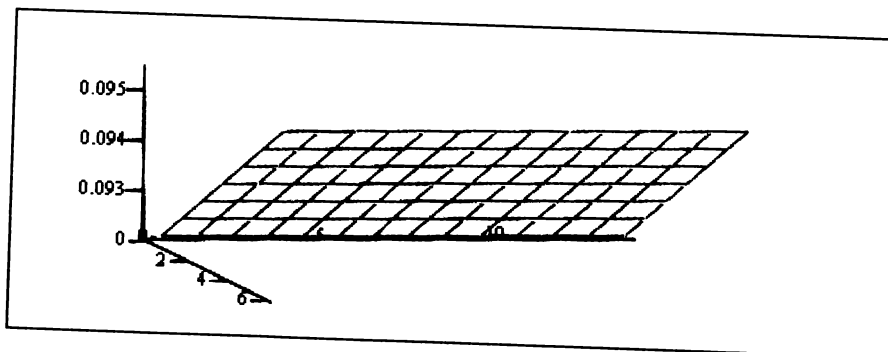
$$XYZ\left(xyz_{p2w}^{(2)},98,14\right)$$

Figure B-1. Nominal and perturbed model top surface nodes for basis set

97
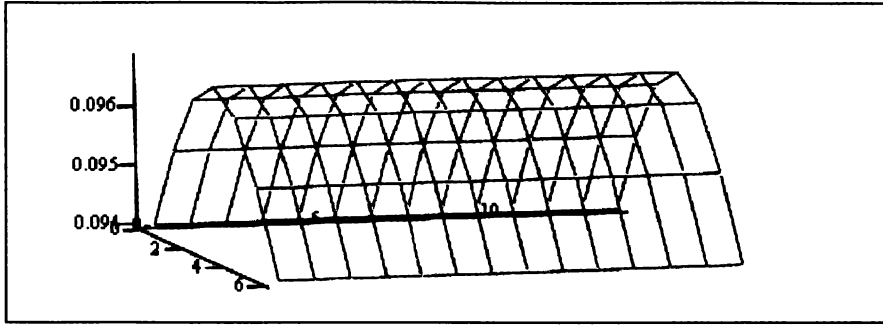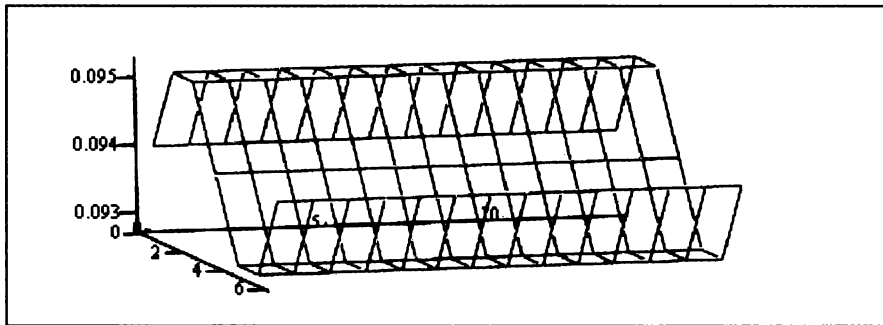
$$\mathrm{XYZ}\!\left(xyz_{p3w}{}^{(2)},98,14\right)$$

$$\mathrm{XYZ}\!\left(xyz_{p4w}{}^{(2)},98,14\right)$$
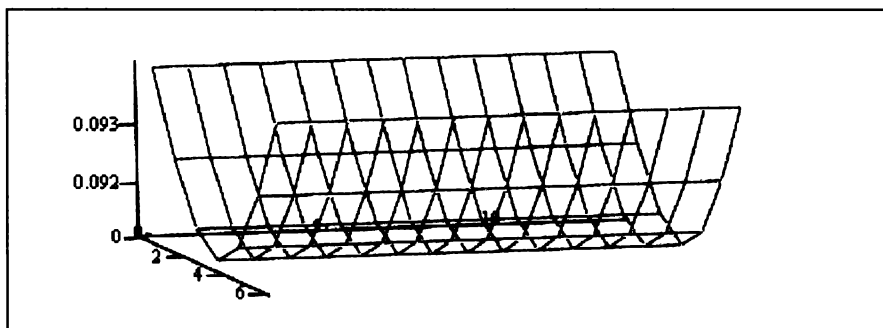
$$\mathrm{XYZ}\!\left(xyz_{pw3c}{}^{(2)},98,14\right)$$

Figure B-1. Nominal and perturbed model top surface nodes for basis set (continued)

98
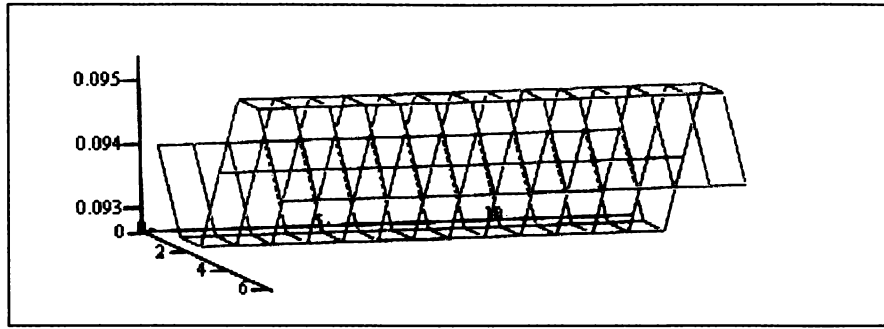
$$XYZ\left(xyz_{pw5s}^{\langle 2\rangle},98,14\right)$$
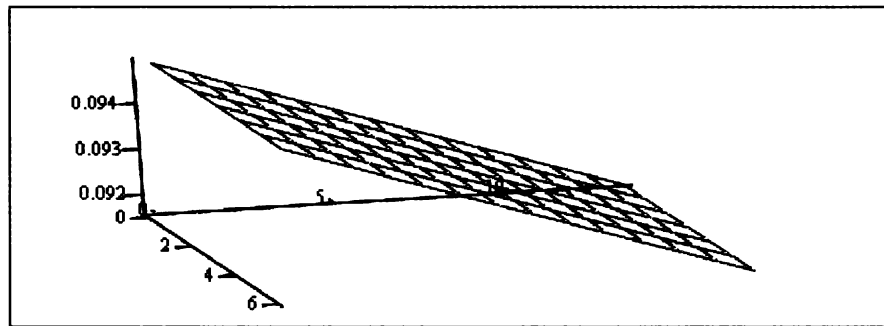
$$XYZ\left(xyz_{p11}^{\langle 2\rangle},98,14\right)$$
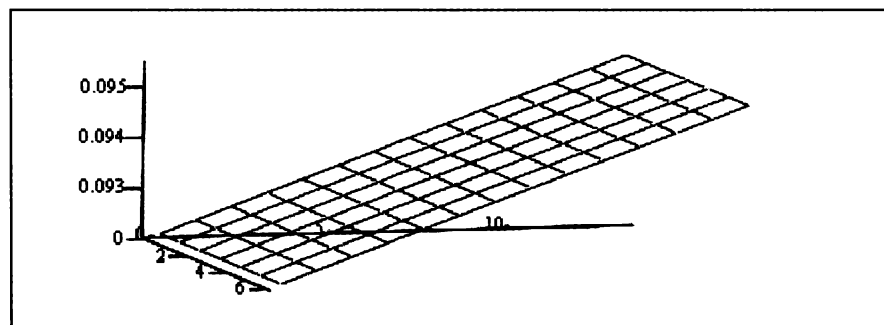
$$XYZ\left(xyz_{p21}^{\langle 2\rangle},98,14\right)$$

Figure B-1. Nominal and perturbed model top surface nodes for basis set (continued)
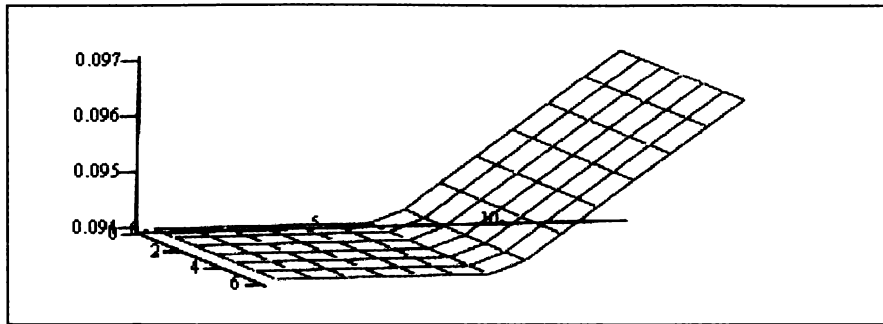
$$XYZ\left(xyz_{g1xy}^{(2)},98,14\right)$$
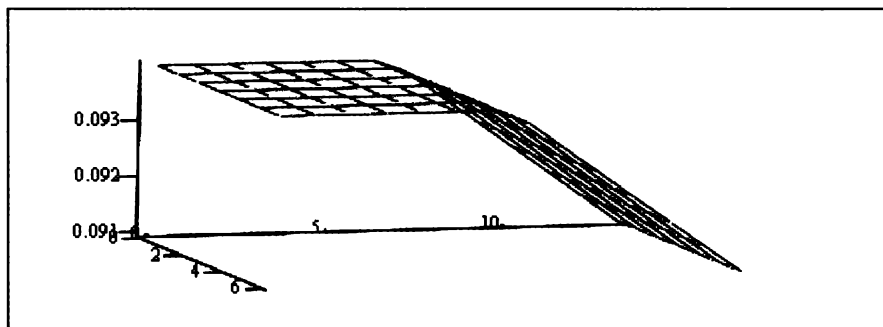
$$XYZ\left(xyz_{g2xy}^{(2)},98,14\right)$$
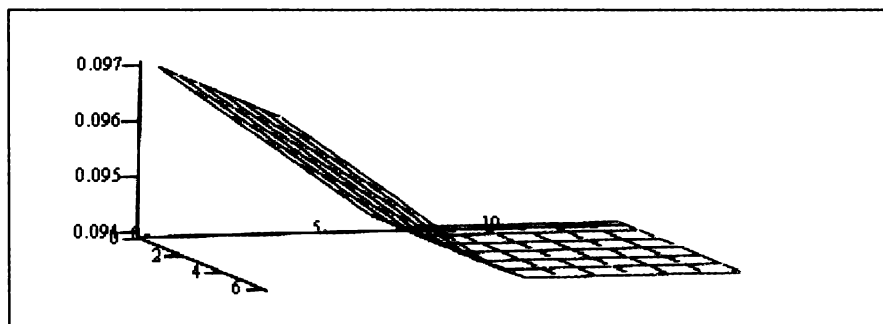
$$XYZ\left(xyz_{g3xy}^{(2)},98,14\right)$$

Figure B-1. Nominal and perturbed model top surface nodes for basis set (continued)

100
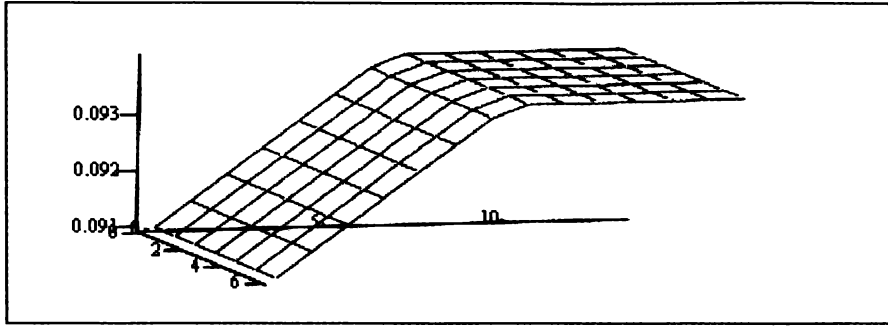
$$XYZ\left(xyz_{g4xy}^{(2)}, 98, 14\right)$$
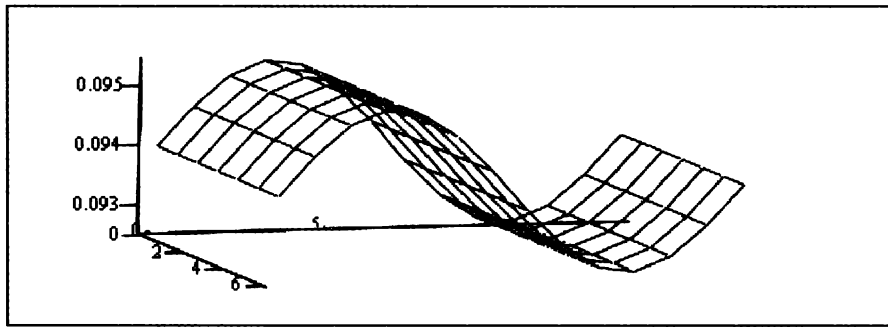
$$XYZ\left(xyz_{p31}^{(2)}, 98, 14\right)$$
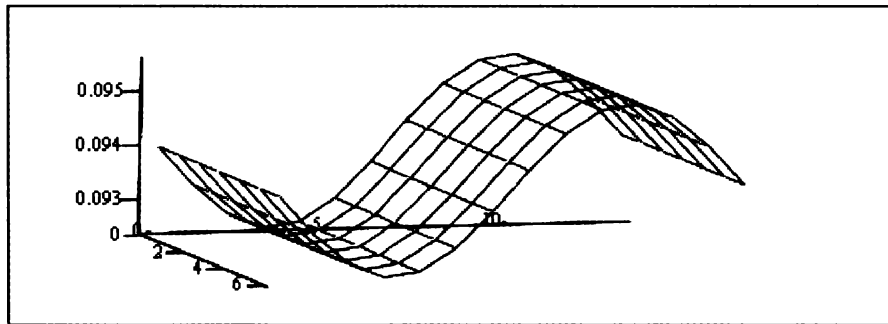
$$XYZ\left(xyz_{p41}^{(2)}, 98, 14\right)$$

Figure B-1. Nominal and perturbed model top surface nodes for basis set (continued)
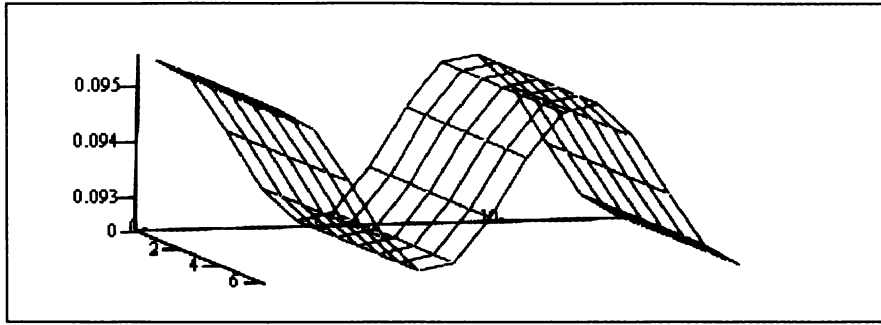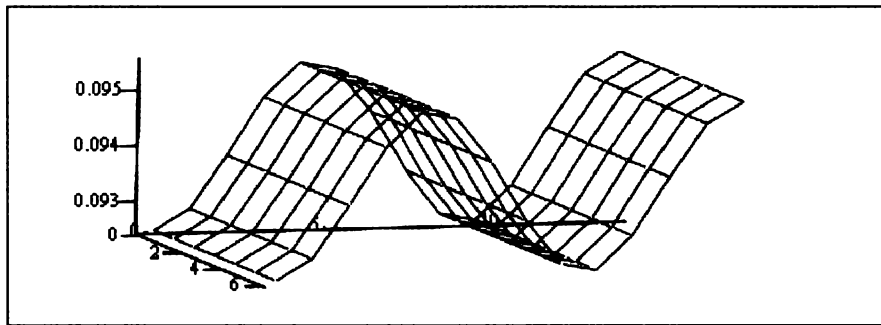
$$XYZ\left(xyz_{p12c}^{\langle 2\rangle}, 98, 14\right)$$

$$XYZ\left(xyz_{p13c}^{\langle 2\rangle}, 98, 14\right)$$
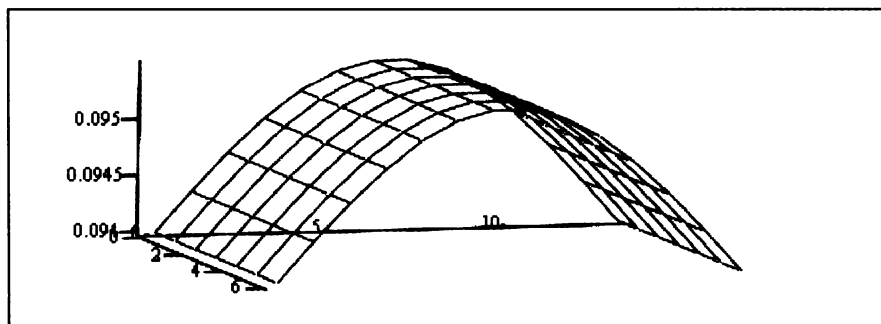
$$XYZ\left(xyz_{p13s}^{\langle 2\rangle}, 98, 14\right)$$

Figure B-1. Nominal and perturbed model top surface nodes for basis set (continued)
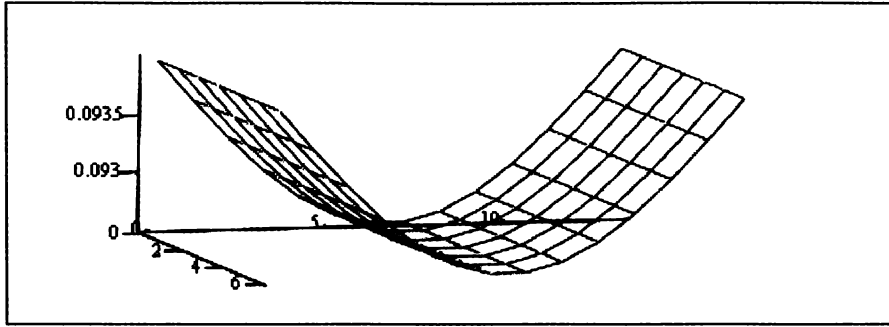
$$\mathrm{XYZ}\!\left({xyz_{\mathrm{pl4s}}}^{(2)}, 98, 14\right)$$
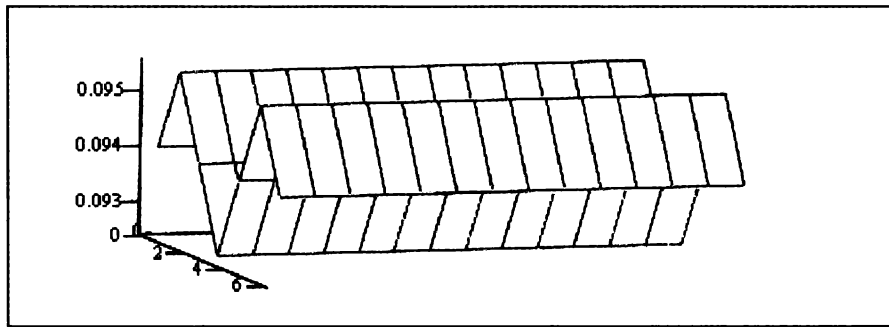
$$\mathrm{XYZ}\!\left({xyz_{\mathrm{pw6s}}}^{(2)}, 98, 14\right)$$
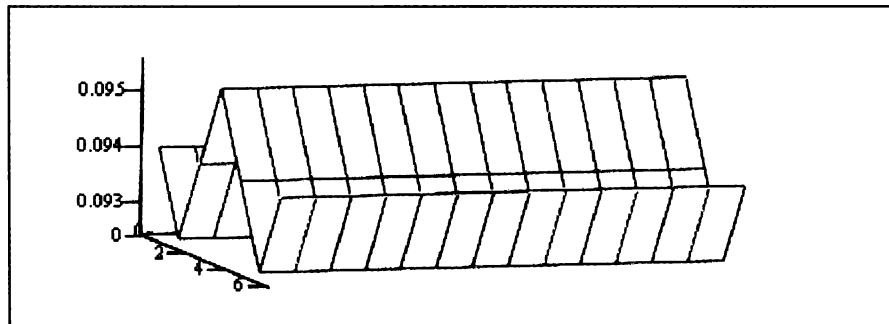
$$\mathrm{XYZ}\!\left({xyz_{\mathrm{pw7s}}}^{(2)}, 98, 14\right)$$

Figure 1

Figure B-1. Nominal and perturbed model top surface nodes for basis set (continued)

Appendix C
Model Updating Code for Geometric Updating

Programs:

This program filters out the ux and uz components for comparsion with the test vector.

$$UYMode(A) := \begin{vmatrix} nc \leftarrow cols(A) \\ j \leftarrow 2 \\ \text{for } i \in 1..\dfrac{nc}{3} \\ \quad \begin{vmatrix} n \leftarrow j \\ B^{\langle i \rangle} \leftarrow A^{\langle n \rangle} \\ j \leftarrow j + 3 \end{vmatrix} \\ B \end{vmatrix}$$

Preapares a mode vector for either graphing or analysis

$$XYZ(\Phi, nr, nc) := \begin{vmatrix} cc \leftarrow 1 \\ rc \leftarrow 0 \\ \text{for } i \in 1..nr \\ \quad \begin{vmatrix} rc \leftarrow rc + 1 \\ M_{cc, rc} \leftarrow \Phi_i \\ \text{if } rc \geq nc \\ \quad \begin{vmatrix} cc \leftarrow cc + 1 \\ rc \leftarrow 0 \end{vmatrix} \end{vmatrix} \\ M \end{vmatrix}$$

This program extracts the test points for the model and simulated test data

$$TP(A, c) := \begin{vmatrix} n \leftarrow cols(A) \\ m \leftarrow rows(c) \\ \text{for } j \in 1..n \\ \quad \text{for } i \in 1..m \\ \qquad B_{i, j} \leftarrow A_{(c_i), j} \\ B \end{vmatrix}$$

This program restacks the model into a vector after the interpolation has been compeleted.

$$\text{Vect}(A) := \begin{vmatrix} nr \leftarrow \text{rows}(A) \\ nc \leftarrow \text{cols}(A) \\ nv \leftarrow nc \cdot nr \\ k \leftarrow 1 \\ j \leftarrow 1 \\ \text{for } i \in 1..nv \\ \quad \begin{vmatrix} V_i \leftarrow A_{k,j} \\ j \leftarrow j + 1 \\ \text{if } j > nc \\ \quad \begin{vmatrix} k \leftarrow k + 1 \\ j \leftarrow 1 \end{vmatrix} \\ k \leftarrow 1 \quad \text{if } k > nr \end{vmatrix} \\ V \end{vmatrix}$$

Modal Assurance Criteria for matching model and test modes.

$$\text{MAC}(A,B) := \begin{vmatrix} nra \leftarrow \text{rows}(A) \\ nca \leftarrow \text{cols}(A) \\ nrb \leftarrow \text{rows}(B) \\ ncb \leftarrow \text{cols}(B) \\ \text{for } j \in 1..ncb \\ \quad \text{for } i \in 1..nca \\ \quad \quad \begin{vmatrix} MN_{i,j} \leftarrow A^{\langle i \rangle} \cdot B^{\langle j \rangle} \\ AL_{i,j} \leftarrow A^{\langle i \rangle} \cdot A^{\langle i \rangle} \\ BL_{i,j} \leftarrow B^{\langle j \rangle} \cdot B^{\langle j \rangle} \\ MC_{i,j} \leftarrow \dfrac{\left(\left|MN_{i,j}\right|\right)^2}{AL_{i,j} \cdot BL_{i,j}} \end{vmatrix} \\ MC \end{vmatrix}$$

Create a permutation matrix to reorder the modes that have beenmatched by the modal assurance criterion.

$$\text{zMAC}(A) := \begin{vmatrix} nc \leftarrow \text{cols}(A) \\ nr \leftarrow \text{rows}(A) \\ \text{for } j \in 1..nc \\ \quad \text{for } i \in 1..nr \\ \quad \quad \begin{vmatrix} B_{i,j} \leftarrow 1 \quad \text{if } A_{i,j} \geq .948 \\ B_{i,j} \leftarrow 0 \quad \text{otherwise} \end{vmatrix} \\ B \end{vmatrix}$$

$$\text{EzeroMAC}(V) := \begin{vmatrix} i \leftarrow 1 \\ \text{for } j \in 1..\text{cols}(V) \\ \quad \text{if } \left(\max\left(V^{\langle j \rangle}\right) \neq 0\right) \\ \quad \quad \begin{vmatrix} U^{\langle i \rangle} \leftarrow V^{\langle j \rangle} \\ i \leftarrow i + 1 \end{vmatrix} \\ U \end{vmatrix}$$

This program completes the interpolation of the model at the test points

$$\text{InterpTest}\left(M, x_m, z_m, x_{tc}, z_{tc}\right) :=$$
$$\begin{vmatrix} \text{nmc} \leftarrow \text{cols}(M) \\ \text{nmr} \leftarrow \text{rows}(M) \\ \text{nxt} \leftarrow \text{rows}\left(x_{tc}\right) \\ \text{nxm} \leftarrow \text{rows}\left(x_m\right) \\ \text{nzt} \leftarrow \text{rows}\left(z_{tc}\right) \\ \text{for } k \in 1..\text{nmc} \\ \quad \begin{vmatrix} Mv \leftarrow \text{XYZ}\left(M^{\langle k \rangle}, \text{nmr}, \text{nxm}\right) \\ \text{for } j \in 1..\text{nxt} \\ \quad \text{for } i \in 1..\text{nzt} \\ \quad\quad \text{Min}_{i,j} \leftarrow \text{polin2}\left(z_m, x_m, Mv, z_{tc_i}, x_{tc_j}\right)1 \\ \text{Mtp}^{\langle k \rangle} \leftarrow \text{Vect}(\text{Min}) \end{vmatrix} \\ \text{Mtp} \end{vmatrix}$$

$$\text{Unwrap}(M) :=$$
$$\begin{vmatrix} V \leftarrow M^{\langle 1 \rangle} \\ \text{for } i \in 2..\text{cols}(M) \quad \text{if cols}(M) > 1 \\ \quad V \leftarrow \text{stack}\left(V, M^{\langle i \rangle}\right) \\ V \end{vmatrix}$$

This program determine the appropriate sign the test mode shape at the measurement points based on the sign of the model mode shhape at the test point loaction. The rationale for this is that the mode shapes are simalar.

$$\text{TestM}(A, M) :=$$
$$\begin{vmatrix} \text{nc} \leftarrow \text{cols}(M) \\ \text{nr} \leftarrow \text{rows}(M) \\ \text{for } j \in 1..\text{nc} \\ \quad \text{for } i \in 1..\text{nr} \\ \quad\quad Mt_{i,j} \leftarrow \dfrac{A_{i,j}}{\left|A_{i,j}\right|} \cdot M_{i,j} \\ \text{Mt} \end{vmatrix}$$

107

This program scales the test vector point for point by the ratio of the maximum Uy of the model mode to the test Uy at the loaction of the model maximum

$$\text{ScaleTest}(M,T) := \begin{vmatrix} \text{nc} \leftarrow \text{cols}(M) \\ \text{for } i \in 1..\text{nc} \\ \quad \begin{vmatrix} \text{maxM} \leftarrow \max\left(M^{\langle i \rangle}\right) \text{ if } \left(\max\left(M^{\langle i \rangle}\right) \neq 0\right) \wedge \left(\max\left(M^{\langle i \rangle}\right) \geq \left|\min\left(M^{\langle i \rangle}\right)\right|\right) \\ \text{maxM} \leftarrow \min\left(M^{\langle i \rangle}\right) \text{ otherwise} \\ \text{Tm} \leftarrow T^{\langle i \rangle} \\ j \leftarrow \text{match}\left(\text{maxM}, M^{\langle i \rangle}\right) \\ \text{sf} \leftarrow \dfrac{\text{maxM}}{\text{Tm}_{j_1, 1}} \\ \text{TS}^{\langle i \rangle} \leftarrow \text{sf} \cdot T^{\langle i \rangle} \end{vmatrix} \\ \text{TS} \end{vmatrix}$$

This program ensures that the test and model eigenvectors have the same phase angle

$$\text{Phase}(M,N) := \begin{vmatrix} n \leftarrow \text{cols}(M) \\ m \leftarrow \text{rows}(M) \\ \text{for } j \in 1..n \\ \quad \text{for } i \in 1..m \\ \qquad \begin{vmatrix} a \leftarrow M_{i,j} - N_{i,j} \\ D_{i,j} \leftarrow (-1 \cdot N)_{i,j} \text{ if } |a| > \left|N_{i,j}\right| \\ D_{i,j} \leftarrow N_{i,j} \text{ otherwise} \end{vmatrix} \\ D \end{vmatrix}$$

This program determine the appropriate sign the test mode shape at the measurement points based on the sign of the model mode shape at the test point loaction. The rationale for this is that the mode shapes are simalar.

$$\text{TestM}(A,M) := \begin{vmatrix} \text{nc} \leftarrow \text{cols}(M) \\ \text{nr} \leftarrow \text{rows}(M) \\ \text{for } j \in 1..\text{nc} \\ \quad \text{for } i \in 1..\text{nr} \\ \qquad \text{Mt}_{i,j} \leftarrow \dfrac{1 \cdot A_{i,j}}{\left|A_{i,j}\right|} \cdot M_{i,j} \\ \text{Mt} \end{vmatrix}$$

$$\text{Phase}(M, N) := \begin{array}{|l} n \leftarrow \text{cols}(M) \\ m \leftarrow \text{rows}(M) \\ \text{for } j \in 1 .. n \\ \quad \begin{array}{|l} \text{for } i \in 1 .. m \\ \quad \begin{array}{|l} a \leftarrow M_{i,j} - N_{i,j} \\ D_{i,j} \leftarrow (-1 \cdot N)_{i,j} \quad \text{if } |a| > |M_{i,j}| \\ D_{i,j} \leftarrow N_{i,j} \quad \text{otherwise} \end{array} \end{array} \\ D \end{array}$$

This program scales the test vector point for point by the ratio of the maximum Uy of the model mode to the test Uy at the loaction of the model maximum

$$\text{ScaleTest}(M, T) := \begin{array}{|l} nc \leftarrow \text{cols}(M) \\ \text{for } i \in 1 .. nc \\ \quad \begin{array}{|l} \text{maxM} \leftarrow \max\left(M^{\langle i \rangle}\right) \quad \text{if } \left(\max\left(M^{\langle i \rangle}\right) \neq 0\right) \wedge \left(\max\left(M^{\langle i \rangle}\right) \geq \left|\min\left(M^{\langle i \rangle}\right)\right|\right) \\ \text{maxM} \leftarrow \min\left(M^{\langle i \rangle}\right) \quad \text{otherwise} \\ Tm \leftarrow T^{\langle i \rangle} \\ j \leftarrow \text{match}\left(\text{maxM}, M^{\langle i \rangle}\right) \\ sf \leftarrow \dfrac{\text{maxM}}{Tm_{j_1, 1}} \\ msf \leftarrow \dfrac{Tm \cdot M^{\langle i \rangle}}{M^{\langle i \rangle} \cdot M^{\langle i \rangle}} \\ TS^{\langle i \rangle} \leftarrow msf \cdot T^{\langle i \rangle} \end{array} \\ TS \end{array}$$

Builds simulation cases for noisy eigenvectors:

$$\text{Noise}(EV, nL, nf, nl) := \begin{array}{|l} n \leftarrow \text{rows}(EV) \\ m \leftarrow \text{cols}(EV) \\ \text{for } j \in 1 .. m \\ \quad \begin{array}{|l} \text{for } i \in 1 .. n \\ \quad \begin{array}{|l} NV_{i,j} \leftarrow EV_{i,j} \quad \text{if } (j < nf) \vee (j > nl) \\ NV_{i,j} \leftarrow EV_{i,j} + EV_{i,j} \cdot \left(\dfrac{nL}{2} - \text{rnd}(nL)\right) \quad \text{otherwise} \end{array} \end{array} \\ NV \end{array}$$

$$\text{Unwrap}(M) := \begin{array}{|l} V \leftarrow M^{\langle 1 \rangle} \\ \text{for } i \in 2 .. \text{cols}(M) \quad \text{if } \text{cols}(M) > 1 \\ \quad V \leftarrow \text{stack}\left(V, M^{\langle i \rangle}\right) \\ V \end{array}$$

Separate the Geometry from the modes:

$$xyz_{nom} := \text{submatrix}(MNOM, 1, \text{rows}(MNOM), 1, 3)$$

$$xyz_{p1w} := \text{submatrix}(P1WMODE, 1, \text{rows}(P1WMODE), 1, 3)$$

$$xyz_{p2w} := \text{submatrix}(P2WMODE, 1, \text{rows}(P1WMODE), 1, 3)$$

$$xyz_{p3w} := \text{submatrix}(P3WMODE, 1, \text{rows}(P3WMODE), 1, 3)$$

$$xyz_{p4w} := \text{submatrix}(P4WMODE, 1, \text{rows}(P4WMODE), 1, 3)$$

$$xyz_{p1l} := \text{submatrix}(P1LMODE, 1, \text{rows}(P1LMODE), 1, 3)$$

$$xyz_{p2l} := \text{submatrix}(P2LMODE, 1, \text{rows}(P2LMODE), 1, 3)$$

$$xyz_{p3l} := \text{submatrix}(P3LMODE, 1, \text{rows}(P3LMODE), 1, 3)$$

$$xyz_{p4l} := \text{submatrix}(P4LMODE, 1, \text{rows}(P4LMODE), 1, 3)$$

$$xyz_{stp} := \text{submatrix}(TPMODES, 1, \text{rows}(TPMODES), 1, 3)$$

$$xyz_{pl3s} := \text{submatrix}(pl3s, 1, \text{rows}(pa4w), 1, 3) \qquad xyz_{pl2c} := \text{submatrix}(pl2c, 1, \text{rows}(pa1w), 1, 3)$$

$$xyz_{pl4s} := \text{submatrix}(pl4s, 1, \text{rows}(pa3w), 1, 3) \qquad xyz_{pl3c} := \text{submatrix}(pl3c, 1, \text{rows}(pa2w), 1, 3)$$

$$xyz_{pw6s} := \text{submatrix}(pw6s, 1, \text{rows}(pa4w), 1, 3) \qquad xyz_{pw3c} := \text{submatrix}(pw3c, 1, \text{rows}(pa1w), 1, 3)$$

$$xyz_{pw7s} := \text{submatrix}(pw7s, 1, \text{rows}(pa3w), 1, 3) \qquad xyz_{pw5s} := \text{submatrix}(pw5s, 1, \text{rows}(pa2w), 1, 3)$$

$$xyz_{pa1w} := \text{submatrix}(pa1w, 1, \text{rows}(pa1w), 1, 3) \qquad xyz_{pa2w} := \text{submatrix}(pa2w, 1, \text{rows}(pa2w), 1, 3)$$

$$xyz_{pa3w} := \text{submatrix}(pa3w, 1, \text{rows}(pa3w), 1, 3) \qquad xyz_{pa4w} := \text{submatrix}(pa4w, 1, \text{rows}(pa4w), 1, 3)$$

$$xyz_{g1xy} := \text{submatrix}(g1xy, 1, \text{rows}(g1xy), 1, 3) \qquad xyz_{g2xy} := \text{submatrix}(g2xy, 1, \text{rows}(g2xy), 1, 3)$$

$$xyz_{g3xy} := \text{submatrix}(g3xy, 1, \text{rows}(g3xy), 1, 3) \qquad xyz_{g4xy} := \text{submatrix}(g4xy, 1, \text{rows}(g4xy), 1, 3)$$

110

Extract y-coordinate mode components:

First extract the modes from the input files

$$M_{nom} := submatrix(MNOM, 1, rows(MNOM), 6, cols(MNOM))$$

$$M_{p1w} := submatrix(P1WMODE, 1, rows(P1WMODE), 6, cols(P1WMODE))$$

$$M_{p2w} := submatrix(P2WMODE, 1, rows(P1WMODE), 6, cols(P2WMODE))$$

$$M_{p3w} := submatrix(P3WMODE, 1, rows(P3WMODE), 6, cols(P3WMODE))$$

$$M_{p4w} := submatrix(P4WMODE, 1, rows(P4WMODE), 6, cols(P4WMODE))$$

$$M_{p1l} := submatrix(P1LMODE, 1, rows(P1LMODE), 6, cols(P1LMODE))$$

$$M_{p2l} := submatrix(P2LMODE, 1, rows(P2LMODE), 6, cols(P2LMODE))$$

$$M_{p3l} := submatrix[P3LMODE, 1, rows(P3LMODE), 6, (cols(P3LMODE))]$$

$$M_{p4l} := submatrix(P4LMODE, 1, rows(P4LMODE), 6, cols(P4LMODE))$$

$$M_{tp} := submatrix(TPMODES, 1, rows(TPMODES), 6, cols(TPMODES))$$

$$M_{pa1w} := submatrix(pa1w, 1, rows(pa1w), 6, cols(pa1w))$$

$$M_{pa2w} := submatrix(pa2w, 1, rows(pa2w), 6, cols(pa2w))$$

$$M_{pa3w} := submatrix(pa3w, 1, rows(pa3w), 6, cols(pa3w))$$

$$M_{pa4w} := submatrix(pa4w, 1, rows(pa4w), 6, cols(pa4w))$$

$$M_{tp} := submatrix(TPMODES, 1, rows(TPMODES), 6, cols(TPMODES))$$

$M_{pa1w} := submatrix(pa1w, 1, rows(pa1w), 6, cols(pa1w))$ $M_{pl2c} := submatrix(pl2c, 1, rows(pa1w), 6, cols(pa1w))$

$M_{pa2w} := submatrix(pa2w, 1, rows(pa2w), 6, cols(pa2w))$ $M_{pl3c} := submatrix(pl3c, 1, rows(pa2w), 6, cols(pa2w))$

$M_{pa3w} := submatrix(pa3w, 1, rows(pa3w), 6, cols(pa3w))$ $M_{pl3s} := submatrix(pl3s, 1, rows(pa3w), 6, cols(pa3w))$

$M_{pa4w} := submatrix(pa4w, 1, rows(pa4w), 6, cols(pa4w))$ $M_{pl4s} := submatrix(pl4s, 1, rows(pa4w), 6, cols(pa4w))$

$$M_{pw3c} := submatrix(pw3c, 1, rows(pa1w), 6, cols(pa1w))$$

$M_{g1xy} := submatrix(g1xy, 1, rows(g1xy), 6, cols(g1xy))$ $M_{pw5s} := submatrix(pw5s, 1, rows(pa2w), 6, cols(pa2w))$

$M_{g2xy} := submatrix(g2xy, 1, rows(g2xy), 6, cols(g2xy))$ $M_{pw6s} := submatrix(pw6s, 1, rows(pa3w), 6, cols(pa3w))$

$M_{g3xy} := \text{submatrix} (g3xy, 1, \text{rows} (g3xy), 6, \text{cols}(g3xy))$ $\quad$ $M_{pw7s} := \text{submatrix} (pw7s, 1, \text{rows} (pa4w), 6, \text{cols}(pa4w))$

$M_{g4xy} := \text{submatrix} (g4xy, 1, \text{rows} (g4xy), 6, \text{cols}(g4xy))$

Separate the y-components from the modes

$MY_{nom} := \text{UYMode} (M_{nom})$ $\qquad$ $MY_{p1w} := \text{UYMode} (M_{p1w})$ $\qquad$ $MY_{pl2c} := 1 \cdot \text{UYMode} (M_{pl2c})$

$MY_{p2w} := \text{UYMode} (M_{p2w})$ $\qquad$ $MY_{p3w} := \text{UYMode} (M_{p3w})$ $\qquad$ $MY_{pl3s} := 1 \cdot \text{UYMode} (M_{pl3s})$

$MY_{p4w} := \text{UYMode} (M_{p4w})$ $\qquad$ $MY_{pll} := \text{UYMode} (M_{pll})$ $\qquad$ $MY_{pl3c} := 1 \cdot \text{UYMode} (M_{pl3c})$

$MY_{p2l} := \text{UYMode} (M_{p2l})$ $\qquad$ $MY_{p3l} := \text{UYMode} (M_{p3l})$

$\qquad\qquad\qquad\qquad\qquad\qquad\qquad\qquad\qquad\qquad MY_{pl4s} := 1 \cdot \text{UYMode} (M_{pl4s})$

$MY_{p4l} := \text{UYMode} (M_{p4l})$ $\qquad\qquad$ $MY_{tpnf} := \text{UYMode} (M_{tp})$

$MY_{pw3c} := 1.0 \, \text{UYMode} (M_{pw3c})$ $\qquad$ $MY_{pw5s} := 1.0 \, \text{UYMode} (M_{pw5s})$

$MY_{pw6s} := 1.0 \, \text{UYMode} (M_{pw6s})$ $\qquad$ $MY_{pw7s} := 1.0 \, \text{UYMode} (M_{pw7s})$

This equation adds noise to the test modes:-> $\qquad$ $MY_{tp} := \text{Noise} (MY_{tpnf}, .0, 1, 13)$

$MY_{pa1w} := \text{UYMode} (M_{pa1w})$ $\qquad$ $MY_{pa2w} := \text{UYMode} (M_{pa2w})$

$MY_{pa3w} := \text{UYMode} (M_{pa3w})$ $\qquad$ $MY_{pa4w} := \text{UYMode} (M_{pa4w})$

$MY_{g1xy} := 1 \cdot \text{UYMode} (M_{g1xy})$ $\qquad$ $MY_{g2xy} := \text{UYMode} (M_{g2xy})$

$MY_{g3xy} := 1 \cdot \text{UYMode} (M_{g3xy})$ $\qquad$ $MY_{g4xy} := \text{UYMode} (M_{g4xy})$

Next provide the simulated test measurement points for the test plates and the coordinates for the Model

$$x_t := \begin{pmatrix} .25 \\ 2 \\ 3.75 \end{pmatrix} \qquad z_t := \begin{pmatrix} 0 \\ 2.165 \\ 4.29 \\ 6.417 \\ 7.48 \\ 8.268 \end{pmatrix}^{\blacksquare}$$

$z_m := \text{submatrix} (MNOM, 1, 14, 3, 3)$

$nr := \text{rows} (xyz_{nom})$ $\qquad$ $nc := 14$

$i := 1 .. \dfrac{nr}{nc}$

$x_{m_i} := MNOM_{nc \cdot i, 1}$

Z coordinates without z=0 at the boundary:--> $\qquad$ $z_t := \begin{pmatrix} 2.165 \\ 4.29 \\ 6.417 \\ 7.48 \\ 8.268 \end{pmatrix}$

$x_m^T = (0 \quad 0.667 \quad 1.333 \quad 2 \quad 2.667 \quad 3.333 \quad 4)$

$z_m^T =$

	1	2	3	4	5	6	7	8	9	10
1	0	0.654	1.308	1.962	2.615	3.269	3.923	4.577	5.231	5.885

$$x_t := \text{submatrix}\left(x_t, 1, 3, 1, 1\right)$$

$$z_t := \text{submatrix}\left(z_t, 1, 5, 1, 1\right)$$

$$x_t = \begin{pmatrix} 0.25 \\ 2 \\ 3.75 \end{pmatrix} \qquad z_t = \begin{pmatrix} 2.165 \\ 4.29 \\ 6.417 \\ 7.48 \\ 8.268 \end{pmatrix}$$

Determine the interpolated model modal displacements at the test points using spline interpolation

$$MY_{tnom} := \text{InterpTest}\left(MY_{noms}, z_m, x_m, z_t, x_t\right) \qquad MY_{tp1l} := \text{InterpTest}\left(MY_{p1l}, z_m, x_m, z_t, x_t\right)$$

$$MY_{tp1w} := \text{InterpTest}\left(MY_{p1w}, z_m, x_m, z_t, x_t\right) \qquad MY_{tp2l} := \text{InterpTest}\left(MY_{p2l}, z_m, x_m, z_t, x_t\right)$$

$$MY_{tp2w} := \text{InterpTest}\left(MY_{p2w}, z_m, x_m, z_t, x_t\right) \qquad MY_{tp3l} := \text{InterpTest}\left(MY_{p3l}, z_m, x_m, z_t, x_t\right)$$

$$MY_{tp3w} := \text{InterpTest}\left(MY_{p3w}, z_m, x_m, z_t, x_t\right) \qquad MY_{tp4l} := \text{InterpTest}\left(MY_{p4l}, z_m, x_m, z_t, x_t\right)$$

$$MY_{tp4w} := \text{InterpTest}\left(MY_{p4w}, z_m, x_m, z_t, x_t\right) \qquad MY_{TP} := \text{InterpTest}\left(MY_{tp}, z_m, x_m, z_t, x_t\right)$$

$$MY_{tpa1w} := \text{InterpTest}\left(MY_{pa1w}, z_m, x_m, z_t, x_t\right) \qquad MY_{tpa2w} := \text{InterpTest}\left(MY_{pa2w}, z_m, x_m, z_t, x_t\right)$$

$$MY_{tpa3w} := \text{InterpTest}\left(MY_{pa3w}, z_m, x_m, z_t, x_t\right) \qquad MY_{tpa4w} := \text{InterpTest}\left(MY_{pa4w}, z_m, x_m, z_t, x_t\right)$$

$$MY_{tg1xy} := \text{InterpTest}\left(MY_{g1xy}, z_m, x_m, z_t, x_t\right) \qquad MY_{tg2xy} := \text{InterpTest}\left(MY_{g2xy}, z_m, x_m, z_t, x_t\right)$$

$$MY_{tg3xy} := \text{InterpTest}\left(MY_{g3xy}, z_m, x_m, z_t, x_t\right) \qquad MY_{tg4xy} := \text{InterpTest}\left(MY_{g4xy}, z_m, x_m, z_t, x_t\right)$$

$$MY_{tpw3c} := \text{InterpTest}\left(MY_{pw3c}, z_m, x_m, z_t, x_t\right) \qquad MY_{tpl2c} := \text{InterpTest}\left(MY_{pl2c}, z_m, x_m, z_t, x_t\right)$$

$$MY_{tpw5s} := \text{InterpTest}\left(MY_{pw5s}, z_m, x_m, z_t, x_t\right) \qquad MY_{tpl3c} := \text{InterpTest}\left(MY_{pl3c}, z_m, x_m, z_t, x_t\right)$$

$$MY_{tpw6s} := \text{InterpTest}\left(MY_{pw6s}, z_m, x_m, z_t, x_t\right) \qquad MY_{tpl3s} := \text{InterpTest}\left(MY_{pl3s}, z_m, x_m, z_t, x_t\right)$$

$$MY_{tpw7s} := \text{InterpTest}\left(MY_{pw7s}, z_m, x_m, z_t, x_t\right) \qquad MY_{tpl4s} := \text{InterpTest}\left(MY_{pl4s}, z_m, x_m, z_t, x_t\right)$$

Use the sorted nominal modes to reorder the test plate data.

Test modes ready for testing method

$$\text{MACYnYt} := \text{MAC}\left(\text{MY}_{\text{tnom}}, \text{MY}_{\text{TP}}\right)$$

$$\text{Pz} := \text{zMAC}(\text{MACYnYt})$$

$$\text{MY}_{\text{tps}} := \text{MY}_{\text{TP}} \cdot \text{Pz}^{\text{T}}$$

$$\text{MY}_{\text{tstP}} := \text{Phase}\left(\text{MY}_{\text{tnom}}, \text{MY}_{\text{tps}}\right)$$

P1W modes ready for testing method (correct phase).

$$\text{MCYtYw1} := \text{MAC}\left(\text{MY}_{\text{tstP}}, \text{MY}_{\text{tp1w}}\right)$$

$$\text{P1w} := \text{zMAC}(\text{MCYtYw1})$$

$$\text{MY1w} := \text{MY}_{\text{tp1w}} \cdot \text{P1w}^{\text{T}}$$

$$\text{MY1wp} := \text{Phase}\left(\text{MY}_{\text{tstP}}, \text{MY1w}\right)$$

P2W modes ready for testing method

$$\text{MCYtYw2} := \text{MAC}\left(\text{MY}_{\text{tstP}}, \text{MY}_{\text{tp2w}}\right)$$

$$\text{P2w} := \text{zMAC}(\text{MCYtYw2})$$

$$\text{MY2w} := \text{MY}_{\text{tp2w}} \cdot \text{P2w}^{\text{T}}$$

$$\text{MY2wp} := \text{Phase}\left(\text{MY}_{\text{tstP}}, \text{MY2w}\right)$$

P3W modes ready for testing method

$$\text{MCYtYw3} := \text{MAC}\left(\text{MY}_{\text{tstP}}, \text{MY}_{\text{tp3w}}\right)$$

$$\text{P3w} := \text{zMAC}(\text{MCYtYw3})$$

$$\text{MY3w} := \text{MY}_{\text{tp3w}} \cdot \text{P3w}^{\text{T}}$$

$$\text{MY3wp} := \text{Phase}\left(\text{MY}_{\text{tstP}}, \text{MY3w}\right)$$

P4W modes ready for testing method

$$\text{MCYtYw4} := \text{MAC}\left(\text{MY}_{\text{tstP}}, \text{MY}_{\text{tp4w}}\right)$$

$$\text{P4w} := \text{zMAC}(\text{MCYtYw4})$$

$$\text{MY4w} := \text{MY}_{\text{tp4w}} \cdot \text{P4w}^{\text{T}}$$

$$\text{MY4wp} := \text{Phase}\left(\text{MY}_{\text{tstP}}, \text{MY4w}\right)$$

P1L modes ready for testing method (correct phase).

$$\text{MCYtYl1} := \text{MAC}\left(\text{MY}_{\text{tps}}, \text{MY}_{\text{tp1l}}\right)$$

$$\text{P1L} := \text{zMAC}(\text{MCYtYl1})$$

$$\text{MY1l} := \text{MY}_{\text{tp1l}} \cdot \text{P1L}^{\text{T}}$$

$$\text{MY1lp} := \text{Phase}\left(\text{MY}_{\text{tstP}}, \text{MY1l}\right)$$

$$MY1l := MY_{tp1l} \cdot P1L^T \qquad\qquad MY1lp := Phase\left(MY_{tstP}, MY1l\right)$$

P2L modes ready for testing method

$$MCYtY12 := MAC\left(MY_{tstP}, MY_{tp2l}\right) \qquad\qquad P2l := zMAC\left(MCYtY12\right)$$

$$MY2l := MY_{tp2l} \cdot P2l^T \qquad\qquad MY2lp := Phase\left(MY_{tstP}, MY2l\right)$$

P3L modes ready for testing method

$$MCYtY13 := MAC\left(MY_{tstP}, MY_{tp3l}\right) \qquad P3l := zMAC\left(MCYtY13\right)$$

$$MY3l := MY_{tp3l} \cdot P3l^T \qquad\qquad MY3lp := Phase\left(MY_{tstP}, MY3l\right)$$

P4L modes ready for testing method

$$MCYtY14 := MAC\left(MY_{tstP}, MY_{tp4l}\right) \qquad P4l := zMAC\left(MCYtY14\right)$$

$$MY4l := MY_{tp4l} \cdot P4l^T \qquad\qquad MY4lp := Phase\left(MY_{tstP}, MY4l\right)$$

Asymmetric modes for comparison

$$MCYtY1aw := MAC\left(MY_{tstP}, MY_{tpa1w}\right) \qquad Pa1 := zMAC\left(MCYtY1aw\right)$$

$$MYa1 := MY_{tpa1w} \cdot Pa1^T \qquad\qquad MY1aw := Phase\left(MY_{tstP}, MYa1\right)$$

$$MCYtY2aw := MAC\left(MY_{tstP}, MY_{tpa2w}\right) \qquad Pa2 := zMAC\left(MCYtY2aw\right)$$

$$MYa2 := MY_{tpa2w} \cdot Pa2^T \qquad\qquad MY2aw := Phase\left(MY_{tstP}, MYa2\right)$$

$$MCYtY3aw := MAC\left(MY_{tstP}, MY_{tpa3w}\right) \qquad Pa3 := zMAC\left(MCYtY3aw\right)$$

$$MYa3 := MY_{tpa3w} \cdot Pa3^T \qquad\qquad MY3aw := Phase\left(MY_{tstP}, MYa3\right)$$

$$MCYtY4aw := MAC\left(MY_{tstP}, MY_{tpa4w}\right) \qquad Pa4 := zMAC\left(MCYtY4aw\right)$$

$$MYa4 := MY_{tpa4w} \cdot Pa4^T \qquad\qquad MY4aw := Phase\left(MY_{tstP}, MYa4\right)$$

$$\text{MCYtYg1xy} := \text{MAC}\left(\text{MY}_{tstP}, \text{MY}_{tg1xy}\right) \qquad \text{Pg1} := \text{zMAC}(\text{MCYtYg1xy})$$

$$\text{MYg1} := \text{MY}_{tg1xy} \cdot \text{Pg1}^T$$

$$\text{MYg1xy} := \text{Phase}\left(\text{MY}_{tstP}, \text{MYg1}\right)$$

$$\text{MCYtYg2} := \text{MAC}\left(\text{MY}_{tstP}, \text{MY}_{tg2xy}\right) \qquad \text{Pg2} := \text{zMAC}(\text{MCYtYg2})$$

$$\text{MYg2} := \text{MY}_{tg2xy} \cdot \text{Pg2}^T \qquad\qquad \text{MYg2xy} := \text{Phase}\left(\text{MY}_{tstP}, \text{MYg2}\right)$$

$$\text{MCYtYg3xy} := \text{MAC}\left(\text{MY}_{tstP}, \text{MY}_{tg3xy}\right) \qquad \text{Pg3} := \text{zMAC}(\text{MCYtYg3xy})$$

$$\text{MYg3} := \text{MY}_{tg3xy} \cdot \text{Pg3}^T \qquad\qquad \text{MYg3xy} := \text{Phase}\left(\text{MY}_{tstP}, \text{MYg3}\right)$$

$$\text{MCYtYg4xy} := \text{MAC}\left(\text{MY}_{tstP}, \text{MY}_{tg4xy}\right) \qquad \text{Pg4} := \text{zMAC}(\text{MCYtYg4xy})$$

$$\text{MYg4} := \text{MY}_{tg4xy} \cdot \text{Pg4}^T \qquad\qquad \text{MYg4xy} := \text{Phase}\left(\text{MY}_{tstP}, \text{MYg4}\right)$$

$$\text{MAC}_{pw3c} := \text{MAC}\left(\text{MY}_{tpw3c}, \text{MY}_{tstP}\right) \qquad \text{zpw3c} := \text{zMAC}\left(\text{MAC}_{pw3c}\right)$$

$$\text{UY}_{pw3c} := \text{MY}_{tpw3c} \cdot \text{zpw3c} \qquad\qquad \text{Upw3c} := \text{Phase}\left(\text{MY}_{tstP}, \text{UY}_{pw3c}\right)$$

$$\text{MAC}_{pw5s} := \text{MAC}\left(\text{MY}_{tpw5s}, \text{MY}_{tstP}\right) \qquad \text{zpw5s} := \text{zMAC}\left(\text{MAC}_{pw5s}\right)$$

$$\text{UY}_{pw5s} := \text{MY}_{tpw5s} \cdot \text{zpw5s} \qquad\qquad \text{Upw5s} := \text{Phase}\left(\text{MY}_{tstP}, \text{UY}_{pw5s}\right)$$

$$\text{MAC}_{pw6s} := \text{MAC}\left(\text{MY}_{tpw6s}, \text{MY}_{tstP}\right) \qquad \text{zpw6s} := \text{zMAC}\left(\text{MAC}_{pw6s}\right)$$

$$\text{UY}_{pw6s} := \text{MY}_{tpw6s} \cdot \text{zpw6s} \qquad\qquad \text{Upw6s} := \text{Phase}\left(\text{MY}_{tstP}, \text{UY}_{pw6s}\right)$$

$$\text{MAC}_{pw7s} := \text{MAC}\left(\text{MY}_{tpw7s}, \text{MY}_{tstP}\right) \qquad \text{zpw7s} := \text{zMAC}\left(\text{MAC}_{pw7s}\right)$$

$$\text{UY}_{pw7s} := \text{MY}_{tpw7s} \cdot \text{zpw7s} \qquad\qquad \text{Upw7s} := \text{Phase}\left(\text{MY}_{tstP}, \text{UY}_{pw7s}\right)$$

$$\text{MAC}_{pl2c} := \text{MAC}\left(\text{MY}_{tpl2c}, \text{MY}_{tstP}\right) \qquad \text{zpl2c} := \text{zMAC}\left(\text{MAC}_{pl2c}\right)$$

$$\text{UY}_{pl2c} := \text{MY}_{tpl2c} \cdot \text{zpl2c} \qquad\qquad \text{Upl2c} := \text{Phase}\left(\text{MY}_{tstP}, \text{UY}_{pl2c}\right)$$

$$\text{MAC}_{pl3c} := \text{MAC}\left(\text{MY}_{tpl3c}, \text{MY}_{tstP}\right) \qquad \text{zpl3c} := \text{zMAC}\left(\text{MAC}_{pl3c}\right)$$

$$\text{UY}_{pl3c} := \text{MY}_{tpl3c} \cdot \text{zpl3c} \qquad\qquad \text{Upl3c} := \text{Phase}\left(\text{MY}_{tstP}, \text{UY}_{pl3c}\right)$$

116

$$MAC_{pl3s} := MAC\left(MY_{tpl3s}, MY_{tstP}\right) \qquad zpl3s := zMAC\left(MAC_{pl3s}\right)$$

$$UY_{pl3s} := MY_{tpl3s} \cdot zpl3s$$

$$Upl3s := Phase\left(MY_{tstP}, UY_{pl3s}\right)$$

$$MAC_{pl4s} := MAC\left(MY_{tpl4s}, MY_{tstP}\right) \qquad zpl4s := zMAC\left(MAC_{pl4s}\right)$$

$$UY_{pl4s} := MY_{tpl4s} \cdot zpl4s$$

$$Upl4s := Phase\left(MY_{tstP}, UY_{pl4s}\right)$$

Stack modes for runnign test case and strip out unmatched modes

$$Mt := Unwrap\left(MY_{tstP}\right) \qquad Mn := Unwrap\left(MY_{tnom}\right)$$

$$Mw3c := Unwrap(Upw3c)$$

$$M1w := Unwrap(MY1wp) \qquad M1L := Unwrap(MY1lp)$$

$$Mw5s := Unwrap(Upw5s)$$

$$Mw6s := Unwrap(Upw6s)$$

$$M2w := Unwrap(MY2wp) \qquad M2L := Unwrap(MY2lp)$$

$$Mw7s := Unwrap(Upw7s)$$

$$M3w := Unwrap(MY3wp) \qquad M3L := Unwrap(MY3lp)$$

$$Ml2c := Unwrap(Upl2c)$$

$$M4w := Unwrap(MY4wp) \qquad M4L := Unwrap(MY4lp)$$

$$M1a := Unwrap(MY1aw) \qquad M2a := Unwrap(MY2aw)$$

$$Ml3c := Unwrap(Upl3c)$$

$$M3a := Unwrap(MY3aw) \qquad M4a := Unwrap(MY4aw)$$

$$Ml3s := Unwrap(Upl3s)$$

$$Ml4s := Unwrap(Upl4s)$$

$$Mg1 := Unwrap(MYg1xy) \qquad Mg2 := Unwrap(MYg2xy)$$

$$Mg3 := Unwrap(MYg3xy)$$

$$Mg4 := Unwrap(MYg4xy)$$

Set up A matrix for the Least squares solution and strpping out unmatched mod

$$A := augment(Mn, M1w, M2w, M3w, M4w, M1L, M2L, M3L, M4L, M1a, M2a, M3a, M4a)$$

$$rank(A) = 13$$

The Test modes are put into the b vector:

$$b := Mt$$

Solve for the basis vector coefficents

$x := \text{geninv}(A) \cdot b$

$x^T =$	1	2	3	4	5	6
1	0.178	0.076	$5.077 \cdot 10^{-3}$	0.106	-0.335	$4.352 \cdot 10^{-3}$

$Ag := \text{augment}(Mg1, Mg2, Mg3, Mg4)$

$Geo1 := \text{augment}\left(xyz_{p1w}^{\langle 2 \rangle}, xyz_{p2w}^{\langle 2 \rangle}, xyz_{p3w}^{\langle 2 \rangle}, xyz_{p4w}^{\langle 2 \rangle} \right)$

$Geo2 := \text{augment}\left(xyz_{p1l}^{\langle 2 \rangle}, xyz_{p2l}^{\langle 2 \rangle}, xyz_{p3l}^{\langle 2 \rangle}, xyz_{p4l}^{\langle 2 \rangle} \right)$

$Geo3 := \text{augment}\left(xyz_{pa1w}^{\langle 2 \rangle}, xyz_{pa2w}^{\langle 2 \rangle}, xyz_{pa3w}^{\langle 2 \rangle}, xyz_{pa4w}^{\langle 2 \rangle} \right)$

$Geo4 := \text{augment}\left(xyz_{g1xy}^{\langle 2 \rangle}, xyz_{g2xy}^{\langle 2 \rangle}, xyz_{g3xy}^{\langle 2 \rangle}, xyz_{g4xy}^{\langle 2 \rangle} \right)$

$Gall := \text{augment}\left(xyz_{nom}^{\langle 2 \rangle}, Geo1, Geo2, Geo3, Geo4 \right)$

$Aall := \text{augment}(A, Ag)$

$\text{cols}(Aall) = 17$

$\text{rank}(Aall) = 17$

$xall := \text{geninv}(Aall) \cdot b$

$Aexw := \text{augment}(Mw3c, Mw5s, Mw6s, Mw7s)$

$Am1 := \text{augment}(A, Aexw)$

$\text{rank}(Aexw) = 4$ $AExall := \text{augment}(Aall, Aexw)$ $\text{rank}(Am1) = 17$

$\text{rank}(AExall) = 21$ $x_{ex} := \text{geninv}(AExall) \cdot b$

$xm1 := \text{geninv}(Am1) \cdot b$

$\text{rank}(Aall) = 17$

$\text{rank}(AExall) = 21$

$Aexl := \text{augment}(Ml2c, Ml3c, Ml3s, Ml4s)$

$Amf := \text{augment}(Am1, Aexl)$

$\text{rank}(Aexl) = 4$

$\text{rank}(Amf) = 21$

$xmf := \text{geninv}(Amf) \cdot b$

118

A matrix for updating solution including all 25 models:

$Axwl := augment(AExall, Aexl)$

$rows(Axwl) = 195$ $cols(Axwl) = 25$

$rank(Axwl) = 25$

$x_{ewl} := geninv(Axwl) \cdot b$

$svds(Axwl)_1 = 3.283 \times 10^3$

Condition number for Axwl is approximately 68400

$svds(Axwl)_{25} = 0.048$

$Gexw := augment\left[xyz_{pw3c}^{\langle 2 \rangle}, \left(xyz_{pw5s} \right)^{\langle 2 \rangle}, xyz_{pw6s}^{\langle 2 \rangle}, xyz_{pw7s}^{\langle 2 \rangle} \right]$

$Gnxy := augment\left(xyz_{nom}^{\langle 2 \rangle}, Geo1, Geo2, Geo3 \right)$

$Gm1 := augment(Gnxy, Gexw)$

$G_{exall} := augment(Gall, Gexw)$

$upm1 := Gm1 \cdot xm1$

$upall := Gall \cdot xall$

$Gexl := augment\left[xyz_{pl2c}^{\langle 2 \rangle}, \left(xyz_{pl3c} \right)^{\langle 2 \rangle}, xyz_{pl3s}^{\langle 2 \rangle}, xyz_{pl4s}^{\langle 2 \rangle} \right]$

$Gmf := augment(Gm1, Gexl)$

$Gawl := augment\left(G_{exall}, Gexl \right)$

$upmf := Gmf \cdot xmf$

$upexwl := Gawl \cdot x_{ewl}$

Save weighting coefficients for plotting:

$B := submatrix(MNOM, 1, rows(MNOM), 4, 5)$

$Nodeup := augment\left(MNOM^{\langle 1 \rangle}, upall, MNOM^{\langle 3 \rangle}, B \right)$

$up_{ex} := G_{exall} \cdot x_{ex}$

$sgeo := csort(geonom, 5)$

$botpl := submatrix(sgeo, 1, 98, 1, 5)$

$UPgp := stack(botpl, Nodeup)$

$UPGEO := csort(UPgp, 4)$ 119

$Gwl := XYZ(upexwl, 98, 14)$

$Gwl =$

	1	2	3	4	5	6	7	8	9
1	0.0941	0.0941	0.0941	0.0941	0.0941	0.0941	0.0941	0.0941	0.0941
2	0.0942	0.0942	0.0942	0.0942	0.0942	0.0942	0.0942	0.0942	0.0942
3	0.0941	0.0941	0.0941	0.0941	0.0941	0.0941	0.0941	0.0941	0.0941
4	0.0943	0.0943	0.0943	0.0943	0.0943	0.0943	0.0943	0.0943	0.0943
5	0.0939	0.0939	0.0939	0.0939	0.0939	0.0939	0.0939	0.0939	0.0939
6	0.0929	0.0929	0.0929	0.0929	0.0929	0.0929	0.0929	0.0929	0.0929
7	0.091	0.0909	0.0909	0.0909	0.0909	0.0909	0.0909	0.0909	0.0909

$upnodall := XYZ(upexwl, 98, 14)$ $tpnode := XYZ\left(TPMODES^{\langle 2 \rangle}, 98, 14\right)$

$$ERa := \frac{\overrightarrow{upnodall - tpnode}}{tpnode} \cdot 100$$

$ERa =$

	1	2	3	4	5	6
1	0.136	0.117	0.112	0.115	0.12	0.122
2	0.21	0.191	0.186	0.189	0.194	0.196
3	0.117	0.098	0.093	0.096	0.101	0.103
4	0.327	0.308	0.303	0.306	0.312	0.313
5	-0.086	-0.105	-0.11	-0.107	-0.102	-0.1
6	0.477	0.458	0.453	0.456	0.461	0.463
7	-0.051	-0.071	-0.076	-0.073	-0.068	-0.066

$Nodeupxl := augment\left(MNOM^{\langle 1 \rangle}, upmf, MNOM^{\langle 3 \rangle}, B\right)$

$UPgpxl := stack(botpl, Nodeupxl)$

$UPGEO := csort(UPgpxl, 4)$

$min(ERa) = -0.119$ $max(ERa) = 0.477$

plate p2 +/- 5% noise

$Gwl, XYZ\left(TPMODES^{\langle 2 \rangle}, 98, 14\right)$

120
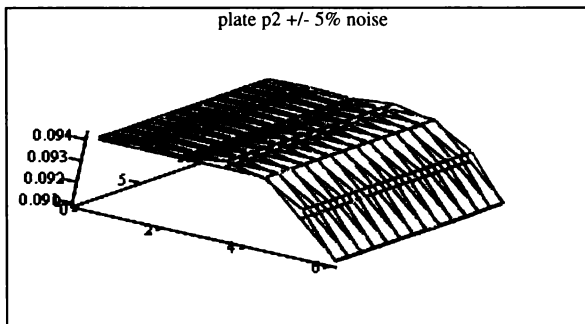
Appendix D
Nominal Model and Test Data

Table D-1. Nominal model modes at the test measruement points

x	z	NOMM1	NOMM3	NOMM5	NOMM6	NOMM7	NOMM8	NOMM9	NOMM10
0.25	0	0.000000	0.000000	0.000000	0.000000	0.000000	0.000000	0.000000	0.000000
0.25	2.165354	0.006917	-0.004038	-0.004608	0.000321	-0.000233	0.001502	-0.000881	0.000215
0.25	4.291339	0.024848	-0.006994	0.000103	-0.000081	-0.000215	-0.002946	-0.000671	-0.000242
0.25	6.417323	0.048797	-0.001543	0.004525	-0.000232	-0.000482	0.001381	0.000107	0.000240
0.25	7.480315	0.061658	0.003636	0.000476	0.000065	-0.000560	0.000558	0.000786	0.000077
0.25	8.267717	0.071298	0.007871	-0.004211	0.000371	-0.000492	-0.002067	0.001182	-0.000244
2	0	0.000000	0.000000	0.000000	0.000000	0.000000	0.000000	0.000000	0.000000
2	2.165354	0.007444	-0.003779	-0.004632	0.000000	0.000029	0.002333	0.000615	0.000000
2	4.291339	0.025397	-0.006361	-0.000307	0.000000	0.000358	-0.001189	0.000886	0.000000
2	6.417323	0.049113	-0.000956	0.003157	0.000000	0.000363	0.002251	-0.000361	0.000000
2	7.480315	0.061888	0.004121	-0.000981	0.000000	0.000383	0.000979	-0.000717	0.000000
2	8.267717	0.071489	0.008298	-0.005664	0.000000	0.000516	-0.001797	-0.000905	0.000000
3.75	0	0.000000	0.000000	0.000000	0.000000	0.000000	0.000000	0.000000	0.000000
3.75	2.165354	0.006917	-0.004038	-0.004608	-0.000321	-0.000233	0.001502	-0.000881	-0.000215
3.75	4.291339	0.024848	-0.006994	0.000103	0.000081	-0.000215	-0.002946	-0.000671	0.000242
3.75	6.417323	0.048797	-0.001543	0.004525	0.000232	-0.000482	0.001381	0.000107	-0.000240
3.75	7.480315	0.061658	0.003636	0.000476	-0.000065	-0.000560	0.000558	0.000786	-0.000077
3.75	8.267717	0.071298	0.007871	-0.004211	-0.000371	-0.000492	-0.002067	0.001182	0.000244

122

Table D-2. R2 Peak displacements for modes

x	z	RP2M1	RP2M3	RP2M5	RP2M6	RP2M7	RP2M8	RP2M9	RP2M10
0.25	0	0	0	0	0	0	0	0	0
0.25	2.165354	0.006558	0.004109	0.005107	0.000322	0.000277	0.00132	0.000996	0.000181
0.25	4.291339	0.024596	0.007069	0.000184	0.000103	0.000193	0.002947	0.00062	0.00022
0.25	6.417323	0.049233	0.001477	0.004554	0.000221	0.000512	0.001134	0.000105	0.000226
0.25	7.480315	0.060652	0.003596	0.000419	9.36E-05	0.000585	0.000206	0.000765	5.42E-05
0.25	8.267717	0.070854	0.007701	0.004323	0.00035	0.000483	0.00241	0.001169	0.000233
2	0	0	0	0	0	0	0	0	0
2	2.165354	0.007082	0.003815	0.004446	8.3E-06	1.22E-05	0.002396	0.000633	8.07E-06
2	4.291339	0.025696	0.00633	0.000171	2.23E-05	0.00036	0.000865	0.000864	1.2E-05
2	6.417323	0.048869	0.000951	0.003064	1.09E-05	0.000324	0.002409	0.000403	1.96E-05
2	7.480315	0.062337	0.004011	0.000908	4.15E-06	0.000362	0.001135	0.000699	1.43E-05
2	8.267717	0.0729	0.008292	0.00552	3.43E-05	0.000542	0.001521	0.000835	1.52E-05
3.75	0	0	0	0	0	0	0	0	0
3.75	2.165354	0.006558	0.00415	0.005002	0.000348	0.000276	0.001386	0.001046	0.000227
3.75	4.291339	0.024818	0.007032	0.000118	0.000114	0.000165	0.00294	0.000572	0.000255
3.75	6.417323	0.049031	0.001449	0.004343	0.000199	0.000493	0.001166	0.000117	0.000267
3.75	7.480315	0.061237	0.003589	0.000419	0.00012	0.000549	0.000197	0.000761	6.48E-05
3.75	8.267717	0.070983	0.00799	0.00408	0.000374	0.000452	0.002556	0.001161	0.000283

123

Table D-3. P1 peak displacements for modes

X	Z	P1M1	P1M3	P1M5	P1M6	P1M7	P1M8	P1M9	P1M10
0.25	0	0	0	0	0	0	0	0	0
0.25	2.165354	0.066468	0.004093	0.005004	0.00039	0.000352	0.00139	0.001037	0.000287
0.25	4.291339	0.02534	0.00702	0.000232	0.00012	0.00027	0.002911	0.00069	0.000317
0.25	6.417323	0.049436	0.001462	0.004537	0.000297	0.000673	0.001142	6.54E-05	0.000307
0.25	7.480315	0.060772	0.0036637	0.000448	8.73E-05	0.000804	0.000292	0.000796	9.33E-05
0.25	8.267717	0.07042	0.00804	0.004493	0.000451	0.00072	0.002522	0.001276	0.000331
2	0	0	0	0	0	0	0	0	0
2	2.165354	0.007011	0.003757	0.004534	7.55E-06	2.12E-05	0.002327	0.00063	8.32E-06
2	4.291339	0.025478	0.006373	0.00016	2.38E-05	0.000443	0.0009979	0.000905	1.13E-05
2	6.417323	0.049011	0.000866	0.003148	9.44E-06	0.000445	0.002362	0.000369	1.94E-05
2	7.480315	0.062076	0.004217	0.001057	8.31E-06	0.000503	0.001064	0.000714	1.41E-05
2	8.267717	0.070391	0.008389	0.005642	4.08E-05	0.000728	0.0016668	0.000866	1.29E-05
3.75	0	0	0	0	0	0	0	0	0
3.75	2.165354	0.00631	0.003982	0.004995	0.00038	0.000307	0.001571	0.000983	0.000242
3.75	4.291339	0.02456	0.00695	0.000142	0.000125	0.000253	0.00292	0.00065	0.000278
3.75	6.417323	0.049159	0.001431	0.004618	0.000232	0.000653	0.001237	6.67E-05	0.00029
3.75	7.480315	0.061622	0.003735	0.000435	0.000138	0.000771	0.000317	0.000799	7.74E-05
3.75	8.267717	0.071121	0.00818	0.004635	0.000459	0.000695	0.002607	0.00133	0.000306

Table D-4. P2 peak displacements for modes

X	Z	P2M1	P2M2	P2M3	P2M4	P2M5	P2M6	P2M7	P2M8	P2M9	P2M10
0.25	0	0	0	0	0	0	0	0	0	0	0
0.25	2.165354	0.00682	0.000143	0.004188	8.01E-05	0.005429	0.0008	0.00032	0.001028	0.001081	0.000143
0.25	4.291339	0.025928	0.000212	0.006992	6.56E-05	2.67E-05	0.000239	0.000187	0.002713	0.000777	0.000161
0.25	6.417323	0.05124	0.000194	0.001639	3.39E-05	0.00489	0.000608	0.000591	0.000665	0.000139	0.000156
0.25	7.480315	0.065486	0.000148	0.003579	6.2E-05	0.000628	0.000201	0.000671	3E-05	0.000927	4.09E-05
0.25	8.267717	0.074808	0.000115	0.007878	8.15E-05	0.004315	0.000906	0.000555	0.002076	0.001389	0.000169
2	0	0	0	0	0	0	0	0	0	0	0
2	2.165354	0.007607	8.54E-05	0.003949	3.53E-05	0.004906	1.76E-05	7.14E-06	0.001973	0.000728	1.39E-05
2	4.291339	0.026876	7.16E-05	0.006482	5.77E-06	0.000212	3.49E-05	0.0004	0.000646	0.000981	1.93E-05
2	6.417323	0.051946	1.15E-05	0.000983	1.73E-05	0.003366	2.11E-05	0.000332	0.002144	0.000436	2.54E-05
2	7.480315	0.065353	6.93E-05	0.004136	8.66E-06	0.001068	1.46E-05	0.00039	0.001032	0.000786	1.79E-05
2	8.267717	0.075027	0.000118	0.00823	3.61E-05	0.005847	0.000103	0.000617	0.001166	0.000974	2.04E-05
3.75	0	0	0	0	0	0	0	0	0	0	0
3.75	2.165354	0.0068	3.23E-05	0.004279	4.4E-05	0.005486	0.000833	0.000308	0.001182	0.001169	9.33E-05
3.75	4.291339	0.025948	5.77E-05	0.007205	8.01E-05	0.00024	0.000284	0.000161	0.002838	0.000657	0.000124
3.75	6.417323	0.051815	0.000201	0.001467	1.59E-05	0.005046	0.000483	0.000594	0.000956	8.48E-05	0.000134
3.75	7.480315	0.065172	0.000282	0.003947	6.85E-05	0.000187	0.000319	0.000666	3.63E-05	0.000895	2.23E-05
3.75	8.267717	0.07521	0.000323	0.008316	0.000125	0.004871	0.000907	0.000526	0.002345	0.00138	0.000114

125

Table D-5. P3 peak displacements for modes

x	z	P3M1	P3M2	P3M3	P3M5	P3M6	P3M7	P3M8	P3M9	P3M10
0.25	0	0	0	0	0	0	0	0	0	0
0.25	2.1653354	0.0065548	0.000119	0.004309	0.005502	0.000433	0.000405	0.001183	0.001422	0.000591
0.25	4.291339	0.024697	0.000152	0.007676	7.47E-05	0.000159	0.000285	0.002875	0.000954	0.00073
0.25	6.417323	0.049323	8.8E-05	0.001778	0.004922	0.000309	0.000742	0.000927	0.000239	0.000713
0.25	7.480315	0.063135	4.76E-05	0.003772	0.000411	0.000148	0.000801	0.0001	0.001215	0.000141
0.25	8.267717	0.07287	4.76E-05	0.008177	0.004548	0.000503	0.000677	0.002108	0.001833	0.000736
2	0	0	0	0	0	0	0	0	0	0
2	2.1653354	0.007213	9.04E-05	0.004107	0.004894	1.47E-05	2.19E-05	0.002003	0.000965	8.04E-06
2	4.291339	0.025424	7.85E-05	0.007068	0.000252	4.92E-05	0.000553	0.000772	0.001341	1.39E-05
2	6.417323	0.049979	4.76E-06	0.001154	0.003414	2.38E-05	0.000454	0.002091	0.000672	1.89E-05
2	7.480315	0.063297	8.42E-05	0.004179	0.001019	1.2E-05	0.000499	0.000919	0.001068	1.32E-05
2	8.267717	0.0729901	0.000117	0.008613	0.005807	7.24E-05	0.000753	0.00131	0.001258	1.23E-05
3.75	0	0	0	0	0	0	0	0	0	0
3.75	2.1653354	0.006416	7.14E-05	0.00433	0.005419	0.000442	0.000377	0.001203	0.001426	0.000606
3.75	4.291339	0.024909	3.33E-05	0.007792	0.000235	0.000165	0.000279	0.002871	0.000983	0.000724
3.75	6.417323	0.050282	9.04E-05	0.001804	0.004934	0.000295	0.000717	0.000971	0.000223	0.000704
3.75	7.480315	0.063822	0.000162	0.003858	0.000342	0.000164	0.000777	0.000113	0.001242	0.000147
3.75	8.267717	0.072885	0.000214	0.008389	0.004594	0.00051	0.000623	0.002142	0.001833	0.000726

126

Table D-6. P4 peak displacements for modes

x	z	P4M1	P4M3	P4M5	P4M6	P4M7	P4M8	P4M9	P4M10
0.25	0	0	0	0	0	0	0	0	0
0.25	2.165354	0.006469	0.004113	0.005314	0.000894	0.000268	0.001239	0.001291	0.000421
0.25	4.291339	0.025133	0.007179	4.36E-05	0.000242	0.00022	0.002696	0.000975	0.000489
0.25	6.417323	0.048853	0.001559	0.005027	0.001329	0.000573	0.000993	5.22E-05	0.000496
0.25	7.480315	0.062255	0.00381	0.000588	0.000252	0.000716	0.000252	0.001072	0.000143
0.25	8.267717	0.072396	0.00839	0.004822	0.001065	0.000611	0.002126	0.001631	0.000531
2	0	0	0	0	0	0	0	0	0
2	2.165354	0.00715	0.003845	0.004764	1.39E-05	1.01E-05	0.001924	0.000829	8.47E-06
2	4.291339	0.025192	0.006343	0.000282	3.93E-05	0.000368	0.000813	0.001223	1.2E-05
2	6.417323	0.04826	0.000973	0.003427	2.31E-05	0.000388	0.002005	0.000436	1.81E-05
2	7.480315	0.061643	0.004288	0.001072	1.12E-05	0.000436	0.000962	0.000928	1.46E-05
2	8.267717	0.072436	0.00872	0.00592	6.94E-05	0.000638	0.001437	0.001178	1.46E-05
3.75	0	0	0	0	0	0	0	0	0
3.75	2.165354	0.006389	0.004083	0.005295	0.000901	0.00026	0.001296	0.00123	0.000426
3.75	4.291339	0.024649	0.007176	8.23E-05	0.000274	0.000196	0.002608	0.000861	0.000488
3.75	6.417323	0.04835	0.001536	0.004969	0.000613	0.000562	0.001014	3.02E-05	0.000493
3.75	7.480315	0.06182	0.003899	0.000391	0.000296	0.000642	0.000254	0.000957	0.000133
3.75	8.267717	0.072255	0.008362	0.004801	0.00104	0.000571	0.002094	0.001569	0.000513
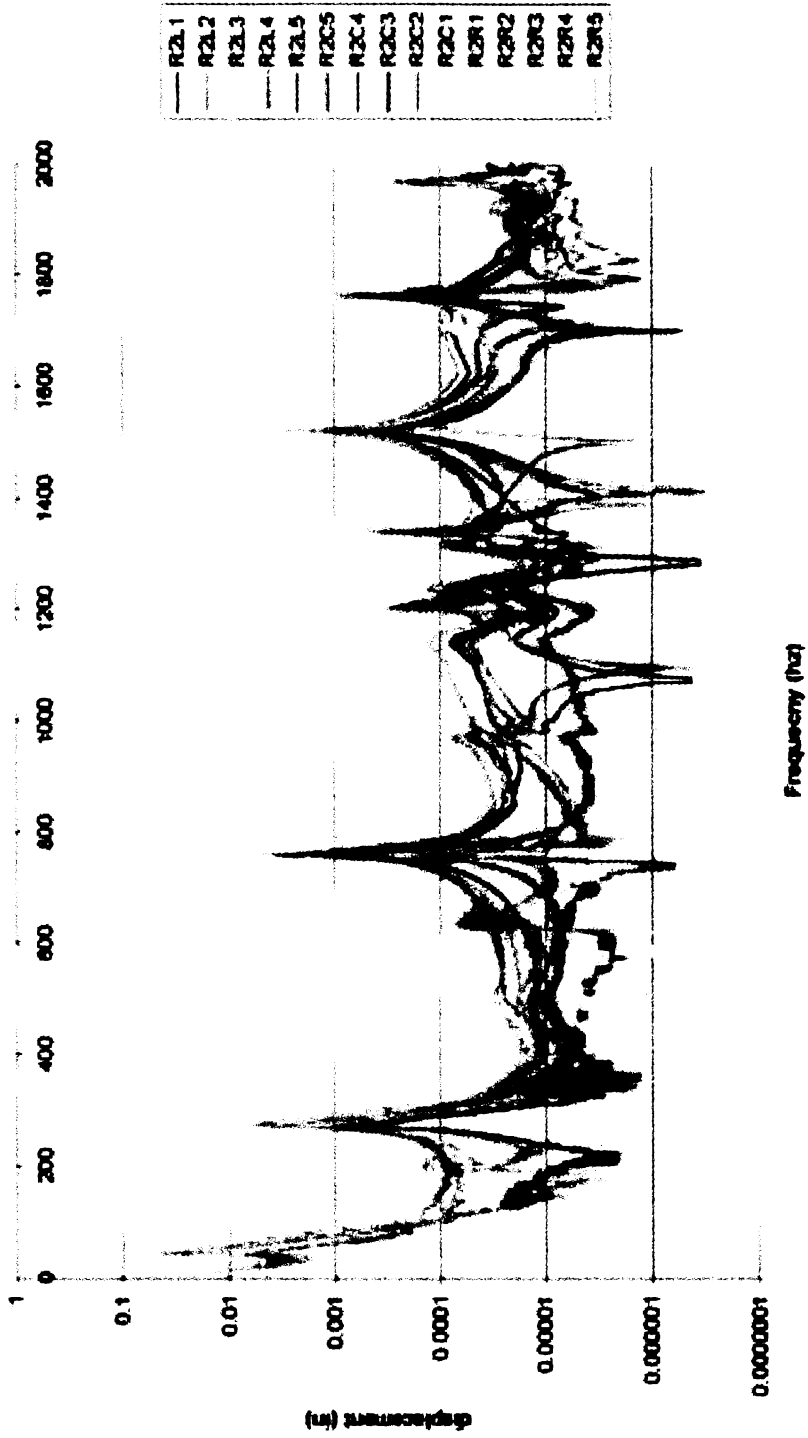
Figure D-1. R2 displacement versus frequency
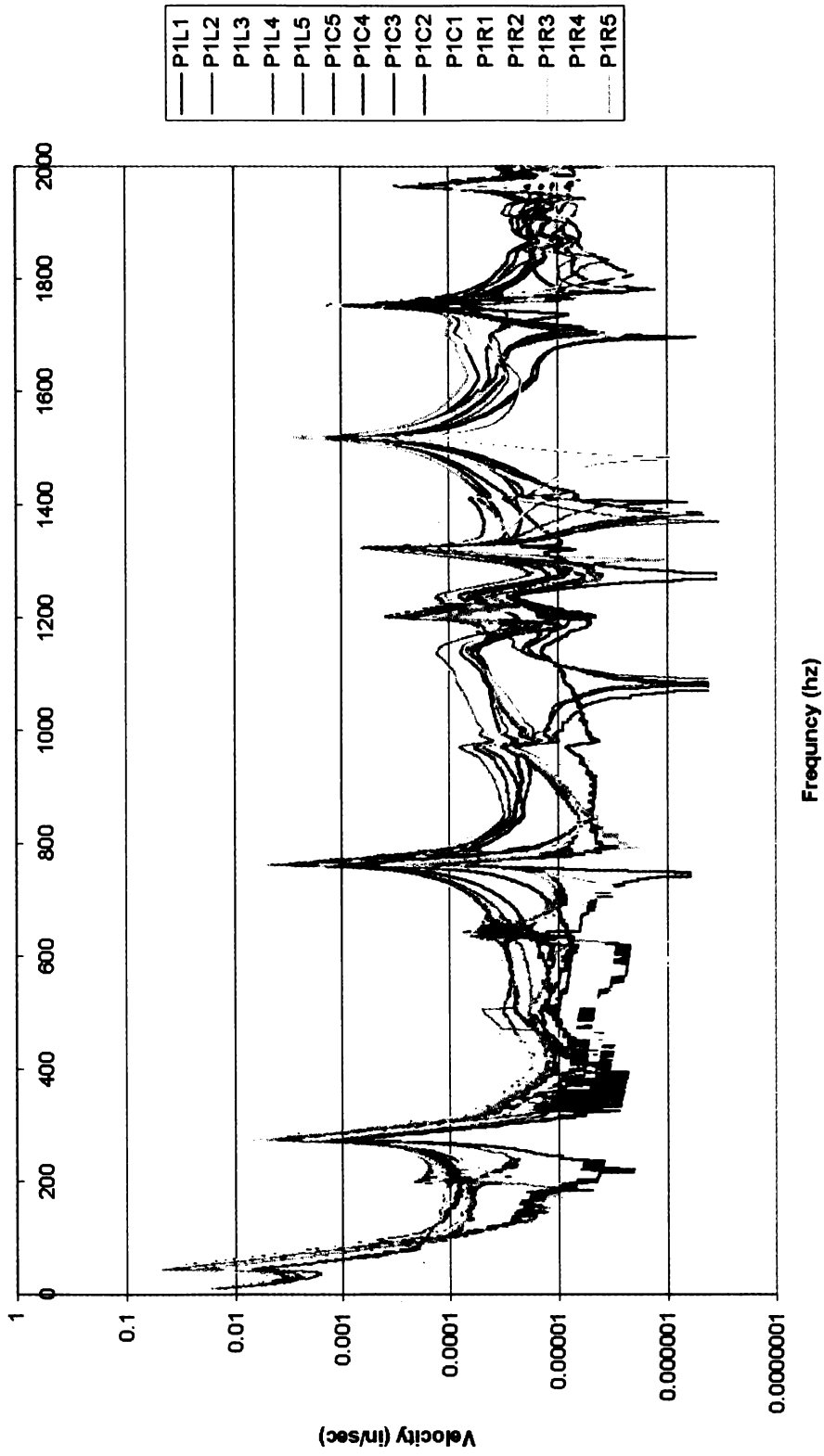
Figure D-2. P1 displacement versus frequency
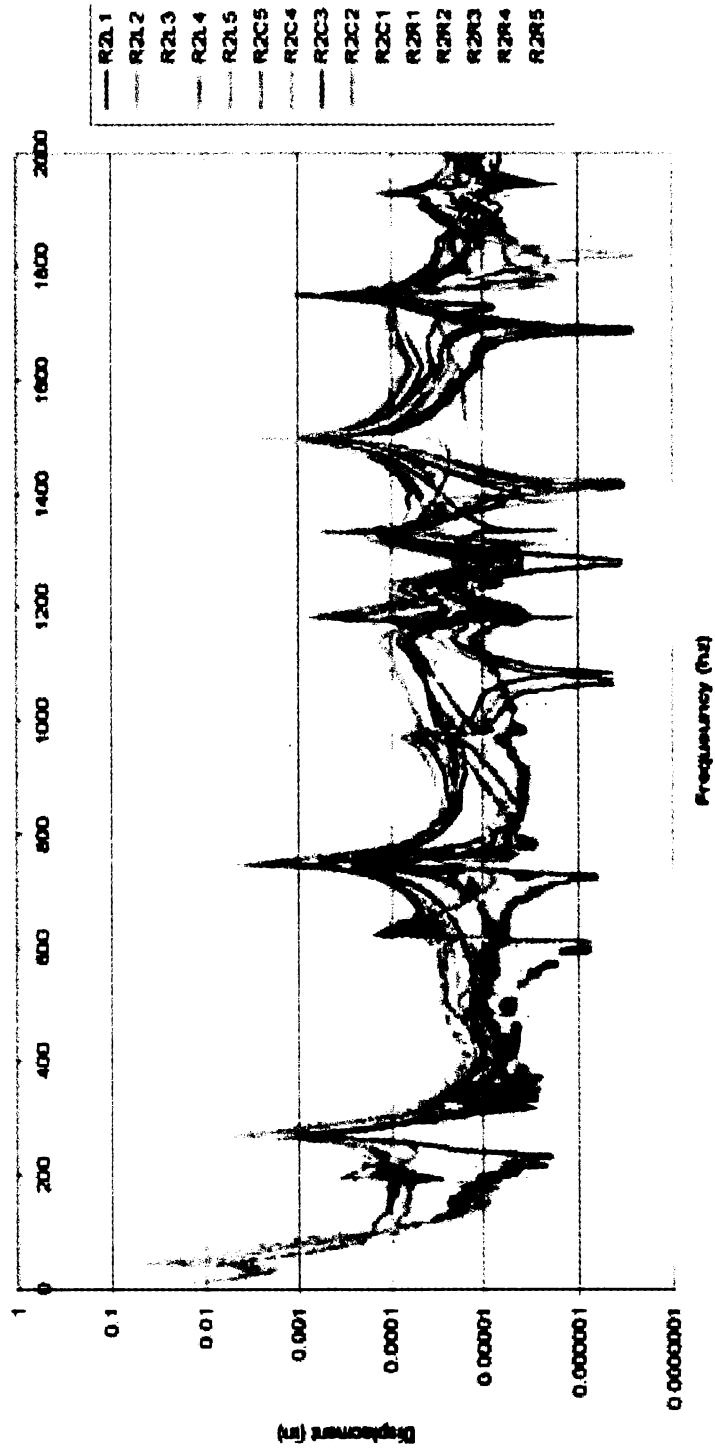
Figure D-3. P2 displacement versus frequency

130
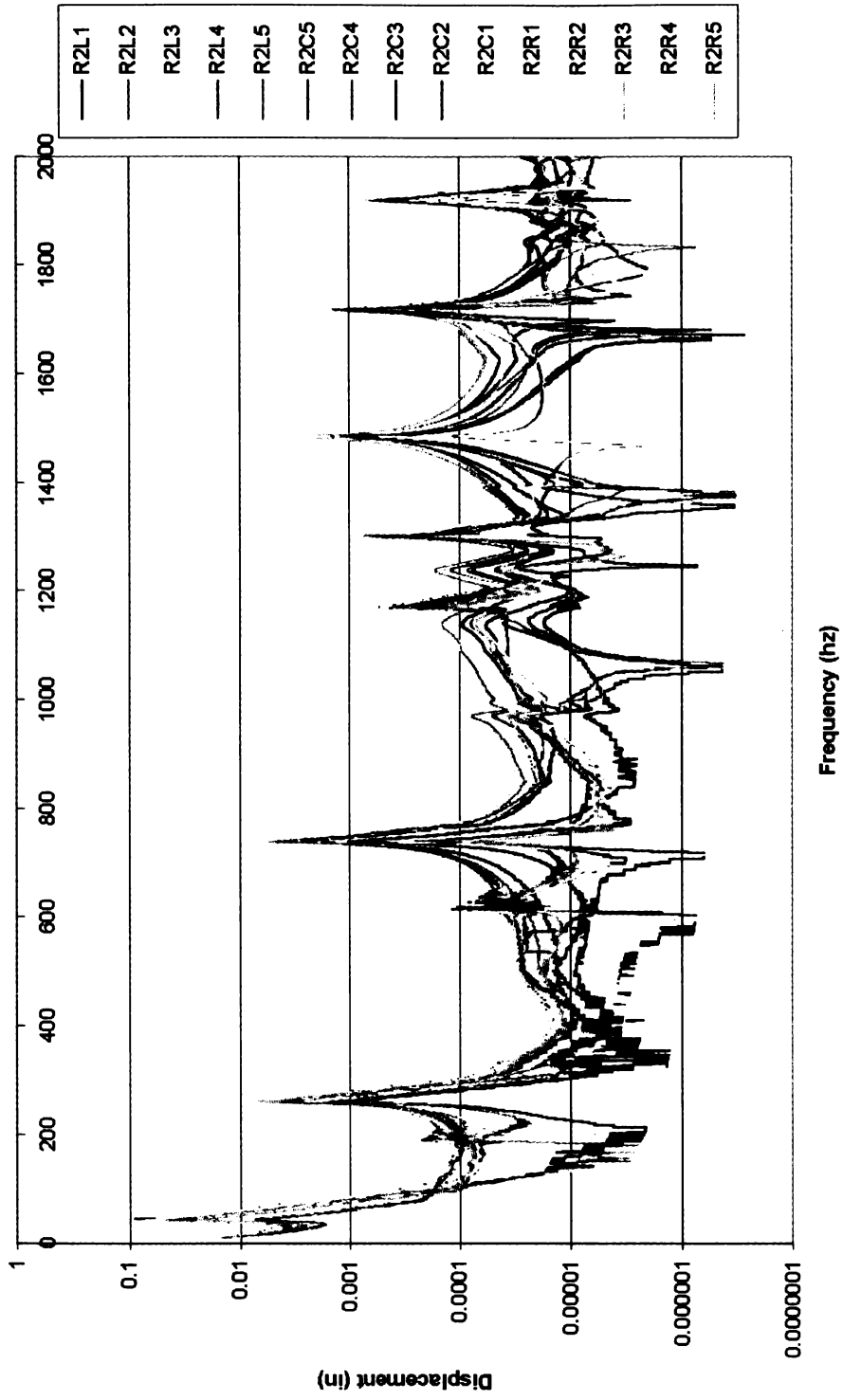
Figure D-4. P3 displacement versus frequency
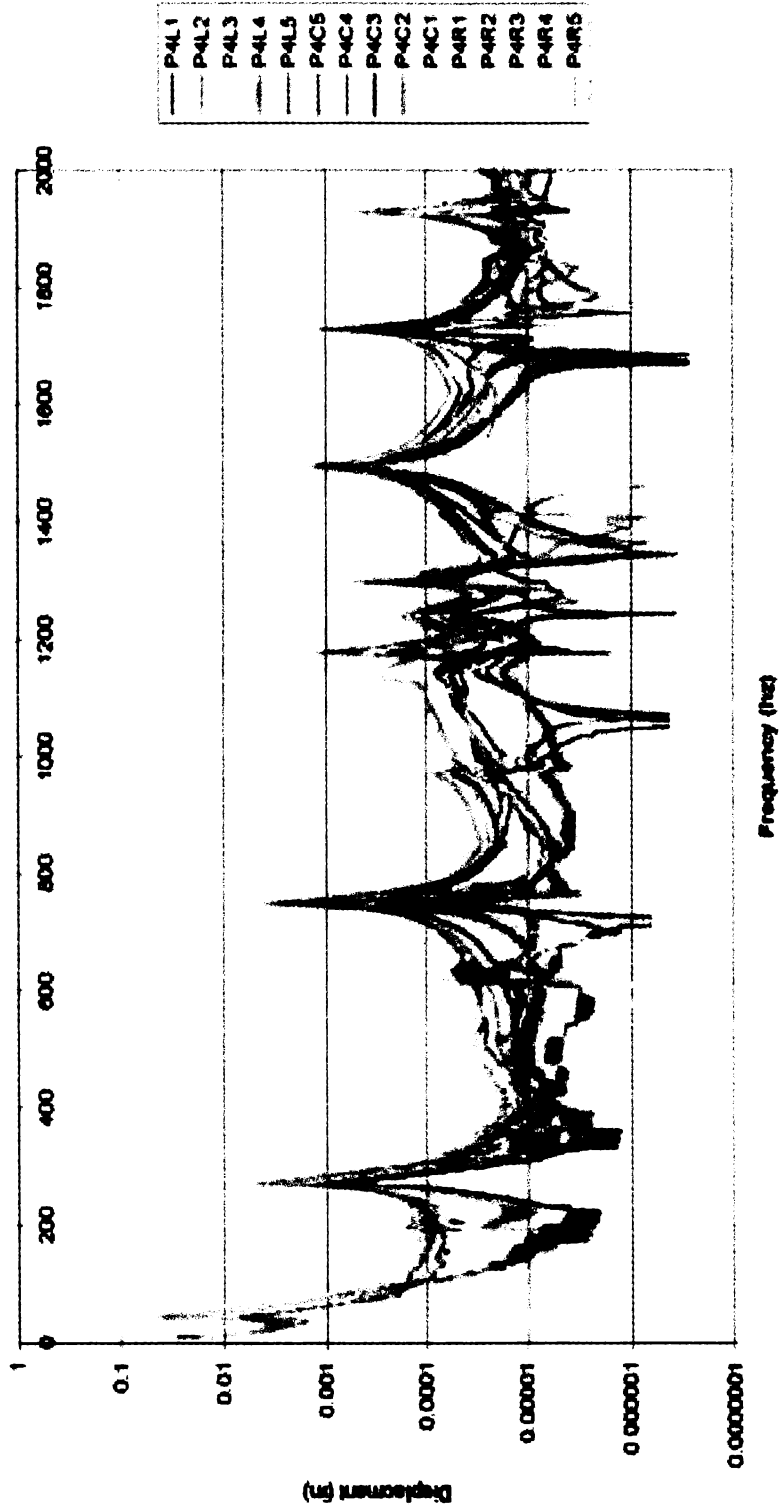
Figure D-5. P4 displacement versus frequency

132

PLATE R2 1B MODE

PLATE R2 2B MODE

PLATE R2 3B MODE

PLATE R2 4B MODE

PLATE R2 3T MODE

PLATE R2 4B MODE

PLATE R2 1C2B MODE

PLATE R2 4T MODE
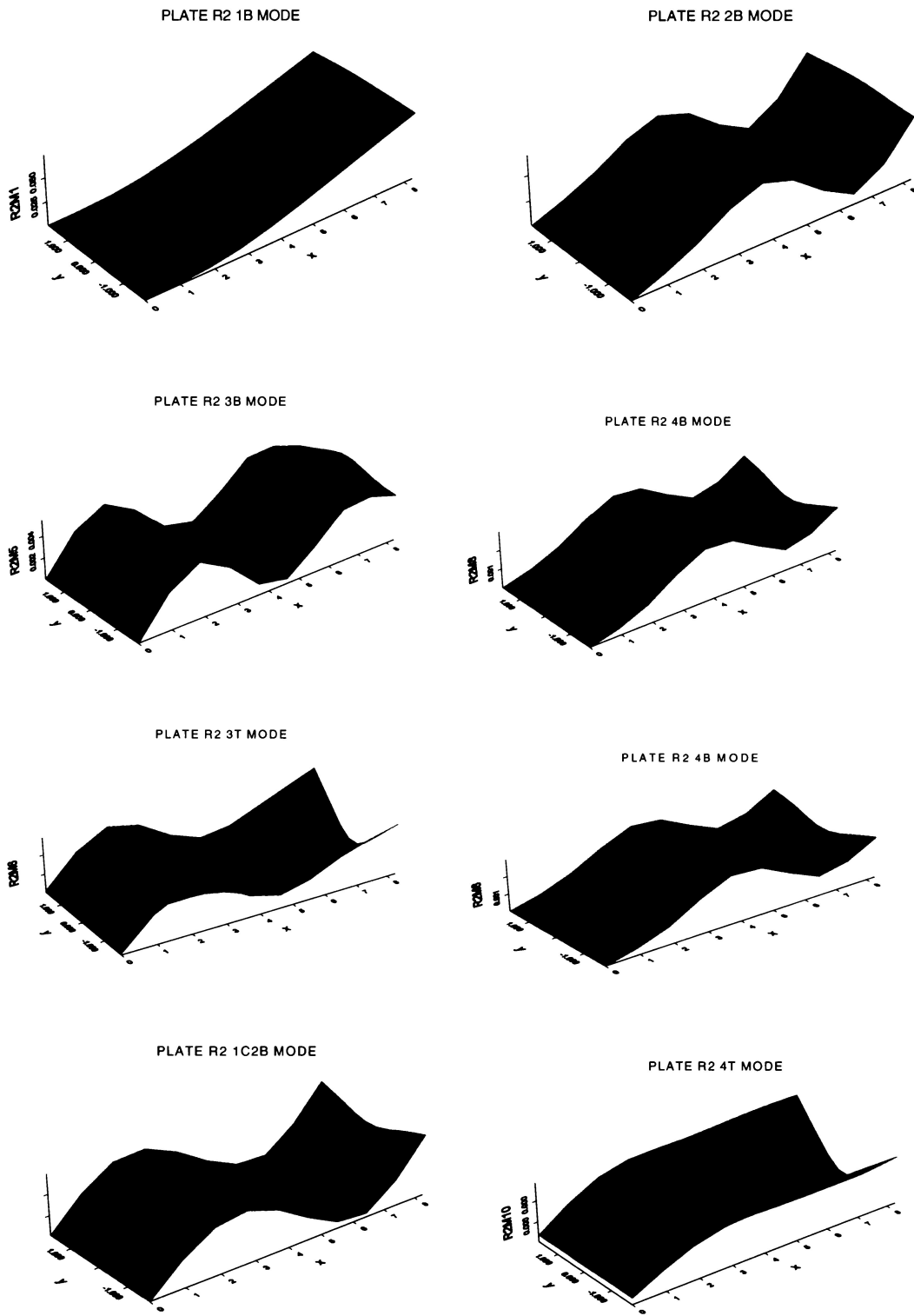
Figure D-6. Absolute value plots of R2 modes

133

PLATE P1 1B MODE

PLATE P1 2B MODE

PLATE P1 2T MODE

PLATE P1 3B MODE

PLATE P1 4B MODE

PLATE P1 3T MODE

PLATE P1 1C2B

PLATE P1 1C1B MODE

PLATE P1 4T MODE
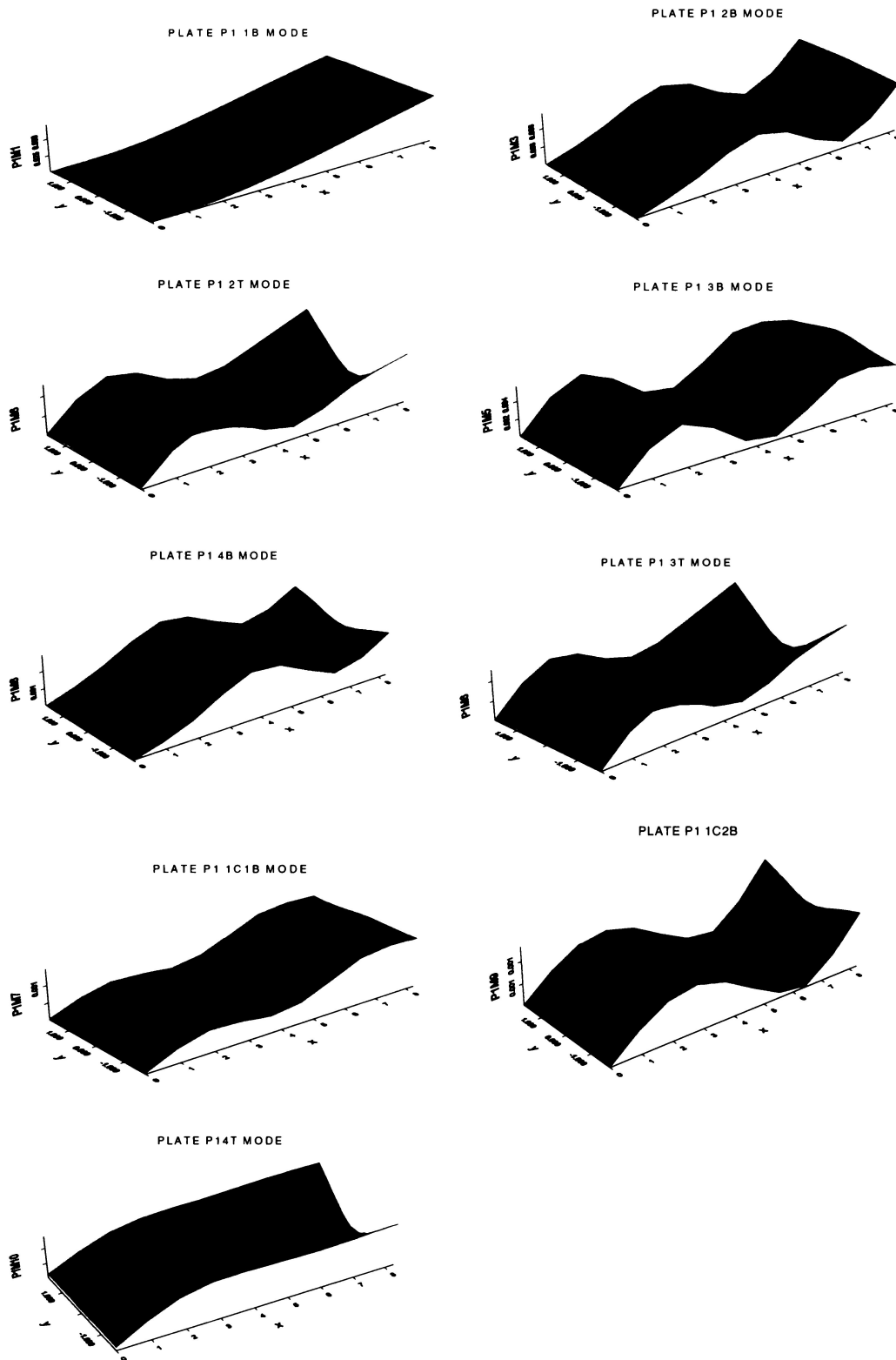
Figure D-7. Absolute Value plots for P1 modes

134

PLATE P2 1B MODE

PLATE P2 1T MODE

PLATE P2 2B MODE

PLATE P2 2T MODE

PLATE P2 3B MODE

PLATE P2 3T MODE

PLATE P2 1C1B

PLATE P2 4B MODE

PLATE P2 1C2B MODE

PLATE P2 4T MODE
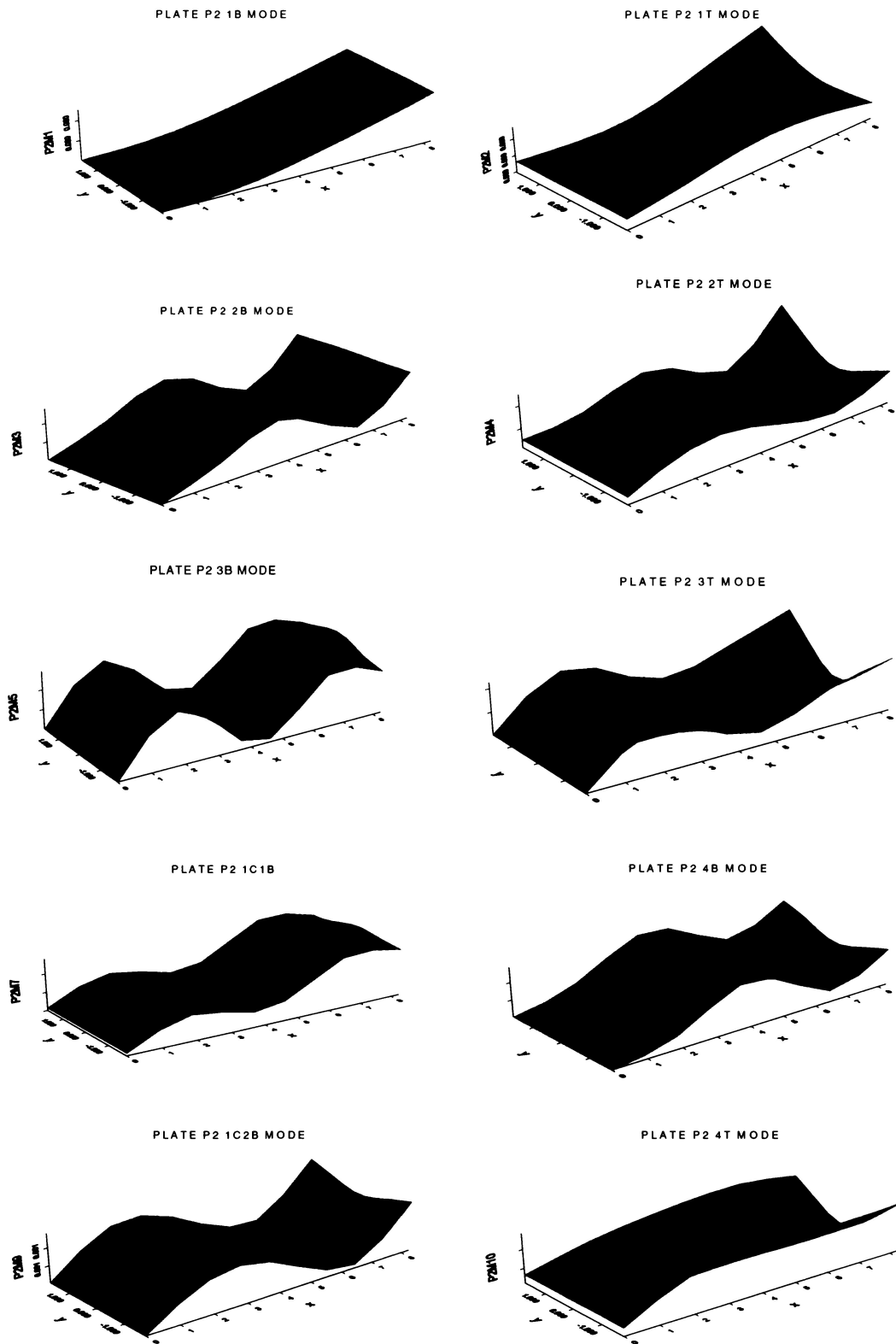
Figure D-8. Absolute value plots for P2 modes

PLATE P3 1B MODE

PLATE P3 1T MODE

PLATE P3 2B MODE

PLATE P3 3B MODE

PLATE P3 3T MODE

PLATE P3 1C1B MODE

PLATE P3 1C2B MODE

PLATE P3 4T MODE
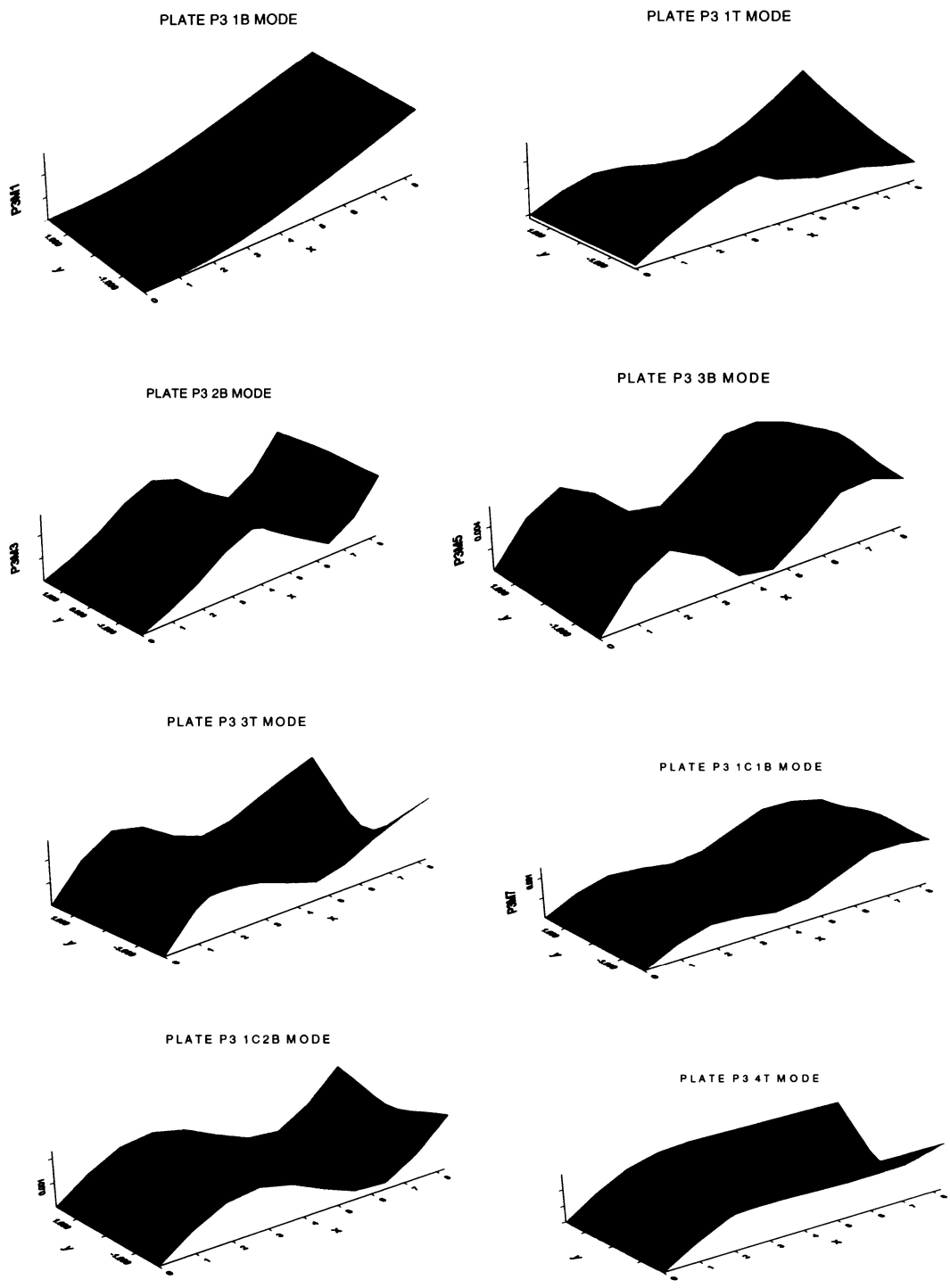
Figure D-9. Absolute value plots for P3 modes

136

PLATE P4 1B MODE

PLATE P4 2B MODE

PLATE P4 3B MODE

PLATE P4 3T MODE

PLATE P4 1C1B MODE
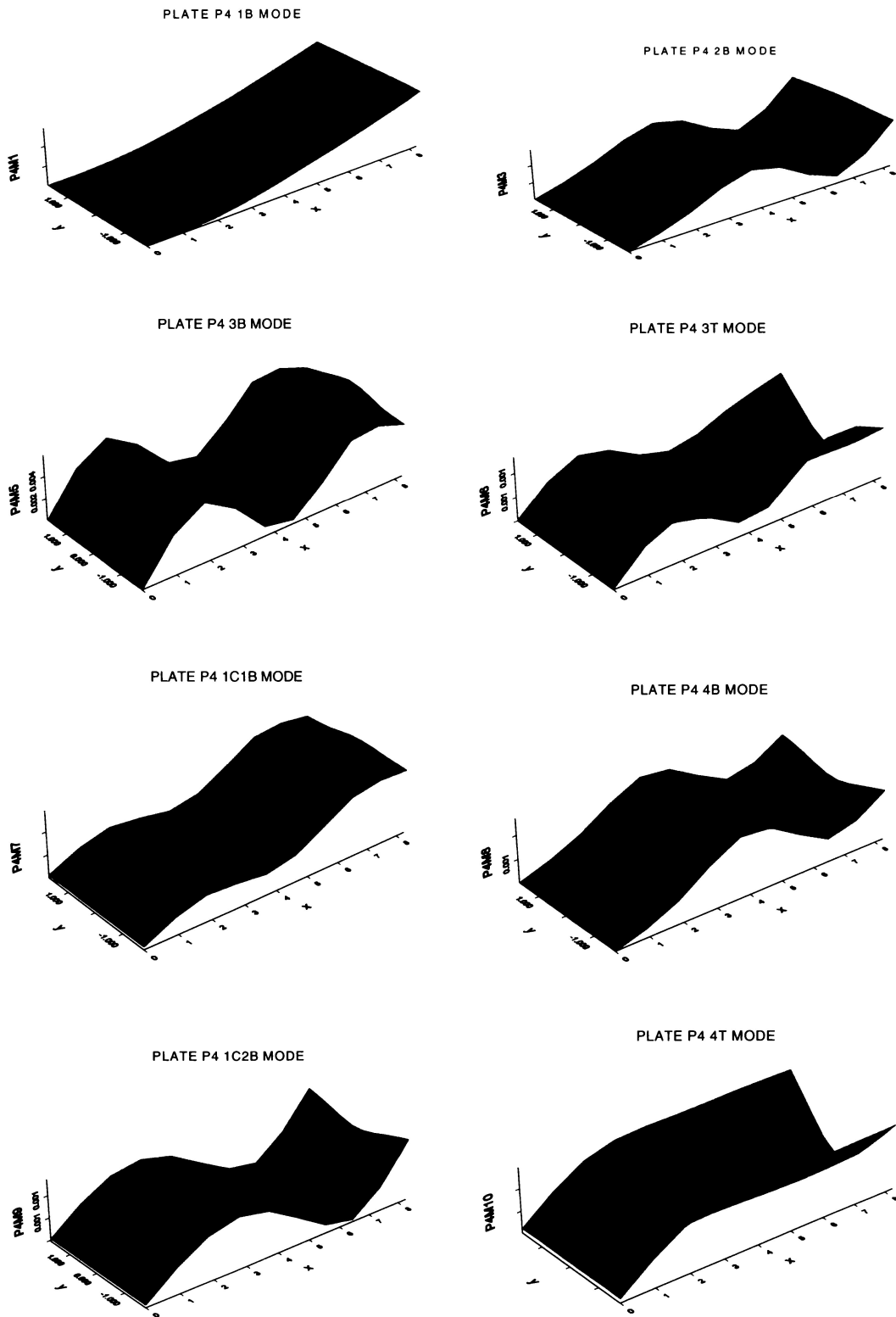
PLATE P4 4B MODE

PLATE P4 4T MODE

PLATE P4 1C2B MODE

Figure D-10. Absolute value for P4 modes

137

Vita

Charles Vining was born in Oshawa, Ontario, Canada on September 4, 1959. He was raised in Swarthmore, Pennsylvania. He was awarded a Bachelors Degree in Mechanical Engineering in 1982 from the University of Delaware, Newark Delaware and a Masters Degree in Engineering Science in 1992, from Pennsylvania State University College Park, Pennsylvania. He currently resides in Tullahoma, Tennessee with his wife and five children. Charles is employed by the Naval Air Systems Command where he works as project manager for Applied Technology at the Arnold Engineering Development Center, Arnold Air Force Base, Tullahoma, Tennessee.